



**Margarida Sofia  
Quintanilha Miranda**

**Transporte Transmembranar de Aniões por  
Recetores Sintéticos**

**Transmembrane Transport of Anions by Synthetic  
Transporters**





**Margarida Sofia  
Quintanilha Miranda**

**Transporte Transmembranar de Aniões por  
Recetores Sintéticos**

**Transmembrane Transport of Anions by Synthetic  
Transporters**

Dissertação apresentada à Universidade de Aveiro para cumprimento dos requisitos necessários à obtenção do grau de Mestre em Química, realizada sob a orientação científica do Doutor Vítor Félix, Professor Associado com Agregação do Departamento de Química da Universidade de Aveiro

Os estudos apresentados nesta dissertação foram realizados com recursos computacionais adquiridos sob o projecto P2020-PTDC/QEQ-SUP/4283/2014, financiado pela Fundação para a Ciência e a Tecnologia I.P. (FCT) e pelo Fundo Europeu de Desenvolvimento Regional (FEDER) através do COMPETE 2020 – Programa Operacional Competitividade e Internacionalização.



Dedico este trabalho aos meus pais.



## **o júri**

presidente

**Prof. Doutor Artur Manuel Soares Silva**  
professor catedrático do Departamento de Química da Universidade de Aveiro

**Prof. Doutor Vítor Manuel Sousa Félix**  
professor associado com agragação do Departamento de Química da Universidade de Aveiro

**Doutor José Richard Baptista Gomes**  
investigador principal do laboratório associado CICECO da Universidade de Aveiro





## **agradecimentos**

Ao prof. Vitor, professor orientador desta tese de mestrado, pela oportunidade e confiança que depositou em mim para a realização deste trabalho. A sua constante disponibilidade e acompanhamento durante todo o processo foram determinantes para a conclusão desta tese, assim com a motivação demonstrada e as condições de trabalho que disponibilizou.

Ao Igor, Pedro e Liliana, do grupo de Molecular Modeling da universidade, pela boa recepção, pela simpatia, pelo bom ambiente e pelo companheirismo que sempre senti ao longo deste ano. Um agradecimento especial ao Igor e ao Pedro que me transmitiram todo o conhecimento necessário à realização do trabalho prático efectuado nesta tese, pela paciência e disponibilidade que demonstraram ao longo deste ano de trabalho em esclarecer quaisquer dúvidas que eu tivesse. Sem a vossa ajuda nada disto seria possível.

To Professor Anthony P. Davis for providing the experimental data that served as base for the present thesis and which allowed its complete elaboration.

À Alexandra, Sílvia e Nádia, as amigas de sempre, pelo apoio nesta “aventura” de me mudar para longe, pela motivação que deram, pela disponibilidade que sempre demonstraram caso algo fosse necessário e por reservarem sempre tempo para nos encontrarmos e convivermos.

Ao meu irmão, pelas inúmeras boleias Gare do Oriente/casa e casa/Gare do Oriente, pelo apoio incondicional em todas as minhas opções e decisões, pelas mensagens inesperadas com piada que muitas vezes me alegraram o dia e pela motivação.

Aos meus pais, por tudo, desde sempre. Pela vossa confiança em mim em todas as circunstâncias e pelo apoio incondicional que demonstraram nas minhas decisões. Por todo o esforço que fizeram para que as minhas aspirações fossem concretizadas, apesar de todos os sacrifícios que isso implicaria, por mostrarem sempre o vosso apoio, carinho e força. Estou-vos eternamente grata!



## palavras-chave

Fibrose cística, POPC, Simulações de dinâmica molecular, Transportadores de aniões cloreto, Transportadores sintéticos, Transporte transmembranar de aniões

## resumo

O transporte de cloreto pela bicamada fosfolipídica, assistido por pequenas moléculas sintéticas, foi estudado através de métodos computacionais, incluindo cálculos quânticos, simulações de dinâmica molecular e cálculos de energia livre. As propriedades de transporte de um conjunto de doze tris-tioureas contendo um anel central de seis membros (cicloexano, cicloexano hexametilado e benzeno) derivatizado com grupos arilo (3,5-trifluorometilo, p-trifluorometilo, p-nitro e fenilo), foram estudados *in silico* tendo como objetivo a compreensão de dados experimentais de transporte reportados.

O estudo computacional iniciou-se com a otimização dos doze complexos em fase gasosa e em dimetilsulfóxido (DMSO), ao nível de teoria de M06-2X/6-31+G\*\*. A força das interações NH...Cl<sup>-</sup> foi determinada através dos valores de  $E^2$  obtidos da teoria de perturbação de segunda ordem, dos índices de ligação de Wiberg e do valor mais positivo de potencial electrostático ( $V_{S,max}$ ). Estes descritores aumentam com as constantes de afinidade, refletindo o carácter electroattractor dos substituintes arilo. Assim, os três transportadores com grupos 3,5-trifluorometilo apresentaram os valores mais altos para estes descritores e para afinidade ao cloreto, demonstrando que estas moléculas conseguem de facto capturar um anião da fase aquosa e proceder ao seu transporte através da bicamada fosfolipídica. Seguiu-se o estudo do processo de difusão passiva para estes três complexos por dinâmica molecular, tendo estes sido colocados tanto na fase aquosa como no centro da bicamada fosfolipídica. Estas simulações revelaram que os transportadores eram capazes de promover os processos de captura e libertação de cloreto. Além disso, os perfis de energia livre para o complexo do ligando cicloexano hexametilado derivatizado com 3,5-trifluorometilo e para o cloreto livre foram obtidos através de cálculos de potencial de força média. O complexo tem que superar uma barreira energética de 2 kcal mol<sup>-1</sup> para atravessar o meio da bicamada enquanto o cloreto livre tem que ultrapassar uma barreira de energia livre de 19.5 kcal mol<sup>-1</sup>, *i.e.* o transporte assistido pelo recetor é energeticamente mais favorável. Outra característica importante das simulações está relacionada com o facto dos complexos de cloreto de inserirem confortavelmente abaixo da interface da membrana, indicando que os recetores conseguem operar como transportadores de cloreto sem sair da bicamada fosfolipídica.



**keywords**

Chloride anion transporters, Cystic fibrosis, Molecular dynamics simulations, POPC, Synthetic transporters, Transmembrane anion transport

**abstract**

The chloride transport across the phospholipid bilayer assisted by small synthetic molecules were studied by computational methods including quantum calculations followed by molecular dynamics simulations and free energy calculations.

A series of twelve tris-thiourea aryl substituted putative transporters, with three different six-membered rings as scaffolds (desmethyl cyclohexane, hexamethyl cyclohexane and benzene) and each of them with four possible aryl substituents (3,5-trifluoromethyl, p-trifluoromethyl, p-nitro and phenyl), were studied in silico in order to understand the experimental transport data previously reported for these molecules.

The computational study started with the DFT optimization of twelve chloride complexes in gas phase and in DMSO at the M062X/6-31+G\*\* theory level. The strength of the N-H...Cl<sup>-</sup> interactions were ascertained through the  $E^2$  values obtained from the second order perturbation theory, the Wiberg bond Indexes and the most positive value of the electrostatic potential ( $V_{S,max}$ ). Overall, these descriptors increases with the binding affinity constants reflecting the electron withdrawing character of the aryl substituents. Thus, the 3,5-trifluoromethyl substituted transporters presented the highest values for the quantum descriptors as well as the highest binding affinity for chloride anion, indicating that these molecules are able to successfully uptake the anion from the water phase and further proceed to its transport across the phospholipid bilayer. Subsequently, the passive diffusion of these chloride complexes were then investigated by MD simulations positioning them either in the bilayer core and water phase. Overall, the MD simulation runs reveal that the transporters were able to promote chloride uptake and release events, consistent with anion carrier transport mechanism. Furthermore, free energy profile for 3,5-trifluoromethyl hexamethyl cyclohexane complex and free chloride were constructed from the potential mean force calculations. The chloride complex has to surpass an energy barrier to cross the middle of the phospholipid bilayer of 2 kcal mol<sup>-1</sup> while for the free chloride this energy increases to 19.5 kcal mol<sup>-1</sup> indicating that the chloride transport assisted by this receptor is energetically favoured. Another remarkable feature from the MD simulations is that the chloride complexes fit comfortably well below the membrane's interface which seems to indicate that the receptors are able to operate as a chloride shuttle without leaving the phospholipid bilayer.



## Index

<b>1. Introduction</b> .....	1
1.1. <i>Membranes</i> .....	1
1.1.1. Methods of transport across the biological membranes .....	3
1.1.1.1. Passive transport .....	3
1.1.1.2. Active transport.....	3
1.1.2. Transporters: carriers and channels .....	5
1.2. <i>The Biological Importance of Ions</i> .....	6
1.2.2. Possible Therapies for Genetic Diseases .....	8
1.3. <i>Design of Synthetic Anion Transporters</i> .....	9
1.3.1. Halogen Bonds on Anion Transport.....	10
1.3.2. Anion- $\pi$ Interactions on Anion Transport.....	11
1.3.3. Chalcogen Bonds on Anion Transport .....	12
1.3.4. CH as Hydrogen Bond Donners on Anion Transport .....	12
1.3.5. Pyrrole and Indole Groups on Anion Transport.....	13
1.3.6. Nitrogen Functional Groups on Anion Transport.....	14
1.3.7. Synthetic Transporters as Druglike Molecules .....	16
1.3.8. Molecules with a Transport Architecture .....	17
1.4. <i>Computational methods and molecular modelling</i> .....	21
1.4.1. First Insights at Atomistic Level by Molecular Dynamics Simulations.....	23
1.4.1.1. Structural Properties of Phospholipid Bilayers.....	26
1.4.1.2. Important Descriptors on Anion Transmembrane Transport.....	27
1.5. <i>The Precedent Work that Lead to this Thesis</i> .....	28
1.6. <i>Objectives</i> .....	31
<b>2. Computational Methods</b> .....	33
2.1. <i>Calculation of atomic RESP Charges for the Transporters</i> .....	33
2.1.1. Structure Assembly for the Free and Complexed Transporters.....	33
2.1.2. Optimization of the Free Transporters .....	33

2.2. Optimization of the chloride complexes .....	34
2.2.1. Natural Bond Orbital Analysis .....	34
2.2.2. Obtaining the Molecular Electrostatic Potential Surfaces .....	35
2.3. Simulations in POPC Bilayer Model.....	35
2.3.1. The Free POPC Bilayer .....	35
2.3.2. Simulation of the Chloride Complexes in the POPC Membrane Model .....	36
2.4. Computation of Potential of Mean Force.....	36
<b>3. Results and Discussion.....</b>	<b>39</b>
3.1. Database Search Analysis.....	39
3.2. DFT Geometry Optimizations .....	41
3.3. Receptor's MD Simulations Analysis .....	49
3.3.1. Structural Impact of the Transporters in the POPC Membrane Model.....	50
3.3.2. Transporters' Diffusion in the Phospholipid Bilayer .....	50
3.3.4. Free Energy Calculations.....	62
<b>4. Conclusion .....</b>	<b>65</b>
<b>5. Bibliography .....</b>	<b>66</b>
<b>Supporting Information .....</b>	<b>74</b>
<i>S1: Multi RESP charges for 51SD, 52SD and 53SD.....</i>	<i>74</i>
<i>S2: Structural parameters of the crystal structure of RUSBIS.....</i>	<i>77</i>
<i>S3: Complete results for the structural parameters of area per lipid and membrane thickness.....</i>	<i>78</i>
<i>S4: Results for the structural parameters of electron density profiles and order parameters.....</i>	<i>79</i>



## Figures Index

Fig. 1 – Graphic representation of a eukaryotic cell with a close up of its biological membrane.....	2
Fig. 2 – Crystal structure of CFTR taken from Protein Data Bank (ref code: 1XMI) with a close up to one of its domains (ref code: 2BBO) where the phenylalanine residue at position 508 is highlighted in pink. ....	7
Fig. 3 – Graphic representation of the mechanism of functioning of the chloride anion channel. ....	8
Fig. 4 – Chemical structure of (a) methyl iodide, representing a non-withdrawing environment for iodine, and (b) trifluoroiodomethane, representing a withdrawing environment for iodine. ....	10
Fig. 5 – (a) Chemical structure of the most efficient chloride transporter according to Stefan Matile and co-workers study <sup>18</sup> on ion transport mediated by halogen bond donors and (b) representation of an halogen bond between the two species. The halogen bond is represented with a dashed line.....	11
Fig. 6 – (a) Chemical structure of pentafluorobenzamide, one of the phenylbenzamide derivatives studied by Michael Giese and co-workers, <sup>19</sup> and (b) respective representation of the interaction between the transporters and the anion. The hydrogen bond is represented in lilac and the anion- $\pi$ interaction is represented in purple, both as dashed lines.....	12
Fig. 7 – (a) Base chemical structure of the 2,2'-bithiophenes studied by Stefan and co-workers <sup>20</sup> and (b) structure of the receptor with best binding energy for the chloride anion. The chalcogen bond is represented by the dashed lines. ....	12
Fig. 8 – (a) Chemical structure of one of the triazolophanes studied by Amar Flood and co-workers <sup>22</sup> and (b) the representation of the hydrogen bonds established by the CH groups and the chloride anion. The hydrogen bonds are represented as dashed lines. ....	13
Fig. 9 – (a) Chemical structure of one of the chiral BINOL-boron substituted $\pi$ -conjugated receptor studied by Hiromitsu Maeda and co-workers <sup>23</sup> and (b) respective representation of the interaction established with the carrier. The hydrogen bonds are represented with dashed lines. ....	14
Fig. 10 – (a) Chemical structure of the squaramide based receptors studied by Philip Gale and co-workers <sup>25</sup> and (b) representation of the hydrogen bonds established between the best transporter and a chloride anion. The hydrogen bonds are represented in dashed lines. ....	16
Fig. 11 – Representation of the tris(2-aminoethyl)amine derivatives studied. ....	17

Fig. 12 – Representation of the simpler organic molecules studied.....	18
Fig. 13 – Representation of the fluorinated tris(2-aminoethyl)amine derivatives.....	18
Fig. 14 – Representation of the bis-indolyureas studied with resource of MD simulations. .....	19
Fig. 15 – Representation of the chemical compounds used to study the electronic effect of different substituents.....	20
Fig. 16 – Approach of one of the tripodal-based molecules to the water-lipid interface in 5 consecutive snapshots Reproduced from tris-thiourea tripodal-based study performed by the Molecular Modelling Group at University of Aveiro. <sup>1</sup> .....	25
Fig. 17 – Representation of the generic chemical structure of cholapods (49) and diureidodecalins (50).....	28
Fig. 18 – Representation of the tris(thio)urea that served as study subject for the present thesis.....	29
Fig. 19 – Sketch representation of the membrane system for setup A used to carry out the MD simulations. ....	36
Fig. 20 – Framework used as query for the CSD Database search, where X = S, O.....	39
Fig. 21 – 3D representation of (a) molecule with the ref code RONJUB, where the purple dashed lines represent the hydrogen bonds between the ligand and the glyphosate molecule, and (b) the anion complex with the ref code RUSBIS, where both the pink and purple dashed lines represent the multiple hydrogen interactions established within the structure's central core.....	40
Fig. 22 – Chemical structures of the twelve transporters being studied in the present thesis, where the numbers 3, 4 and 6 represent the scaffold, the “S” identifies the presence of thiourea groups and the letters “D”, “F”, “N” and “P” symbolize the aromatic substituents. .....	41
Fig. 23 – Optimized structure of the twelve transporters with a theory level of M062X/6- 31+G**, in gas phase.....	42
Fig. 24 – Electrostatic potential mapped on the molecular electron density surface (0.001 electron per Bohr <sup>3</sup> ) of 3SD, 3SP, 4SD, 4SP, 6SD and 6SP. The three highest values for each transporter are represented as black dots on the molecular surfaces. The colour scales range from blue to red from -16 kcal mol <sup>-1</sup> to 77 kcal mol <sup>-1</sup> , <sup>1</sup> in all representations.	45
Fig. 25 – Plot of the $V_{S,max}$ values against log( $K_a$ ) for the three series of transporters in gas phase (unfilled dots) and in DMSO (solid dots). For the 3S series $R^2=0.013$ and $R^2=0.351$ , for gas phase and DMSO, respectively. For the 4S series $R^2=0.657$ and $R^2=0.662$ , for gas	

phase and DMSO, respectively. For the 6S series $R^2=0.936$ and $R^2=0.906$ , for gas phase and DMSO, respectively. ....	46
Fig. 26 – Plot of the $E^2$ values against $\log(K_a)$ (provided in Anthony Davis' paper regarding these transporters) <sup>54-55</sup> and for $V_{S,max}$ against $\log(E^2)$ for the 4S series in gas phase (unfilled dots) and in DMSO (solid dots). The correlation coefficients for the $E^2$ vs $\log(K_a)$ plot in gas phase and in DMSO are $R^2 = 0.600$ and $R^2 = 0.996$ , respectively. As for the $V_{S,max}$ vs $\log(E^2)$ plot they are $R^2 = 0.735$ and $R^2 = 0.733$ in the gas phase and DMSO, respectively. ....	46
Fig. 27 – Plot of the $E^2$ values against the WBI for the three series of transporters in gas phase (unfilled dots) and in DMSO (solid dots). The correlation coefficients for the 3S series are $R^2 = 0.978$ and $R^2 = 0.999$ in gas phase and DMSO, respectively; for the 4S series are $R^2 = 0.999$ and $R^2 = 0.0998$ in gas phase and DMSO, respectively; as for the 6S series are $R^2 = 0.923$ and $R^2 = 0.997$ in gas phase and DMSO, respectively. ....	48
Fig. 28 – Schematic representation of both MD setups used. The tripodal structures are represented as a black stool-like shape. ....	49
Fig. 29 – Chemical structure of the three transporters put through MD simulations (3SD, 4SD and 6SD, from left to right) where the atoms that define $Core_{COM}$ are highlighted in red and the atoms that define $CF_{3COM}$ are highlighted in blue. ....	51
Fig. 30 – Evolution of the $P_{int} \cdots Core_{COM}$ (in red) and the $P_{int} \cdots CF_{3COM}$ (in blue) distances for the 3SD transporter. The water/lipid interface is at a relative position of 0 Å. The counting of hydrogen bonds to chloride anions and phospholipid head groups is represented in green and orange, respectively. The data for $P_{int} \cdots Core_{COM}$ and $P_{int} \cdots CF_{3COM}$ was smoothed with Bézier curves. ....	52
Fig. 31 – Evolution of the $P_{int} \cdots Core_{COM}$ (in red) and the $P_{int} \cdots CF_{3COM}$ (in blue) distances for the 4SD transporter. The water/lipid interface is represented at a relative position of 0 Å. Remaining details as given in Fig.30. ....	52
Fig. 32 – Evolution of the $P_{int} \cdots Core_{COM}$ (in red) and the $P_{int} \cdots CF_{3COM}$ (in blue) distances for the 6SD transporter. The water/lipid interface is represented line at a relative position of 0 Å. Remaining details as given in Fig.30. ....	52
Fig. 33 – Snapshots of the interactions between the transporters (a) 3SD, (b) 4SD and (c) 6SD with the phosphate head groups of the bilayer membrane and water molecules at a distance of 3 Å. The carbon atoms of the transporters are represented in salmon, purple and dark blue for (a), (b) and (c), respectively, while the hydrogen atoms are represented in white, the nitrogen atoms in blue and the sulfur atoms in yellow. The chloride and phosphorus atoms are represented as green and orange spheres, respectively, as for the	

carbon atoms of the POPC lipids are represented as grey lines. The snapshot in (a) was taken from A <sub>1</sub> 3SD, from A <sub>2</sub> 4SD for (b) and A <sub>1</sub> 6SD for (c).....	54
Fig. 34 – Evolution of the number of water molecules at a distance of 3.4 Å of the three binding sites of 3SD (in three different shades of blue) and evolution of the number of hydrogen bonds with the phosphate head groups (in orange). The hydration data was smoothed with Bézier curves. ....	55
Fig. 35 – Evolution of the number of water molecules at a distance of 3.4 Å for the three binding sites of 4SD (in three different shades of blue) and evolution of the number of hydrogen bonds with the phosphate head groups (in orange). The hydration data was smoothed with Bézier curves. ....	55
Fig. 36 – Evolution of the number of water molecules at a distance of 3.4 Å for the three binding sites of 6SD (in three different shades of blue) and evolution of the number of hydrogen bonds with the phosphate head groups (in orange). The hydration data was smoothed with Bézier curves. ....	56
Fig. 37 – Five frames of A <sub>1</sub> 3SD demonstrating 3SD entering the membrane bilayer. 3SD is represented in a space filling model with carbon atoms in salmon, hydrogen atoms in white, nitrogen atoms in blue and sulfur atoms in yellow. The chloride and phosphorus atoms are represented as green and orange spheres, respectively, and the POPC lipids are drawn in grey lines (the hydrogen atoms in the C-H bonds of POPC lipids and the sodium atoms were omitted for clarity).....	56
Fig. 38 – Five frames of A <sub>2</sub> 4SD demonstrating the transporter entering the membrane bilayer. 4SD is represented in a space filling model with carbon atoms in purple. Remaining details as given in Fig. 37.....	57
Fig. 39 – Five frames of A <sub>1</sub> 6SD demonstrating the transporter entering the membrane bilayer. 6SD is represented in a space filling model with carbon atoms in blue. Remaining details as given in Fig. 37.....	57
Fig. 40 – Evolution of the P <sub>int</sub> ⋯ Core <sub>COM</sub> (in red) and the P <sub>int</sub> ⋯ CF <sub>3COM</sub> (in blue) distances for the 3SD transporter. The water/lipid interface is represented at a relative position of 0 Å. Remaining details as given in Fig.30.....	58
Fig. 41 – Evolution of the P <sub>int</sub> ⋯ Core <sub>COM</sub> (in red) and the P <sub>int</sub> ⋯ CF <sub>3COM</sub> (in blue) distances for the 4SD transporter. The water/lipid interface is represented at a relative position of 0 Å. Remaining details as given in Fig.30.....	58
Fig. 42 – Evolution of the P <sub>int</sub> ⋯ Core <sub>COM</sub> (in red) and the P <sub>int</sub> ⋯ CF <sub>3COM</sub> (in blue) distances for the 6SD transporter. The water/lipid interface is represented at a relative position of 0 Å. Remaining details as given in Fig.30.....	59

Fig. 43 – Evolution of the number of water molecules at a distance of 3.4 Å of the three binding sites of 3SD (in three different shades of blue) and evolution of the number of hydrogen bonds with the phosphate head groups (in orange). The hydration data was smoothed with Bézier curves.....	59
Fig. 44 – Evolution of the number of water molecules at a distance of 3.4 Å of the three binding sites of 4SD (in three different shades of blue) and evolution of the number of hydrogen bonds with the phosphate head groups (in orange). The hydration data was smoothed with Bézier curves.....	59
Fig. 45 – Evolution of the number of water molecules at a distance of 3.4 Å of the three binding sites of 6SD (in three different shades of blue) and evolution of the number of hydrogen bonds with the phosphate head groups (in orange). The hydration data was smoothed with Bézier curves.....	60
Fig. 46 – Snapshots of the interactions between the transporters (a) 3SD, (b) 4SD and (c) 6SD with the phosphate head groups of the bilayer membrane and water molecules at a distance of 3 Å. The snapshot in (a) was taken from B <sub>1</sub> 3SD, from B <sub>1</sub> 4SD for (b) and B <sub>1</sub> 6SD for (c). Remaining detail as given in Fig.33.....	60
Fig. 47 – Evolution of the $P_{int} \cdots Core_{COM}$ for the 3SD transporter in setup A (red continuous line) and in setup B (dark red dashed line). The water/lipid interface is represented at a relative position of 0 Å. Data was smoothed with Bézier curves. ....	61
Fig. 48 – Evolution of the $P_{int} \cdots Core_{COM}$ for the 4SD transporter in setup A (red continuous line) and in setup B (dark red dashed line). The water/lipid interface is represented at a relative position of 0 Å. Data was smoothed with Bézier curves. ....	61
Fig. 49 – Evolution of the $P_{int} \cdots Core_{COM}$ for the 6SD transporter in setup A (red continuous line) and in setup B (dark red dashed line). The water/lipid interface is represented at a relative position of 0 Å. Data was smoothed with Bézier curves. ....	62
Fig. 50 – Histogram obtained for the 4SD complex showing the correct overlapping of neighboring windows.....	63
Fig. 51 – Free energy profiles for the 4SD chloride complex (in red) and the free chloride anion (in green). ....	64
Fig. 52 – Sketch of the spatial dispositions adopted by the chloride complex that would (a) reflect the free energy profile plotted in Fig. 51 and (b) a symmetric free energy profile. .	64

## Tables Index

Table 1 – Binding and transport data regarding the tris(thio)urea studied by Anthony P. Davis and co-workers. ....	30
Table 2 – Summary of the DFT optimization results for all transporters in gas phase and in DMSO (values in italic). ....	43
Table 3 – Summary of quantum descriptors for all transporters in gas phase and in DMSO (values in italic). The values for $K_a$ and $t_{1/2}^f$ were taken from previous studies. <sup>54-55</sup> .....	47
Table 4 – Summary of the results obtained for area per lipid and membrane thickness, for the three transporters in study, in both setups, in comparison with the values for the POPC model.....	50
Table 5 – Average $P_{int}$ ... $Core_{COM}$ distances for the last 50 ns of MD simulations for the three transporters in both setups.....	62
Table 6 – Atom type and correspondent charge for all atoms of 51SD obtained after the multi RESP analysis.....	74
Table 7 – Atom type and correspondent charge for all atoms of 52SD obtained after the multi RESP analysis.....	75
Table 8 – Atom type and correspondent charge for all atoms of 53SD obtained after the multi RESP analysis.....	76
Table 9 – Results for the dimensions of the interactions established in the crystal structure of RUSBIS: .....	77
Table 10 – Results obtained for area per lipid and membrane thickness for the last 100 ns of MD simulation of the three transporters being studied, in both setups, in comparison with the values for the POPC model.....	78

## Schemes Index

Scheme 1 – Summary of the different existing types of transport with examples and characteristics of each case (adapted from “Lehninger Principles of Biochemistry” chapter 11 – Biological Membranes and Transport). .....	5
Scheme 2 – Summary of possible therapies for genetic and inherited diseases. ....	8
Scheme 3 – Chemical structure and identification of pyrrole and indole groups. ....	14
Scheme 4 – Chemical structure and identification of the mostly used functional groups in synthetic transporters. ....	15
Scheme 5 – Representation of the chemical structure of the most common lipids used in the simulation of lipid bilayer membranes. ....	25
Scheme 6 – Summary of all the steps involved in obtaining the energy profiles for the transporters being studied. ....	37
Scheme 7 – Schematic representation of the main spatial dispositions adopted by the transporters throughout the MD simulations. The tripodal structures are represented as a black stool-like shape. ....	53

## Abbreviations

$^{13}\text{C}$ NMR	Carbon-13 Nuclear Magnetic Resonance
$^1\text{H}$ NMR	Proton Nuclear Magnetic Resonance
$^2\text{H}$ NMR	Deuterium Nuclear Magnetic Resonance
ADP	Adenosine Diphosphate
ATP	Adenosine Triphosphate
CF	Cystic Fibrosis
<i>CFTR</i>	Cystic Fibrosis Transmembrane Conductance Regulator
CGenFF	CHARMM General Force Field
CHARMM	Chemistry at Harvard Molecular Mechanics
COM	Centre of Mass
DLPC	1,2-Dilauroyl- <i>sn</i> -Glycero-3-Phosphocholine
DMPC	1,2-Dimyristoyl- <i>sn</i> -Glycero-3-Phosphocholine
DMSO	Dimethylsulfoxide
DOPC	1,2-Dioleoyl- <i>sn</i> -Glycero-3-Phosphocholine
DOPE	1,2-Dioleoyl- <i>sn</i> -Glycero-3-Phosphoethanolamine
DPPE	1,2-Dipalmitoyl- <i>sn</i> -Glycero-3-Phosphocholine
$E^2$	Second Order Perturbation Energy
$EC_{50}$	Half Maximum Effective Concentration
EDP	Electron Density Profile
ESP	Electrostatic Potential
GAFF	General AMBER Force Field
GPUs	Graphics Processing Units
HF	Hartree-Fock Functional
$K_a$	Binding Affinity Constants
M06-2X	Minnesota '06 Family Functional
MD	Molecular Dynamic
MEP	Molecular Electrostatic Potential
MM	Molecular Mechanics
NBDs	Nucleotide-Binding Domains
NBO	Natural Bond Orbital
NMR	Nuclear Magnetic Resonance
NPT	Isothermal-Isobaric Ensemble
NVT	Canonical Ensemble
OPLS	Optimized Potentials for Liquid Simulations



PC	Phosphatidylcholines
PE	Phosphatidylethanolamines
P <sub>i</sub>	Inorganic Phosphate
<i>PKD1</i>	Polycystin 1
PMC	Polarizable Continuum Model
PME	Particle Mesh Ewald
PMF	Potential Mean Force
POPC	1-Palmitoyl-2-Oleoyl- <i>sn</i> -Glycero-3-Phosphocholine
POPE	1-Palmitoyl-2-Oleoyl- <i>sn</i> -Glycero-3-Phosphoethanolamine
PSA	Polar Surface Area
QM	Quantum Mechanics
RESP	Restrained Electrostatic Potential
S <sub>CD</sub>	Deuterium-Order Parameter
<i>SCN1A</i>	Sodium Voltage-Gated Channel $\alpha$ Subunit 1
SGLT1	Sodium-Glucose Linked Transporter
SMD	Steered Molecular Dynamics
<i>sn</i> -1	Stereospecific number 1
<i>sn</i> -2	Stereospecific number 2
TIP3P	Transferable Intermolecular Potential 3 Point
TSA	Total Surface Area
UFF	Universal Force Field
US	Umbrella Sampling
V <sub>s</sub>	Electrostatic Potential
V <sub>s,max</sub>	Maximum value for Electrostatic Potential
V <sub>s,min</sub>	Minimum value for Electrostatic Potential
WBI	Wiberg Bond Indexes

## 1. Introduction

The world, as the dynamic system it is, is in perpetual evolution. This progress brings many simplifications and benefits for our society and human life in general, however this development is far from over and carries a number of responsibilities.

A great example of this ongoing advance is the use of science and technology in a continuously more efficient and sustainable manner to overcome future problems and challenges.

Based on this broad view, from the association between computer technology and science, namely chemistry, emerges the main idea for the present thesis. All of the work here presented was developed within the research interests of the Molecular Modelling Group of University of Aveiro. This research group carries extensive molecular dynamics studies as well as quantum mechanics calculations to investigate, among other subjects, the transport of anions across lipid bilayers<sup>1</sup> or the behaviour of interlocked structures (*e.g.* rotaxanes),<sup>2</sup> being these studies directly related to health matters, such as the treatment of well know channelopathies (*e.g.* cystic fibrosis – CF) or the development of molecular machines that change shape depending on the chemical environment of the system they belong. To do so, the group is equipped with powerful computational resources as well as a great know-how in these matters, being one of the few research groups that studies the transport of anions and having heavily contributed with molecular dynamic studies for this topic. This level of commitment and cutting edge work lead to the establishment of important collaborations, both nationally and internationally, showing the great importance of this type of studies.

Hence, this chapter will serve as an overall look on the most important aspects regarding the theme of this thesis, transmembrane transport of anions by synthetic transporters. This means that topics such as cell membranes, methods of transport, the importance of ions on biologic systems, CF, insights on the developments made in this area as well as computational tools used in these studies will all be mentioned as a way to provide a deeper and wider understanding of transmembrane transport. Further ahead, all the results obtained will be shown and discussed to reach significant conclusions concerning the present topic.

### 1.1. Membranes

Eukaryotic cells are composed of many organelles and are limited by a phospholipid bilayer, commonly designated as cell membrane (portrayed in Fig. 1). Membranes define the limit of cells and regulate the exchange of molecular compounds between the outside

environment and the cytosol, and vice-versa.<sup>3</sup> These cellular boundaries have extremely important characteristics like flexibility, self-sealing ability and absent permeability towards most polar or charged solutes, exhibiting permeability to nonpolar compounds.<sup>3</sup>

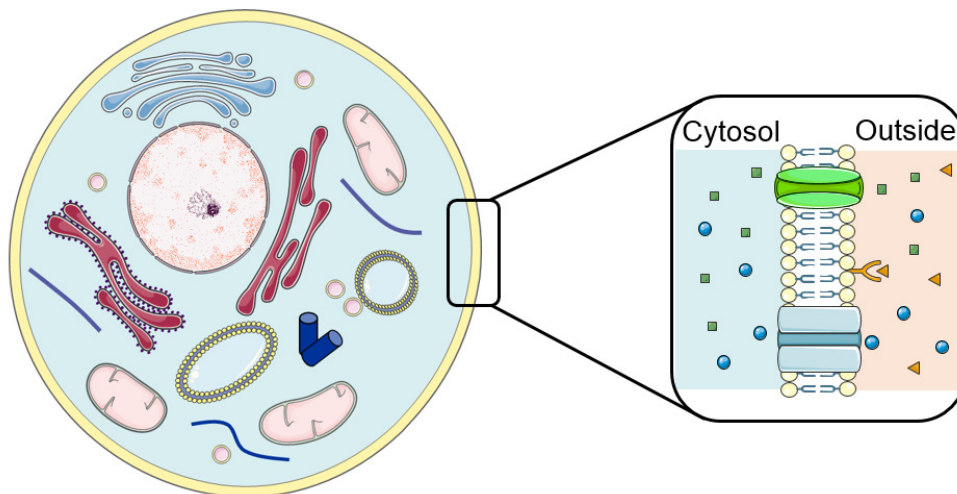


Fig. 1 – Graphic representation of a eukaryotic cell with a close up of its biological membrane.

This selectivity process happens due to the fact that the two phospholipid layers are arranged so that the hydrophobic tails point towards each other, to form a hydrophobic centre, while the ionic head-groups are placed at the inner and outer surfaces of the cell membrane.<sup>4</sup> The resulting structure is stable since the hydrophilic head-groups interact with the polar aqueous media present on both the inside and the outside of the cell, whereas the hydrophobic tails maximize hydrophobic interactions with each other and are kept away from these polar environments.<sup>4</sup> Nonetheless, membranes are not merely passive barriers, meaning that lipid bilayers are composed of biological molecules, such as lipids and proteins, in varying combinations, depending on their location and function, which allows the cell to have a regulated flow of substrates, according to its needs.<sup>3</sup> At the cell surface, there can be transporters that move specific organic solutes and inorganic ions across the membrane, or receptors whose function is to sense extracellular signals and trigger molecular changes in the cell. There can even be adhesion molecules that hold neighbouring cells together.<sup>3</sup> Within the cell, membranes can also organize cellular processes such as the synthesis of lipids and certain proteins, as well as the energy transductions in mitochondria (and chloroplasts for plants and algae).<sup>3</sup>

### 1.1.1. Methods of transport across the biological membranes

To maintain the correct equilibrium in all living cells, and hence their normal functioning, every cell must acquire from its surroundings all the substrates needed for biosynthesis and for energy production, while simultaneously releasing, to its environment, the by-products of its metabolism.<sup>3</sup> To do so, the membranes exhibit different alternatives of transmembrane movement, depending on the type of compound that needs to get across and if it is necessary to provide energy during that process. With this in mind, the transport of substrates across biological membranes can be divided in two families: passive transport and active transport. The difference between the two is that the former does not need any form of energy to occur while the latter does.

#### 1.1.1.1. Passive transport

In passive transport, the transported species always move down their concentration gradient, which is from the location where they have a higher concentration to the location where they are less concentrated.<sup>3</sup> This happens in simple diffusion and in facilitated diffusion which are further explored below:

- In simple diffusion a certain solute will move from one side of the membrane to the other, right through the membrane itself, until the state of equilibrium is achieved. A good example of this type of passive transport is the process of osmosis.
- In facilitated diffusion the solute goes through the membrane with the help of proteins. The purpose of these membrane proteins is to lower the activation energy for the transport of slightly more polar compounds so they can follow their concentration gradient.<sup>3</sup> This type of transport is quite common in biological processes, for instance, the transport of  $\beta$ -galactosides, such as lactose, is aided by specific membrane proteins designated as permeases.<sup>3</sup>

#### 1.1.1.2. Active transport

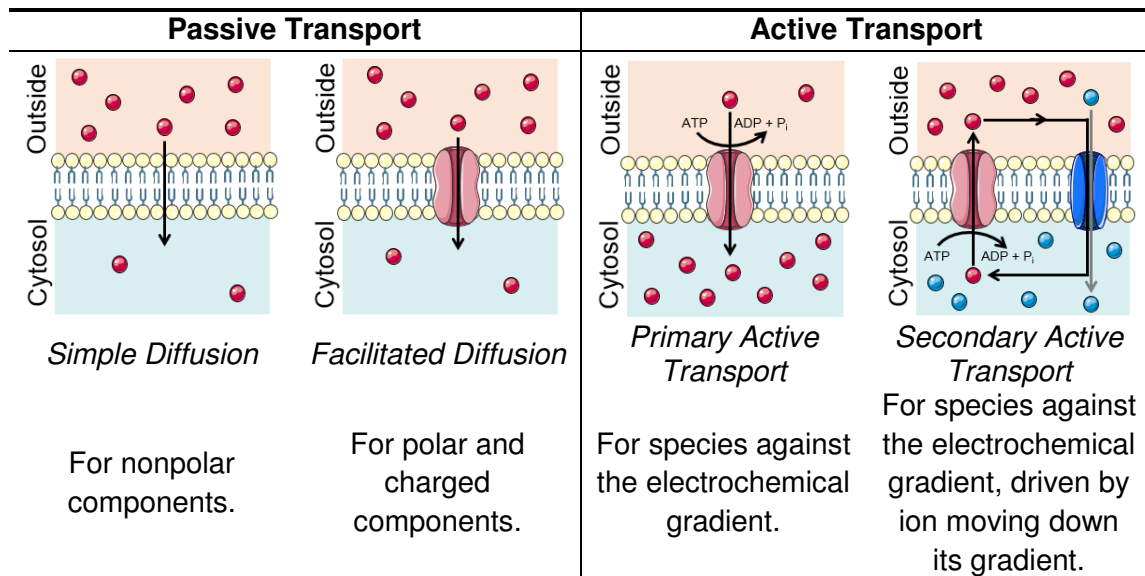
This type of transport requires energy to occur, consequently this method of transport has to be coupled with processes that release energy. Some examples of such processes include the absorption of sunlight, oxidation reactions or the breakdown of ATP (Adenosine Triphosphate).<sup>3</sup> As part of being a thermodynamically unfavourable process the solute is usually accumulated in one of the sides of the membrane at concentrations above the equilibrium point.<sup>3</sup>

Just like in passive transport, there are also two types of transport: primary active transport and secondary active transport. These are described in more depth below:

- In the primary active transport the passage of a certain solute is a process directly coupled to chemical reactions that require energy, just as the breakdown of ATP.<sup>3</sup> As an example, one can consider calcium pumps, which are responsible for the exclusion of calcium cations from eukaryotic cells, allowing the regulation of this cation in both the intracellular and the extracellular medium.<sup>5</sup>
- In the secondary active transport the passage of a solute is a process that also requires energy, however this energy is provided by the primary active transport of a different solute, usually an ion, which in turn originates an ion gradient at the expense of ATP.<sup>3</sup> This type of transport may also be referred as co-transport since it involves two different species moving simultaneously across the lipid bilayer. Here one can state the example of sodium-potassium pumps that allow the symport of both cations across biological membranes.<sup>6</sup>

When considering the transport of more than one species across the cell membrane one is able to classify that process as antiport or symport, depending on the direction of the species implicated on the process. Thus, one may classify the transport as antiport when the species move across the membrane in opposite directions.<sup>3</sup> The sodium-calcium exchanger is a well-studied antiporter membrane protein and belongs to a class of ion transporters composed of eleven transmembrane segments widely spread in the heart, kidney, brain and other tissues. This protein maintains the regular levels of  $\text{Ca}^{2+}$  in the cell by promoting the entry of  $\text{Na}^+$  in the cell as well as the exit of  $\text{Ca}^{2+}$  so that the intracellular concentration of free  $\text{Ca}^{2+}$  can be maintained.<sup>7</sup> As for symport transport, which occurs when both species move in the same direction, one may take the example of the *SGLT1* (Sodium-Glucose Linked Transporter).<sup>8</sup> This membrane protein belongs to the sodium/glucose co-transporter family and helps with the absorption of D-glucose and D-galactose. This process is made in a symport fashion since it is the  $\text{Na}^+$  electrochemical gradient, in the same direction as the glucose transport, which triggers the whole transport process to occur.<sup>8</sup>

The four different types of transport are summarised in Scheme 1 below for a better understanding of their function and occurrence in biological membranes.



Scheme 1 – Summary of the different existing types of transport with examples and characteristics of each case (adapted from “Lehninger Principles of Biochemistry” chapter 11 – Biological Membranes and Transport).

### 1.1.2. Transporters: carriers and channels

One can divide transporters into two categories that are essentially different in the way they lead a certain substrate through the cell membrane. Thus, one may have:

- Carriers, a species that is capable of binding to a certain substrate with high selectivity being able to catalyse its transport rates to lower them below the limits of free diffusion.<sup>3</sup> Carriers are saturable, meaning that above a certain concentration the rate of transport will stabilize, just like enzymes.<sup>3</sup>
- Channels, a hollow structure that can be gated- or voltage-triggered.<sup>3</sup> Besides being less selective than carriers, channels allow transmembrane movement at rates of greater magnitudes when comparing the two transporters, as a consequence, they are usually not saturable.<sup>3</sup>

These two types of transporters have been extensively studied throughout the years and, besides the differences in their intrinsic characteristics, these structures also differ in the method of transport used. For instance, carriers establish selective interactions, with one or multiple binding sites, to a certain substrate, usually polar or charged. This assembly diffuses across the lipid bilayer and the species is released on the other side of the membrane. On the other hand, channels provide a hydrophilic path through the biological membrane which selectively allows polar and charged compounds, such as ions, to move down their electrical or chemical concentration gradients.<sup>3</sup>

## 1.2. The Biological Importance of Ions

After a closer look at the characteristics and method of transport of both carriers and channels, it is also important to take into account the type of substrates that they help across the phospholipid bilayer, namely ions. Cells contain ions, such as sodium, potassium, calcium or chloride, whose concentrations differ from the inside to the outside of the cell, originating a concentration gradient across the cell membrane.<sup>4</sup> The presence of these ions ensures a number of essential functions in the cell, such as the transmission of nerve signals (which involves the sodium and potassium channels),<sup>4</sup> or the transport of CO<sub>2</sub> to the lungs (that is aided by the chloride-bicarbonate exchanger).<sup>3</sup>

Likewise, one must note that due to their representation in living beings, as well as the functions that they take part in, anion channels are scarcer when compared to cation channels.<sup>1</sup> Consequently, their malfunctioning may lead to serious health issues, commonly designated as channelopathies, which will be discussed ahead, and may influence the regulation of several essential ions to the cell since, as stated before, some processes depend on more than one ion.<sup>1</sup> Therefore, one can conclude that the presence of both ions and working receptors/transporters is crucial.

Mutations may occur for several reasons, even the smallest change, just as a change in one amino acid on the primary structure of a protein, can induce a mutation with serious consequences. For instance, the change of one amino acid in the amino acid sequence may influence greatly the ion selectivity of a certain channel.<sup>4</sup> Serving as example, it is known that a mutation on the *SCN1A* (sodium voltage-gated channel  $\alpha$  subunit 1) gene encodes a defective neuronal sodium voltage-gated channel originates generalized epilepsy with febrile seizures, which can only be managed by lifelong medication of anticonvulsants.<sup>3</sup> Other examples include a mutation on the *PKD1* (polycystin 1) gene that leads to a deficient calcium channel which gives raise to polycystic kidney disease, whose treatment relies on permanent medication, or a defective *CFTR* (cystic fibrosis transmembrane conductance regulator) gene results on a defective chloride channel that in turn instigates CF, a disease intrinsically associated with deficient chloride transport, without a known cure and with a life expectancy of around 30 years.<sup>3</sup>

This work will focus mainly on the transport of chloride anions through cell membranes, which is intrinsically connected to CF. The present thesis hopes to help in the discovery of a way of overcoming poorly working chloride channels. As an alternative to these channels, we propose the development of small organic molecules that are capable of assuring

transmembrane chloride transport, which consequently, allows them to replace deficient *CFTR* channels. Therefore, it is important not just to have a better understanding of what is CF but also how and with what means we can study if a particular set of organic molecules can work, or not, as effective anion carriers in a biological system.

CF is mainly caused by the deletion of the phenylalanine residue at position 508 in *CFTR*, see Fig. 2.<sup>3</sup> As a consequence of this mutation the protein folds incorrectly.<sup>3</sup> This regulator functions as a chloride channel in the plasma membrane of epithelial cells, regulating the concentration of the anion in the environment outside the cell, especially in the lungs.<sup>9</sup> As CF is an autosomal recessive disease, one must carry both copies of the mutated gene to develop the disease.<sup>9</sup>

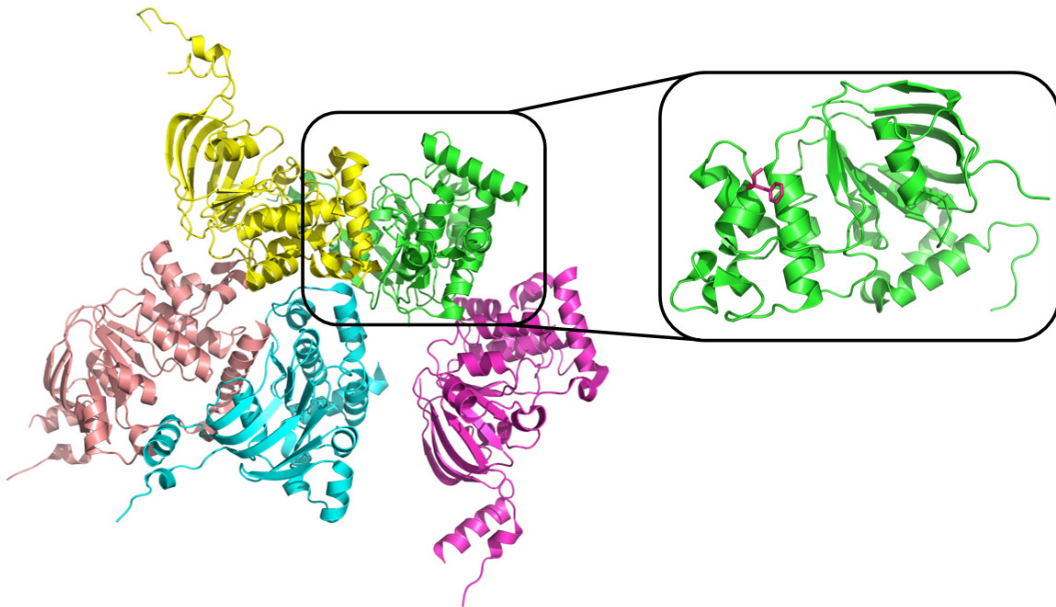


Fig. 2 – Crystal structure of CFTR taken from Protein Data Bank (ref code: 1XMI) with a close up to one of its domains (ref code: 2BBO) where the phenylalanine residue at position 508 is highlighted in pink.

A functional working channel conducts the chloride anion across the plasma membrane when both NBDs (Nucleotide-Binding Domains) are bonded to ATP. The channel then closes when the ATP on one of the NBDs is broken down to ADP (Adenosine Diphosphate) and  $P_i$  (inorganic phosphate), as shown in Fig. 3.<sup>9</sup> In contrast, when the protein is mutated and folds incorrectly it causes interferences in its insertion in the plasma membrane, as a result, the movement of chloride anions across the cell membrane is reduced.<sup>3,9</sup>



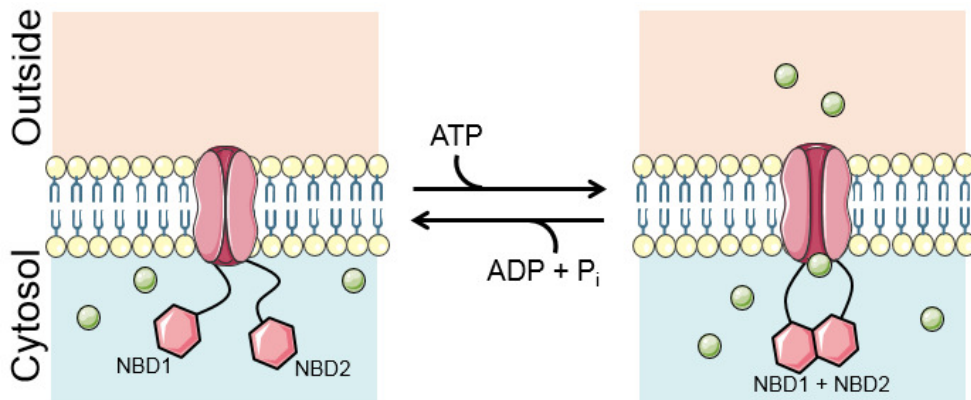
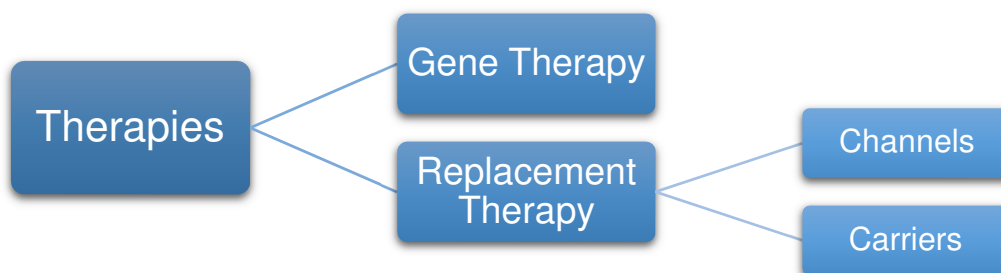


Fig. 3 – Graphic representation of the mechanism of functioning of the chloride anion channel.

In most cases this disease leads to death by respiratory failure, as there is currently no cure for this disease. However, the scientific community is thinking and testing solutions that might lead to a better management for this disease. One of the solutions includes the development of ionophores that function as synthetic transporters, which selectively promote chloride transport across cell membranes.<sup>3</sup> To date, a considerable amount of work has been developed regarding this matter, some of which will be discussed ahead. Therefore, with the successful development of such molecules one could establish the proper circulation of chloride anions on individuals with CF. Therefore, the use of ionophores is of great importance since these can be used in replacement therapies for the treatment of channelopathies.

### 1.2.2. Possible Therapies for Genetic Diseases

Described above are solely a few examples of the serious consequences associated to defective ion-channels. The seriousness of such genetic or inherited health complications urges solutions and, over the years, researchers have studied and developed new therapies to create a definitive treatment to such diseases. These therapies can be divided into two categories as illustrated in Scheme 2.



Scheme 2 – Summary of possible therapies for genetic and inherited diseases.

For instance, gene therapy can be used to either replace or inactive defective genes, or to introduce new genes that may help the treatment or prevention of a genetic disease.<sup>3</sup> Besides being presented as a promising solution, this type of therapy is still being studied and tested so that, in the future, it can be used as an effective and practical form of intervention.<sup>3</sup>

As for channel replacement therapies, they are used, as the name suggests, to replace defective ion channels. There are two ways of replacing it, either by introducing another channel that is capable of establishing the normal movement of ions across the cell membrane, or by using carriers that are also capable of performing that transport process.<sup>3</sup> In the present thesis the focus will be on the channel replacement therapies using carriers. Here one can take the example of a chloride ion-channel not functioning properly. In this particular case, a possible form of disease management suggests that the task supposed to be carried out by the chloride ion-channel will be performed by a carrier, also designated as a synthetic transporter. This carrier is a small organic molecule that is selective towards the chloride anion, hence it will be able to capture ions, either intracellularly or extracellularly. Once the carrier and anion establish an interaction, the complex is then capable of diffusing through the lipid bilayer, releasing the anion on the opposite side. As a consequence, the concentration of anions in the cell can be regulated, ending the accumulation of anion in one of the sides of the phospholipid bilayer. By maintaining the patients' levels of chloride balanced this form of management also allows better life conditions and a greater life expectancy.

### *1.3. Design of Synthetic Anion Transporters*

The process of ion transport is a subject addressed by supramolecular chemistry. Two well-known concepts of this field of study are complementarity and preorganization, therefore these concepts are also associated with ion transport. For this process to occur both the transporter and the ion need to show complementarity among each other, not only in terms of conformation, but also in terms of electronic interactions. In addition, both carrier and ion should present higher level of organization, which is associated with lesser energy spent.<sup>10</sup> By combining greater complementarity and preorganization one is promoting a stronger binding and a better selectivity and efficiency in terms of ion transport.<sup>10</sup>

As stated above, the transport of anions is of the utmost importance in biological systems. Moreover, scientists are also finding other areas of application for this type of transport such as a possible usage as anticancer agents, due to the strong correlation observed between transport rates of transmembrane transport and anticancer activity *in vitro*.<sup>11-12</sup>

Nonetheless, it is also important to note that it is not exactly clear to the research groups that carry these studies how to design a selective and efficient anion transporter, however important steps are being taken towards that goal.<sup>13</sup>

In the past years, the topic “Synthetic Transporters” has been approached in distinct manners from metal-organic architectures to  $\pi$ - $\pi$  architectures and anion- $\pi$  interactions.<sup>14</sup> Pairing with these architectures came a variety of structures such as small anion transporters, macrocycles and polyion-counterion systems that add to the (now considered) classic structures (*i.e.*, steroids, cyclodextrins or synthetic polymers).<sup>14</sup>

With this in mind, one can say that synthetic transporters need to fulfil a very important requirement: they have to function in the biological membrane.<sup>15</sup>

To think of molecules capable of carrying ions across biological membranes, one has to consider some key factors, such as the presence of functional groups capable of interacting selectively with ions, or the type of interactions that are established between the carrier and the anion.<sup>16</sup>

### 1.3.1. Halogen Bonds on Anion Transport

Halogen bonds consist of non-covalent interaction between a halogen (in an electron-withdrawing environment) and a negative site, for instance a Lewis base.<sup>17</sup> This type of interaction can be seen in receptors and is able to compete and interfere with hydrogen bonding, however it is only observable with species containing bromide or iodine and sometimes chloride.<sup>17</sup> The interaction is established due to the fact that, in a withdrawing environment (such as the one depicted in Fig. 4 (b)), the electronegative properties of the atom halogen iodine are overpowered giving rise to a positive region, commonly designated as “ $\sigma$ -hole”.<sup>17</sup> This “hole” can then interact with negative site of other compounds establishing, as a result, a halogen bond.<sup>17</sup>

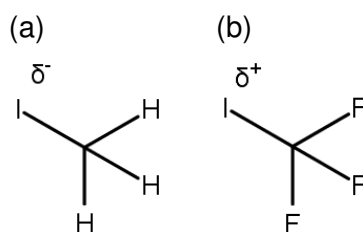


Fig. 4 – Chemical structure of (a) methyl iodide, representing a non-withdrawing environment for iodine, and (b) trifluoriodomethane, representing a withdrawing environment for iodine.

As an example, one may consider the study carried out by Stefan Matile and co-workers regarding the transport of chloride anion across the lipid, where they analysed a number of

small perfluorinated molecules that had on their constitution strong halogen bond donors.<sup>18</sup> These researchers concluded that the best transporter (Fig. 5(a)) was able to encapsulate a chloride anion with up to 6 molecules.<sup>18</sup> In Fig. 5(b) is depicted a representation of the interaction establish between the transporter and the chloride anion.

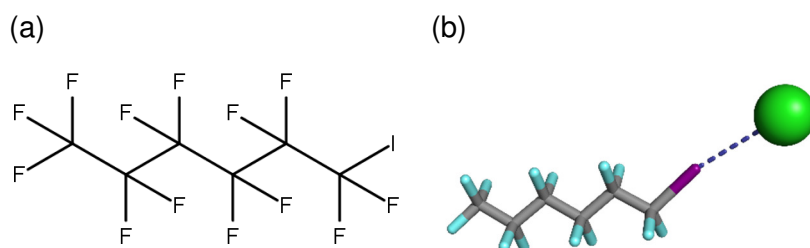


Fig. 5 – (a) Chemical structure of the most efficient chloride transporter according to Stefan Matile and co-workers study<sup>18</sup> on ion transport mediated by halogen bond donors and (b) representation of an halogen bond between the two species. The halogen bond is represented with a dashed line.

### 1.3.2. Anion- $\pi$ Interactions on Anion Transport

This type of interaction, as the name implies, is also non-covalent and occurs between an anion and an electron deficient  $\pi$ -system.<sup>16</sup> Besides the fact that it is much less known than the cation- $\pi$  interaction, this type of interaction has been receiving a greater degree of attention due to its reported anion binding properties.<sup>16</sup> One can look at the example of pentafluorobenzamide represented in Fig. 6 and studied by Michael Giese and co-workers.<sup>19</sup> Here one can clearly see an interaction between a bromide anion and the  $\pi$ -system of the  $C_6F_5$  group. In this particular case, the bromide anion is not centred relatively to the centre of the ring due to the presence of the NH group that also establishes an interaction with the anion.<sup>19</sup> These researchers compared the mentioned compound with other derivatives and concluded the strength of the anion binding increased in the order  $I^- < Br^- < Cl^-$ .<sup>19</sup> They also noticed that the binding strength was directly related to the electron-withdrawing effect of the arene group, meaning that, when the benzene moiety had more electronegative substituents, the interaction between the receptor and the ion was greater.<sup>15</sup>

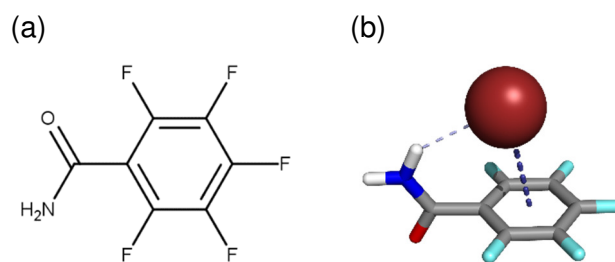


Fig. 6 – (a) Chemical structure of pentafluorobenzamide, one of the phenylbenzamide derivatives studied by Michael Giese and co-workers,<sup>19</sup> and (b) respective representation of the interaction between the transporters and the anion. The hydrogen bond is represented in lilac and the anion- $\pi$  interaction is represented in purple, both as dashed lines.

### 1.3.3. Chalcogen Bonds on Anion Transport

Chalcogen bonds resemble halogen bonds, however, in the former interaction, the positive electrostatic potential arises due to the presence of a low energy C-X  $\sigma^*$  orbital, where X can be sulfur, selenium or tellurium. This “ $\sigma$ -hole-like positive” region is then available to establish an interaction with a negative site, such as an anion.<sup>20-21</sup>

Work developed by Stefan Matile and co-workers can serve as an example for this type of interactions and their application in the anion transport subject.<sup>20</sup> In this research, the transport activity of chloride anions by derivatives of 2,2'-bithiophenes (generically represented in Fig. 7(a)) was studied. The researchers concluded that the best binding energies emerged from the receptors with deepest  $\sigma$ -holes, such as the receptor represented in Fig. 7(b).

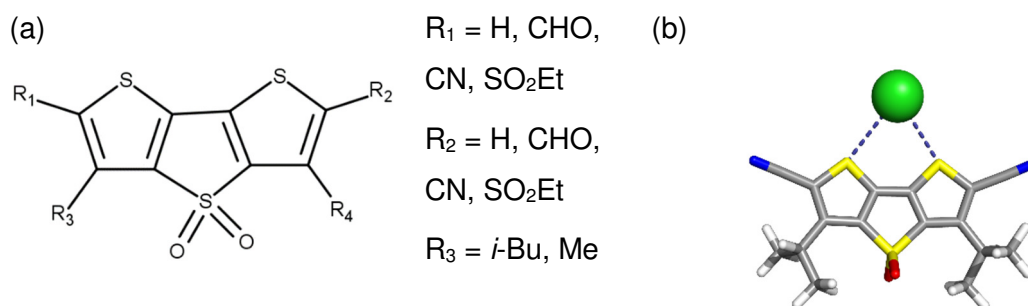


Fig. 7 – (a) Base chemical structure of the 2,2'-bithiophenes studied by Stefan and co-workers<sup>20</sup> and (b) structure of the receptor with best binding energy for the chloride anion. The chalcogen bond is represented by the dashed lines.

### 1.3.4. CH as Hydrogen Bond Donners on Anion Transport

Much has been said regarding hydrogen bonds involving NH or OH groups, for obvious reasons. These groups are, in fact, the most common regarding the establishment of hydrogen bonds, however, a number of structures are starting to be studied where this type

of interaction is established by CH groups. At first glance, a CH group would not be the immediate choice for this type of interaction with an anion since these groups have small electronegativity difference and show reduced bond dipole.<sup>22</sup> However, these groups only establish weaker hydrogen bonds in particular cases, such as when the binding cavity is lined with positive charges and hence the CH groups contribute with secondary interactions, combined with intrinsically polarized heteroatom based donors.<sup>22</sup> Therefore, CH groups can be used for strong hydrogen bonding if they are extrinsically polarized by electron-withdrawing groups.<sup>22</sup> Following this line of thought, one can take into consideration the study performed by Amar Flood and co-workers.<sup>22</sup> These researchers studied the binding properties of receptors containing aryl-triazole, namely triazolophanes just like the one represented in Fig. 8(a) and concluded that these compounds exhibited high binding affinity for chloride anions.<sup>16</sup> This behaviour was attributed to the pre-organization of the structure, size complementarity of the receptor and the chloride anion, as well as to the CH hydrogen bond donor groups.

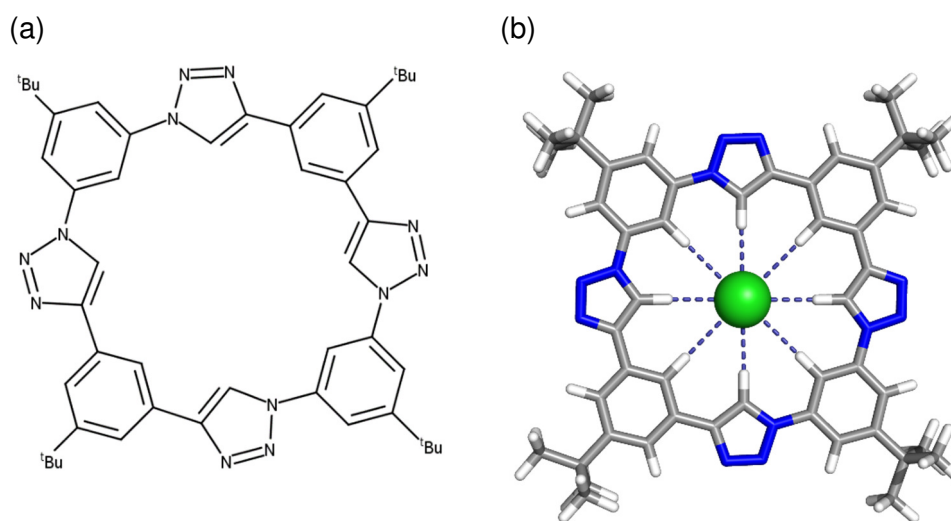
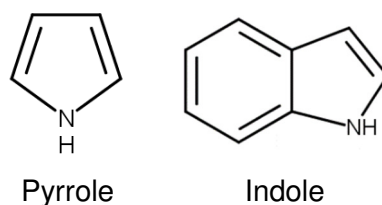


Fig. 8 – (a) Chemical structure of one of the triazolophanes studied by Amar Flood and co-workers<sup>22</sup> and (b) the representation of the hydrogen bonds established by the CH groups and the chloride anion. The hydrogen bonds are represented as dashed lines.

### 1.3.5. Pyrrole and Indole Groups on Anion Transport

As important as the interactions between receptors and anions are the moieties responsible for those interactions. Thus, receptors associated with anion transport may be composed of pyrrole or indole groups. These pyrroles and indoles (represented in Scheme 3) are capable of establishing hydrogen bonds due to the presence of hydrogen bond receptor groups, however they do not have hydrogen bond acceptor groups, which may pose as an

advantage since it allows them to avert aggregation and competition for hydrogen bond donor sites.<sup>16</sup> This feature turns pyrrole and indole containing receptors into interesting systems that are increasingly being studied for anion transport purposes.



Scheme 3 – Chemical structure and identification of pyrrole and indole groups.

To better understand how the interaction between the chloride anion and the pyrrole groups is established, one can look at the representation of the structure of a dipyrrolyldiketone based receptor studied by Hiromitsu Maeda and co-workers, represented in Fig. 9(b).<sup>23</sup> The mentioned study aimed at the analysis of anion recognition properties and, as we can see, the receptor is able to recognize and establish interactions with the anion through hydrogen bonds.<sup>23</sup> Thus, as previously mentioned, this type of interaction may be used not only for anion transmembrane transport but also in receptors with anticancer activity.<sup>24</sup>

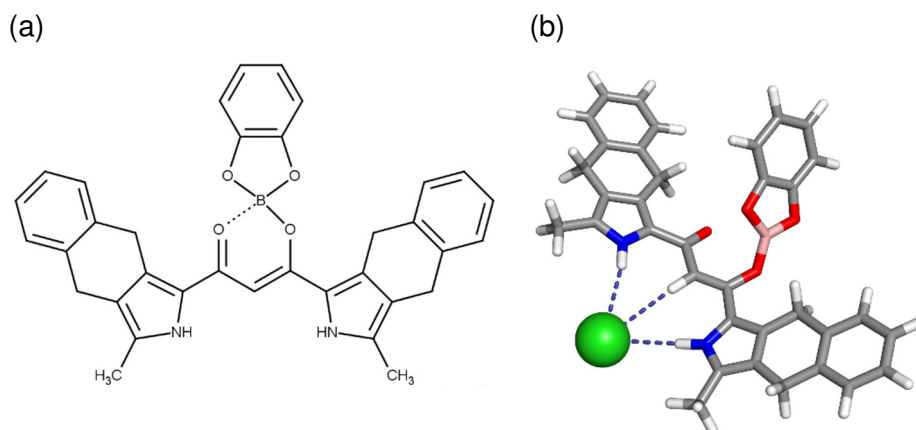
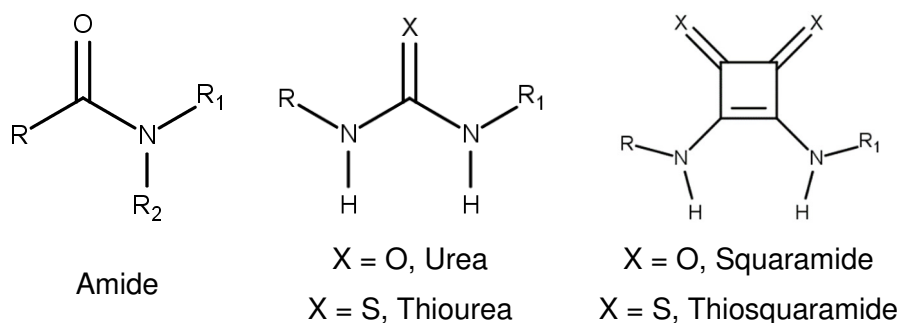


Fig. 9 – (a) Chemical structure of one of the chiral BINOL-boron substituted  $\pi$ -conjugated receptor studied by Hiromitsu Maeda and co-workers<sup>23</sup> and (b) respective representation of the interaction established with the carrier. The hydrogen bonds are represented with dashed lines.

### 1.3.6. Nitrogen Functional Groups on Anion Transport

Lastly, the focus is turned to an extremely common constituent of anion receptors: nitrogen functional groups. In this broad category one can find receptors composed of amide, (thio)urea or (thio)squaramide functional groups (presented in Scheme 4). These are used

in great extent due to their simple synthesis and easily controllable acidity on the proton of the NH group (when present).<sup>16</sup>



Scheme 4 – Chemical structure and identification of the mostly used functional groups in synthetic transporters.

Receptors containing nitrogen functional groups are capable of establishing hydrogen bonds with anions as well as electrostatic interactions, when they are protonated. Urea and thiourea own two NH hydrogen bond donors whilst amide only has one. This allows the former systems to coordinate anions through multiple hydrogen bonds. (Thio)squaramides also have two hydrogen bond donors and are becoming increasingly popular among researchers interest due to their high anion affinity and selectivity.<sup>16</sup>

Many studies have shown that these systems of transport are particularly good at transporting chloride anions,<sup>11</sup> which is a major point of interest in the present thesis. These studies often focus on binding affinities and transport rates regarding the transport of chloride, however, some of them also explore the factors that relate to or influence transmembrane transport.<sup>11</sup> Examples of such factors may include the effect of electron withdrawing substituents near NH, or the role of pre-organization in the system's binding strength, affinity and selectivity towards the chloride anion.<sup>11</sup>

Since both urea and thiourea groups will be discussed ahead, one may analyse an example of the interactions established by a squaramide and a chloride anion.<sup>25</sup> In this case, the researchers compared the squaramide derivatives presented in Fig. 10(a) with their urea and thiourea analogues.<sup>25</sup> The results of this study show that the squaramide based compounds surpass their analogues in term of anion transport by closely one order of magnitude. This conclusion was justified by the possible increase in the anion binding strength of the squaramide based receptors (interaction represented in Fig. 10(b)).<sup>25</sup> This conclusion also justifies the continuous and increasing interest in studying squaramides as possible transmembrane transporters.<sup>25</sup>



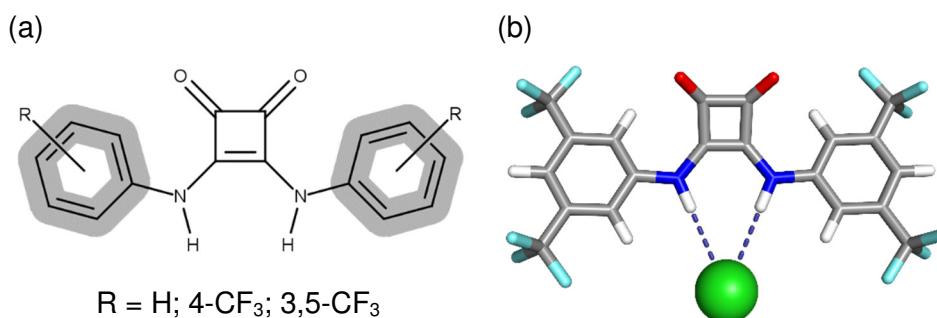


Fig. 10 – (a) Chemical structure of the squaramide based receptors studied by Philip Gale and co-workers<sup>25</sup> and (b) representation of the hydrogen bonds established between the best transporter and a chloride anion. The hydrogen bonds are represented in dashed lines.

### 1.3.7. Synthetic Transporters as Druglike Molecules

The research and development of synthetic transporters is highly associated with medicinal chemistry due to their possible usage in genetic or inherited conditions, thus it becomes important, besides considering the physical and chemical properties and behaviour of these systems, to also consider adjusting the transporter characteristics for pharmaceutical applications. At the moment there is no method of administration reported for synthetic transporters. For oral administration, the most common method, one should consider the Lipinski's rule of five. This rule consists of a combination of simple guidelines that help to determine if a particular chemical compound is likely to be orally active to humans.<sup>26-27</sup> In other words, this rule helps to determine the druglikeness of that particular chemical compound. The guidelines are presented below:<sup>26-27</sup>

- The molecular mass should be inferior to 500 Da.
- There should be no more than 5 hydrogen bond donors.
- There should be no more than 10 hydrogen bond acceptors.
- The log P (octanol-water partition coefficient) value should be inferior to 5.

This rule functions as a set of rules of thumb and as such they should not be blindly followed, in fact there are many exceptions.<sup>26</sup> Thus, these guidelines should be considered for orientation purposes only, regarding the design of organic molecules with pharmaceutical usage.

Nonetheless, to increase the accuracy of such guidelines, and consequently to improve the efficiency of drug design, this rule has been improved over the years.<sup>28</sup> As a result the definition of a druglike molecule evolved from the simple set of guidelines to a more specific combination of conditions. For instance, the molecular mass should be set in the interval of 160 Da and 480 Da, the total number of atoms should go from 20 to 70, the logP value

should be comprehended between -0.4 and 5.6 and the molar refractivity should stay between 40 and 130.<sup>28</sup> These are just a few examples of the amendments made to the original rule of five established by Lipinski, however there are many other corrections.<sup>29-30</sup> So, depending on the on the target the transporters has to reach and the obstacles it may face other methods of administration should be considered. For instance, for CF patients the treatment should be administered by inhalation for a quicker and more direct response.

### 1.3.8. Molecules with a Transport Architecture

The focus will be turned to the previously mentioned receptors containing urea and thiourea moieties. The emphasis on these is justified by the fact that the receptors being studied on the present thesis are also composed of these nitrogen groups. However it is important to note that the following studies, which will allow an in depth view on this matter, were not arbitrary chosen, since they were carried in a collaboration between the Molecular Modelling Group at the University of Aveiro and the research group of Philip A. Gale. Therefore, one should start with the research involving tripods, namely tris(2-aminoethyl)amine derivatives, represented in Fig. 11. This study shown that receptors containing urea were either inactive or poorly active antiport agents whilst molecules with thiourea showed the exact opposite behaviour, displaying good activity levels.<sup>13</sup>

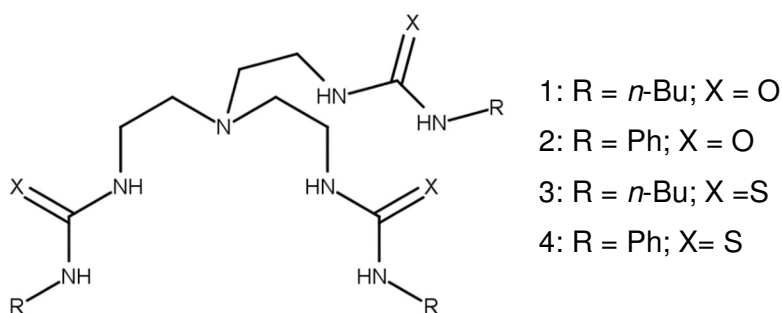


Fig. 11 – Representation of the tris(2-aminoethyl)amine derivatives studied.

Following this study the same researchers reiterated these conclusions by carrying out very similar experiments on simpler organic molecules (shown in Fig. 12). Here, just like before, the researchers observed that the molecules containing thiourea groups performed favourably in terms of transport activity when compared to their urea analogous.<sup>13</sup> Consequently, these previous studies point out an evident advantage for the thiourea systems as antiport agents.<sup>11</sup>

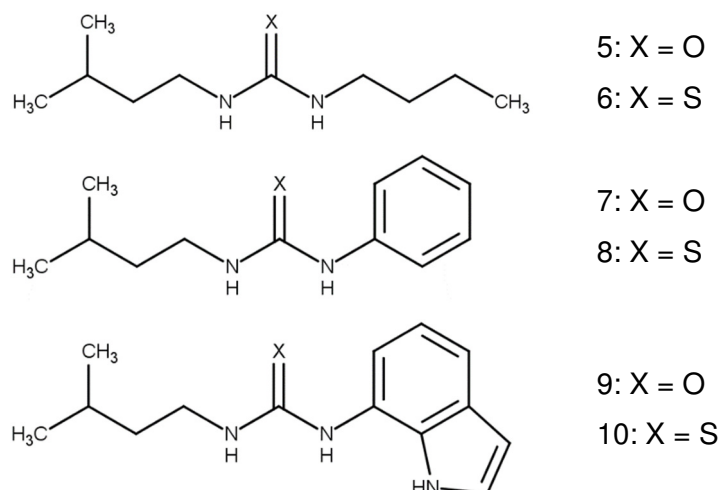
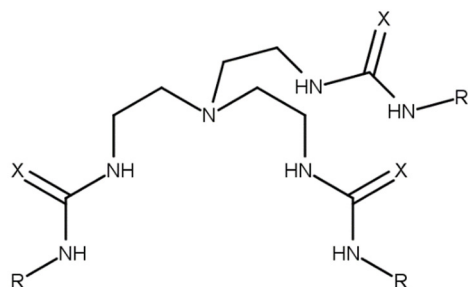


Fig. 12 – Representation of the simpler organic molecules studied.

With such compelling evidences regarding the efficiency of anion transport across biological membranes, it became rather tempting to build a bridge between the results obtained and the possibility of using them for medical purposes. Nonetheless, to cover the gap between these two realities, the researchers had to adapt the design of molecules in order for them to have pharmaceutical usage. Despite the fact that the small organic structures exhibited promising results, researchers should also bear in mind that to design effective pharmaceutical compounds, these need to be optimized in terms of absorption, distribution, metabolism, excretion and toxicity (ADMET) which consist of a set of properties of the utmost importance for medicinal chemistry.<sup>13</sup> The researchers continued the study of the small organic molecules, however they added fluorinated groups to their structures (depicted in Fig. 13).<sup>31</sup> This is a frequently used approach in medicinal chemistry to enhance the physiological properties of chemical compounds, since it increases lipophilicity and hydrogen bond acidity, which leads to an improvement on anion binding properties.<sup>31</sup>

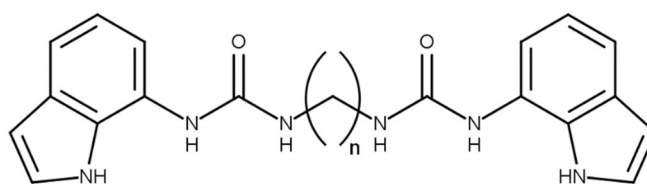


- 11: R = *p*-C<sub>6</sub>H<sub>4</sub>F; X = O      15: R = *p*-C<sub>6</sub>H<sub>4</sub>F; X = S  
12: R = C<sub>6</sub>F<sub>5</sub>; X = O      16: R = C<sub>6</sub>F<sub>5</sub>; X = S  
13: R = *p*-C<sub>6</sub>H<sub>4</sub>(CF<sub>3</sub>); X = O      17: R = *p*-C<sub>6</sub>H<sub>4</sub>(CF<sub>3</sub>); X = S  
14: R = 3,5-C<sub>6</sub>H<sub>3</sub>(CF<sub>3</sub>)<sub>2</sub>; X = O      18: R = 3,5-C<sub>6</sub>H<sub>3</sub>(CF<sub>3</sub>)<sub>2</sub>; X = S

Fig. 13 – Representation of the fluorinated tris(2-aminoethyl)amine derivatives.

From this study the researchers concluded that fluorinated transporters, do in fact, show greater anion transport activity, maintaining the observations concerning the urea and thiourea moieties.<sup>31</sup> This increase concerning activity is related to the lipophilicity of the compounds with fluorinated groups, since this group confers an increase in lipophilicity values allowing the transporter and, consequently, the anion complex to partition into the membrane more favourably.<sup>32</sup> Following this line of thought, the use of fluorinated aromatic substituents would also lead to greater lipophilicity and hence facilitate the movement of the transporter (or the anion complex) across biological membranes.<sup>32</sup>

As the search for a better understanding of these transport systems continued, other studies emerged. These focused on another important aspect of the transport process which is the factor (or factors) that allow transporters to be considered active in their function.<sup>32</sup> For this the researchers studied 9 bis-indolyureas that only differed on the length of the alkyl chain (represented in Fig. 14) and ran a series of experimental procedures with the help of Molecular Dynamic (MD) simulations.<sup>32</sup>



18 – 26: n = 4 - 12

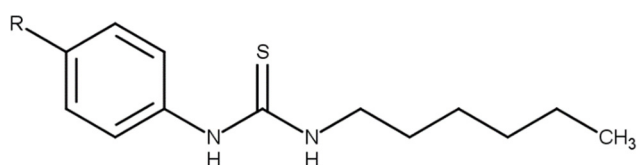
Fig. 14 – Representation of the bis-indolyureas studied with resource of MD simulations.

As stated before, it has been proven that receptors containing urea groups are not active transporters, however, a chemical compound composed of urea and indole groups appears to be an active antiport agent.<sup>32</sup> For this study, parameters such as  $EC_{50\ 270s}$  (which corresponds to the measurement of receptor's concentration to mediate 50% of the ion efflux in 270 seconds), the Hill coefficient (which corresponds to an estimative of the number of molecules needed to carry a single ion),  $\log P$ , the PSA (Polar Surface Area) and the TSA (Total Surface Area) were determined. The researchers also plotted the percentage of chloride efflux.<sup>32</sup> All this allowed the researchers to draw several conclusions. For instance, greater transport activity is directly correlated with increasing values of lipophilicity until a certain turning point, where a bigger chain length originates slower transport rates and consequently slower partitioning.<sup>32</sup> This is a general behaviour, however, as pointed out by

the researchers, there are exceptions as a fairly active molecule has a clogP value of 11.03.<sup>33</sup>

The researchers also concluded that the synthetic transporters follow a carrier mechanism and hence do not function as a channel.<sup>32</sup> This was proven by the relation established between the thickness of the biological membrane and the transport efficiency, since the increase of former originated a decrease in the latter.<sup>32</sup> The fact that the MD simulations, carried by the Molecular Modelling Group of University of Aveiro, showed that all transporters exhibited an outstanding mobility within the phospholipid tails, which helped to prove this point.<sup>32</sup> Other conclusions on this study regarded the advantage of possessing a bigger number of binding sites and the availability of these same compounds to function as anion transporters.<sup>32</sup>

More recent studies have shown a direct relation between the electronic effect of the substituent and the interaction of the transporter with the anion.<sup>34</sup> Here the researchers observed the behaviour of numerous receptors composed of thiourea groups that only differ on the *para*-substituent of the phenyl group (portrayed in Fig. 15).



27: R = Br	33: R = COOMe	38: R = O(CO)Me	43: R = SO <sub>2</sub> Me
28: R = CF <sub>3</sub>	34: R = F	39: R = OCF <sub>3</sub>	44: R = CH <sub>3</sub>
29: R = Cl	35: R = H	40: R = OEt	45: R = CH <sub>2</sub> CH <sub>3</sub>
30: R = CN	36: R = I	41: R = OMe	46: R = (CH <sub>2</sub> ) <sub>2</sub> CH <sub>3</sub>
31: R = COCF <sub>3</sub>	37: R = NO <sub>2</sub>	42: R = SMe	47: R = (CH <sub>2</sub> ) <sub>3</sub> CH <sub>3</sub>
32: R = COMe			48: R = (CH <sub>2</sub> ) <sub>4</sub> CH <sub>3</sub>

Fig. 15 – Representation of the chemical compounds used to study the electronic effect of different substituents.

Our research group played a major role in this study and concluded that the strongest binding happened on the chemical compound with the most electron withdrawing substituent.<sup>34</sup> It also noticed that the electronic effect influences the acidity of the protons present on the NH groups that interact with the anion, making this interaction stronger for more acidic protons.<sup>34</sup> As a result, it was possible to observe that the transport ability

increased as the substituents went from an hydrogen atom to a nitro functional group in the following order:  $H < F \approx Cl < CF_3 < CN < NO_2$ .<sup>34-35</sup> Lipophilicity appears once more as a crucial aspect to obtain an efficient anion transporter, along with increased anion-binding ability and decreased molecular size.<sup>34</sup>

To sum up, most of the previous studies have shown that for simple chemical compounds to work properly and efficiently as transmembrane chloride transporters, there has to be an equilibrium between aqueous solubility and lipophilicity.<sup>36</sup> According to those same studies, one should also take in consideration the substituent groups adjacent to the urea or thiourea moieties, which influence the acidity of the protons of the NH group that, in turn, will influence the binding strength of the receptor. Additional factors to contemplate would be the number of binding sites, as well as the influence of fluorinated groups when trying to design transporters with pharmaceutical purposes. In agreement with the studies presented in this section, all these aspects should be considered to design chemical compounds that ought to be able to function as anion carriers.<sup>36</sup>

#### 1.4. Computational methods and molecular modelling

At this point it becomes important to consider some concepts regarding molecular modelling as way of understanding in full all the work developed in the present thesis. First of all, one should take in consideration that computational methods can resort either to quantum mechanics (QM) or to molecular mechanics (MM).

In QM one is able to determine electronic properties since the electrons of the system are taken into account during calculations.<sup>37</sup> These calculations are based on solving the time-independent Schrödinger's equation, described by eq. (1).<sup>37</sup>

$$\left( -\frac{\hbar^2}{2m} \nabla^2 + V(r) \right) \Psi(r) = E\Psi(r) \leftrightarrow \hat{H}\Psi = E\Psi \quad (1)$$

Since solving this equation is only possible for the hydrogen atom, or one-electron particles, one has to resort to approximation to be able to apply QM calculations for larger systems.<sup>37</sup> If, on the one hand, QM allows one to obtain results with great accuracy, on the other hand, these calculations demand high computational resources and time, placing QM out of the picture for larger systems such as lipid cell membranes.<sup>37</sup> For these larger systems, force field methods, or MM, appear as a solution. For instance, the fact that MM does not consider

the electronic part of the system allows this method to obtain the energy from the coordinates of its constituents in less time and with fewer computer resources.<sup>37</sup> As one could predict, one of the downfalls of MM relies on its inability to calculate electronic properties.

At this stage, it is important to define the term force field: Force field methods provide the energy of the system considering four components: bonds, angles, torsions and nonbonding interactions:<sup>37</sup>

$$E = \sum_{bonds} \frac{k_i}{2} (l_i - l_{i,0})^2 + \sum_{angles} \frac{k_i}{2} (\theta_i - \theta_{i,0})^2 + \sum_{torsions} \frac{V_n}{2} (1 + \cos(n\omega - \gamma)) + \sum_{i=1}^N \sum_{j=i+1}^N \left( 4\varepsilon_{ij} \left[ \left( \frac{\sigma_{ij}}{r_{ij}} \right)^{12} - \left( \frac{\sigma_{ij}}{r_{ij}} \right)^6 \right] + \frac{q_i q_j}{4\pi\varepsilon_0 r_{ij}} \right) \quad (2)$$

On eq. (2)  $l$ ,  $\theta$ , and  $\omega$  specify the bond lengths, valence angles and torsion angles, respectively, obtained from the molecular geometry.<sup>38</sup> In turn, the terms  $l_{i,0}$  and  $\theta_{i,0}$  correspond to equilibrium values regarding bonds and angles whilst  $k_i$  corresponds to the force constants.<sup>38</sup> For the torsion term,  $V_n$  corresponds to the amplitude and  $\gamma$  is the phase for each multiplicity  $n$ .<sup>38</sup> On the last term of the equation,  $\varepsilon_0$  comes as the dielectric constant,  $q_i$  and  $q_j$  designate the partial atomic charges on atoms  $i$  and  $j$ .<sup>38</sup> Lastly, in the van der Waals term,  $\varepsilon_{ij}$  corresponds to the well depth,  $\sigma_{ij}$  is the radius and  $r_{ij}$  describes the distance between atoms  $i$  and  $j$ .<sup>38</sup>

Therefore, a force field can be defined as a set of parameters (represented in the constants  $k_i$ ,  $V_n$  and  $\sigma_{ij}$ ) allowing one to obtain structural properties. Thus, the choice of the most appropriate force field is crucial to obtain accurate calculation for the system being studied so, over the years, there has been a need to develop force fields that could correctly be applied to a wide variety of structures. For instance, one can use CHARMM (Chemistry at HARvard Molecular Mechanics) for biomolecules,<sup>39</sup> OPLS (Optimized Potentials for Liquid Simulations) also for biomolecules and some organic systems<sup>40</sup> or UFF (Universal Force Field) as a general force field that covers all the elements in the periodic table.<sup>41</sup> However, none of these force fields were used in the present work and theoretically all of them could. For instance, CHARMM is capable of being applied to biological macromolecular systems, moreover an extension of this force field, designated as CHARMM General Force Field (CGenFF) along with CHARMM36, could be used to study organic molecules.<sup>42</sup> Nonetheless, this extension is unable to properly and accurately simulate certain functional groups, such as urea and thiourea groups.<sup>42</sup> Another example is UFF, which is a general

force field, and consequently lacks the accuracy and precision required in such studies, being often used for inorganic molecules. Since in the present thesis the small organic molecules studied for transmembrane chloride transport were composed of thiourea groups, the studies were performed using GAFF (General AMBER Force Field)<sup>43-44</sup> to describe the studied anions transporters, along with Lipid14<sup>45</sup> for the phospholipid molecules of the bilayer.

GAFF was inspired by previous AMBER force fields allowing them to be compatible. As a result, GAFF follows the parameters in Parm99, meaning that it serves itself of the parameterization of AMBER for proteins and nucleic acids and complements its parameter set with information regarding most of the organic and pharmaceutical molecules.<sup>43</sup> As a result, GAFF presents itself as a complete force field and as functional tool for the study of pharmaceutical compounds. Nevertheless, GAFF, by itself, cannot be used for phospholipid bilayer model simulations, a key part of the thesis, due to the fact that it cannot properly reproduce membrane properties. Still, it was used as a starting point for the development of two independent lipid force fields (Lipid11<sup>46</sup> and GAFFlipid<sup>47</sup>), which later gave rise to Lipid14. This framework enables the simulation of several lipids by mixing different head and tail groups, thus allowing the tensionless simulation of lipid bilayers.<sup>45</sup>

#### 1.4.1. First Insights at Atomistic Level by Molecular Dynamics Simulations

A closer look at MD is also important since this can be seen as one of the fundamental tools of a molecular modeller. These simulations need information regarding the potential energy function of the system's components that will interact with each other. In turn, that information is derived from a force field, which is based on MM, as mentioned above. The end result of MD simulations is a trajectory file that gathers the changes of positions and velocities of all the system's components through the simulation time. From this file one is able to predict structural and energetic properties and to study processes such as the diffusion of molecules into solids, as well as observe the behaviour of large molecular systems.

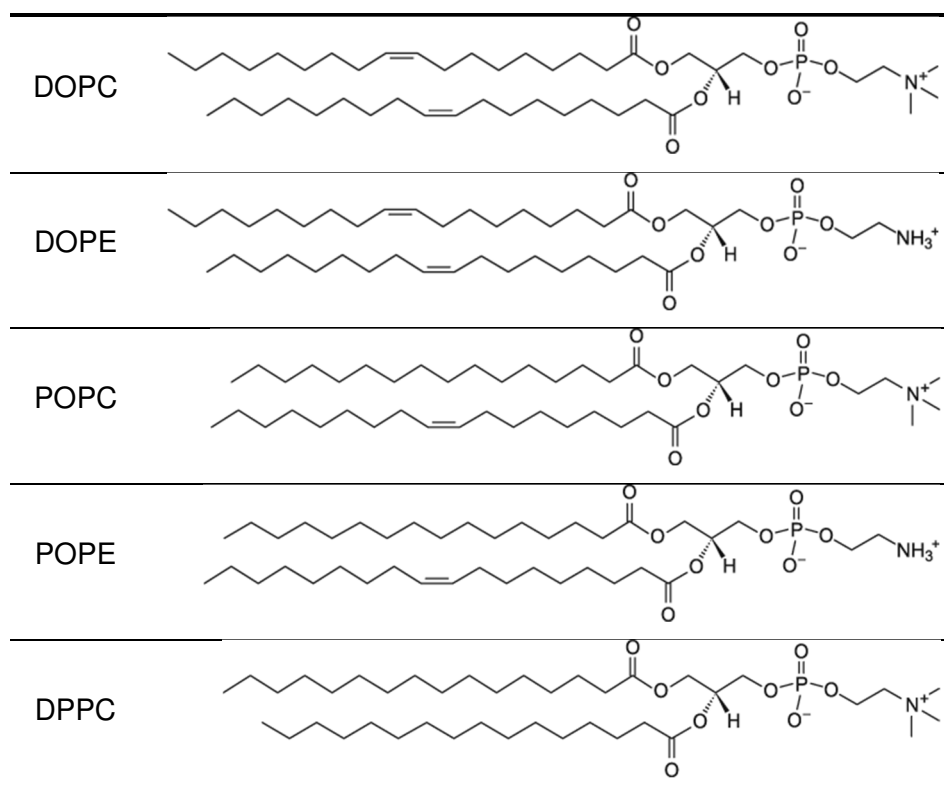
There are several models that turn the simulation on lipid membranes possible and, just as before, simpler models allow the simulation of larger systems and longer time scales, at the compromise of atomic detail.<sup>45</sup> The models used to simulate membranes go from all-atom (where hydrogen atoms are included in the simulation),<sup>48</sup> to united-atom (where the hydrogen atoms of methylenes and terminal methyl are replaced by effective van der Waals spheres)<sup>49</sup> or coarse-grained models (where small groups of atoms are represented by

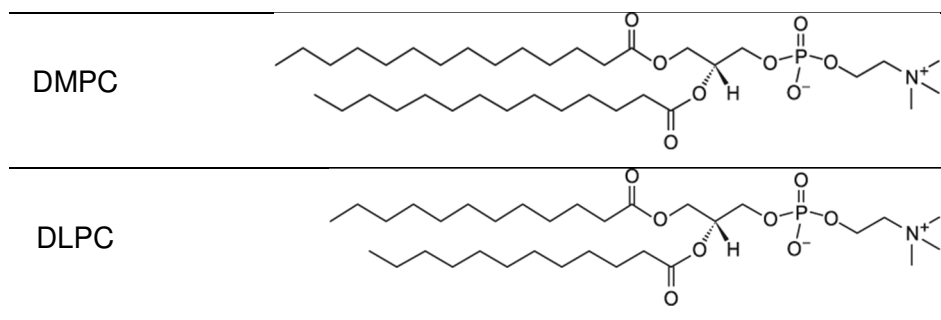


single interaction sites).<sup>50</sup> These models are used in some of the force fields previously mentioned and, once again, their choice heavily depends on the characteristics of the system being studied.

In the particular case of simulations with lipid bilayer membranes the model used is the all-atom since it has the ability to reproduce Nuclear Magnetic Resonance (NMR) order parameters and it can be easily associated with all-atom protein, nucleic acid, carbohydrate and small molecule force fields.<sup>45</sup>

Although Lipid14 supports several lipid types, the choice of the phospholipid should rely on the objective of the research being carried out, hence some of the most common membranes used in MD simulations composed of either phosphatidylcholines (PC) or phosphatidylethanolamines (PE) lipids, two very common classes of phospholipids in eukaryotic cell membranes. A few examples of such phospholipids are 1,2-dioleoyl-*sn*-glycero-3-phosphocholine (DOPC), 1,2-dioleoyl-*sn*-glycero-3-phosphoethanolamine (DOPE), 1-palmitoyl-2-oleoyl-*sn*-glycero-3-phosphocholine (POPC), 1-palmitoyl-2-oleoyl-*sn*-glycero-3-phosphoethanolamine (POPE), 1,2-dipalmitoyl-*sn*-glycero-3-phosphocholine (DPPC), 1,2-dimyristoyl-*sn*-glycero-3-phosphocholine (DMPC) and 1,2-dilauroyl-*sn*-glycero-3-phosphocholine (DLPC) (all represented in Scheme 5).





Scheme 5 – Representation of the chemical structure of the most common lipids used in the simulation of lipid bilayer membranes.

For instance, in particular cases, membranes can be complemented with certain biological structures, such as cholesterol. This sterol can be introduced in the bilayer for MD simulations, in a controlled ratio, as a way to ascertain the variation in activity of the chemical compounds being studied.<sup>32</sup> This is important since the presence of cholesterol increases the viscosity of the membrane, intensifying the difficulty in the diffusion of the carrier-anion complex and hence reducing its activity.<sup>32</sup>

The Molecular Modelling Group at University of Aveiro has both a great know-how and computational resources, being capable of carrying out MD simulations that have been published in a number of papers with several collaborations. As an example, this group studied tris-thiourea tripodal-based molecules, such as the one represented in Fig. 11. The group's work was fully focused on MD simulations regarding that receptor. They concluded that the molecules have low impact on the phospholipid bilayer's structure and that the molecules being studied are also capable of diffusing, with the chloride anion, to the membrane, as represented in Fig. 16. This is of great importance since these observations correspond to the ideal conditions for transmembrane transport of chloride anion to function properly.<sup>1</sup>

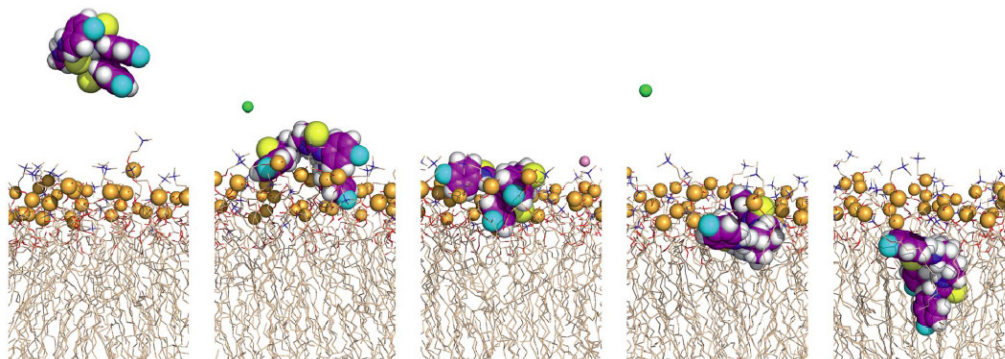


Fig. 16 – Approach of one of the tripodal-based molecules to the water-lipid interface in 5 consecutive snapshots. Reproduced from tris-thiourea tripodal-based study performed by the Molecular Modelling Group at University of Aveiro.<sup>1</sup>

#### 1.4.1.1. Structural Properties of Phospholipid Bilayers

The analysis of the structural properties of the lipid bilayers should also be taken into account when performing MD simulations. Such properties can be the area per lipid, order parameters, electron density or the thickness of the lipid membrane, allowing one not only to examine the phospholipid bilayer's behaviour when interacting with a receptor or a complex, but also how this interaction changes the structural properties of the membrane. The area per lipid corresponds to the surface area that each lipid occupies on the membrane. It is a way of understanding if the lipid bilayer is in the correct phase at a given temperature.<sup>45</sup> To ascertain it, one only has to divide the lateral area of the simulation box by the number of phospholipids per layer, as represented in eq. (3).<sup>51</sup>

$$A_L = \frac{\text{Box } x \text{ dimension} \times \text{Box } y \text{ dimension}}{\text{number of phospholipids per layer}} \quad (3)$$

One may also calculate the order parameter to determine the ordering of the lipid acyl chains.<sup>51</sup> The values obtained are compared to experimental values, which in turn are obtained by NMR spectroscopy *via* the deuterium-order parameter ( $S_{CD}$ ), particularly acquired from deuterium ( $^2\text{H}$ ) NMR or proton-carbon-13 ( $^1\text{H}$ - $^{13}\text{C}$ ) NMR.<sup>45</sup> The measurement of the ordering regards the orientation of the C-D bonds with respect to the lipid membrane normal. As a result the  $S_{CD}$  can be calculated with the equation represented in eq. (4).<sup>45</sup>

$$S_{CD} = 0.5 \langle 3\cos^2(\theta) - 1 \rangle \quad (4)$$

In eq. (4),  $\theta$  denotes the angle between the bilayer normal and the vector joining a certain carbon atom  $C_i$  to the respective deuterium atom, while the angle brackets express an ensemble average.<sup>45</sup>

When observing the experimental results for all membranes one can expect a common behaviour in all of them. The graphical representation of this property depicts that the head groups of the *sn*-1 chains present greater  $S_{CD}$  values than the correspondent *sn*-2 chains.<sup>45</sup> Also, for unsaturated chains, there is a distinctive drop at the *cis* double bond.<sup>45</sup>

The Electron Density Profiles (EDP) can be calculated and graphically represented as a combination of all the contributors in a system. The representation of each contributor individually is unusual.<sup>45</sup> Whichever the case may be, the graphical representations along

the membrane normal should always be symmetrical for a pure membrane system and presented on an absolute scale.<sup>45</sup> The usage of this scale increases the relative error of the scaling factor, however the increase is not considered critical for the purposes used.<sup>51</sup>

Lastly one may also analyse the thickness of the lipid bilayer, that is, the total length of the membrane from the head groups of one layer to the head groups of the other layer. The thickness can be calculated in different manners.<sup>45</sup> It can be obtained as the peak-to-peak distance from the EDP of the membrane, or it can be calculated using the z-dimension of the simulation box and the integral of the probability distribution of the water density along the Z axis.<sup>45</sup> For the purpose of this thesis, membrane thickness was accessed by calculating the average position of the phosphorus atoms of each leaflet, regarding the phospholipid bilayer's normal, and subtracting these values.

#### 1.4.1.2. Important Descriptors on Anion Transmembrane Transport

Besides the membrane properties one should also consider the properties of the receptor being studied. Such properties include the lipophilicity or the electrostatic potential ( $V_s$ ).

As previously mentioned, the lipophilicity of the receptor under scrutiny is of the utmost importance since it can aid the prediction of the pharmaceutical disposition of that molecule and its druglikeness. This property can be obtained through the calculation of the value of logP, which, in turn, can be obtained through different methods.<sup>52</sup> Therefore, one may use substructure based methods that rely in calculations of logP values of fragments of the receptor and in the end presents the sum of the individual contributions of the different fragments, or one may opt for a property based methods where the logP value is calculated by using the whole molecule.<sup>52</sup> One software capable of performing these calculations is VCCLab, which allows the calculation of logP using the different methods described.<sup>52</sup>

For determining the binding affinity of the receptor regarding the anion one should take in consideration its  $V_s$ . This property was firstly reported by the Molecular Modelling Group at University of Aveiro and allows the assessment of the binding activity since it values non-covalent interactions where the electrostatic component is the major contributor.<sup>53</sup> The  $V_s$  at any point of a certain molecule can be obtained by eq. (5).<sup>17</sup>

$$V_S = \sum_i \frac{Z_i}{|R_i - r|} - \int \frac{\rho(r') dr'}{|r' - r|} \quad (5)$$

In eq. (5),  $Z_i$  represents the charge on a certain atom  $i$ , which is located in the position  $R_i$ . The  $\rho(r)$  corresponds to the electronic density of the molecule being studied.<sup>17</sup>

As a result, one obtains a maximum value ( $V_{S,max}$ ) as well as a minimum value ( $V_{S,min}$ ). The former is related to the hydrogen-bond acidity and hence to the receptor's binding ability. On the contrary, the latter regards the anion hydrogen-bond basicity.<sup>53</sup> The most frequent manner of presenting the obtained results is through a representation of the electron density surface of the receptor, where these maximum and minimum regions are easily perceptible.<sup>53</sup>

### 1.5. The Precedent Work that Lead to this Thesis

Lastly one should consider the work that lead to this thesis. The Molecular Modelling group has developed, over the years, an important and consistent work regarding, among other research interests, transmembrane transport of chloride anion. This gave rise to relevant publications and collaborations, just as previously mentioned collaboration with Philip A. Gale. For the present thesis, the molecules being studied came from the work developed by Anthony P. Davis, another example of the group's collaborations. Thus, the aim of this thesis is to investigate the ability of tris-thiourea derivatives as efficient synthetic transporters.<sup>54-55</sup> To do so, the structures are to be optimized and submitted to a series of computational methods, simulations and calculations.

The achievements accomplished so far evoked the curiosity of deepening the knowledge for characteristics and behaviour of tripods which are the structural base of the chemical compounds handled on this thesis.

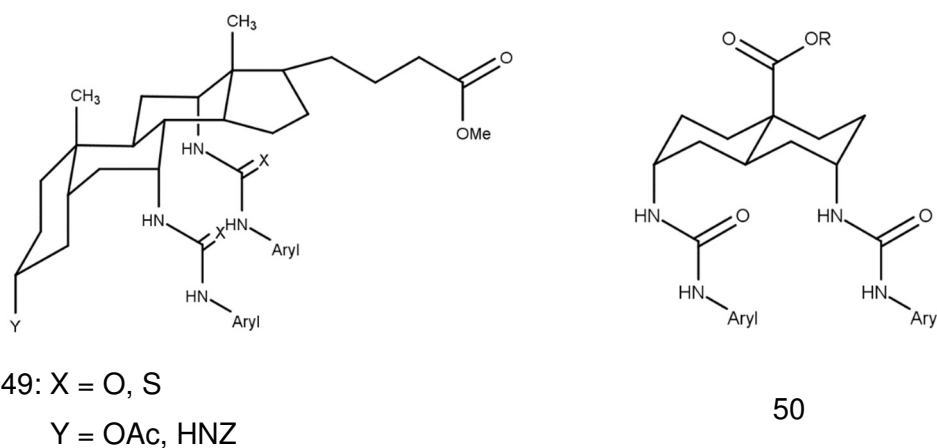


Fig. 17 – Representation of the generic chemical structure of cholapods (49) and diureidodecalins (50).

For a long time, cholapods and diureidodecalins (represented in Fig. 17) were considered the best anion transporters, showing astonishing results for both binding affinity and for transport rate.<sup>54</sup> Nonetheless, these chemical compounds require a long and complex synthesis, involving numerous steps and reagents.<sup>55</sup>

Considering all the studies and conclusions previously mentioned as well as this last aspect, Anthony P. Davis and his co-workers turned to a new group of chemical compounds as an alternative. These new compounds consist of tris(thio)urea receptors (depicted in Fig. 18) and are easily synthesized (the cyclohexane-based structures take 4 to 5 steps to be synthesized while the triethylbenzene-based structure takes solely 1 step, from commercially available triamine, to be synthesized).<sup>55</sup>

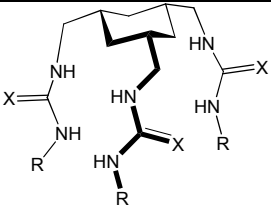
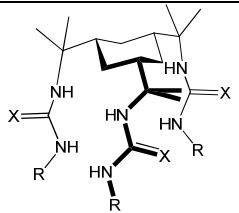
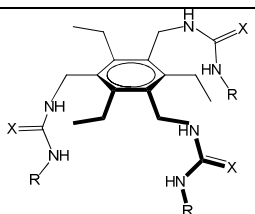
	51OD: X = O, R = C <sub>6</sub> H <sub>3</sub> (CF <sub>3</sub> ) <sub>2</sub>	51SD: X = S, R = C <sub>6</sub> H <sub>3</sub> (CF <sub>3</sub> ) <sub>2</sub>
	51OF: X = O, R = C <sub>6</sub> H <sub>4</sub> CF <sub>3</sub>	51SF: X = S, R = C <sub>6</sub> H <sub>4</sub> CF <sub>3</sub>
	51ON: X = O, R = C <sub>6</sub> H <sub>4</sub> NO <sub>2</sub>	51SN: X = S, R = C <sub>6</sub> H <sub>4</sub> NO <sub>2</sub>
	51OP : X = O, R = C <sub>6</sub> H <sub>5</sub>	51SP : X = S, R = C <sub>6</sub> H <sub>5</sub>
	52OD: X = O, R = C <sub>6</sub> H <sub>3</sub> (CF <sub>3</sub> ) <sub>2</sub>	52SD: X = S, R = C <sub>6</sub> H <sub>3</sub> (CF <sub>3</sub> ) <sub>2</sub>
	52OF: X = O, R = C <sub>6</sub> H <sub>4</sub> CF <sub>3</sub>	52SF: X = S, R = C <sub>6</sub> H <sub>4</sub> CF <sub>3</sub>
	52ON: X = O, R = C <sub>6</sub> H <sub>4</sub> NO <sub>2</sub>	52SN: X = S, R = C <sub>6</sub> H <sub>4</sub> NO <sub>2</sub>
	52OP : X = O, R = C <sub>6</sub> H <sub>5</sub>	52SP : X = S, R = C <sub>6</sub> H <sub>5</sub>
	53OD: X = O, R = C <sub>6</sub> H <sub>3</sub> (CF <sub>3</sub> ) <sub>2</sub>	53SD: X = S, R = C <sub>6</sub> H <sub>3</sub> (CF <sub>3</sub> ) <sub>2</sub>
	53OF: X = O, R = C <sub>6</sub> H <sub>4</sub> CF <sub>3</sub>	53SF: X = S, R = C <sub>6</sub> H <sub>4</sub> CF <sub>3</sub>
	53ON: X = O, R = C <sub>6</sub> H <sub>4</sub> NO <sub>2</sub>	53SN: X = S, R = C <sub>6</sub> H <sub>4</sub> NO <sub>2</sub>
	53OP : X = O, R = C <sub>6</sub> H <sub>5</sub>	53SP : X = S, R = C <sub>6</sub> H <sub>5</sub>

Fig. 18 – Representation of the tris(thio)urea that served as study subject for the present thesis.

The compounds depicted in Fig. 18 were studied in terms of binding affinity towards the chloride anion and anion transport.<sup>54-55</sup> The results for the receptors were compared to a derivative of a cholapod receptor. The results obtained were gathered and are presented in Table 1.<sup>54-55</sup>

The binding affinity studies were carried out in wet dimethylsulfoxide (DMSO-*d*<sub>6</sub>/H<sub>2</sub>O) in a ratio of 200:1 with tetrabutylammonium chloride (Bu<sub>4</sub>N<sup>+</sup>Cl<sup>-</sup>) as substrate and in chloroform with tetraethylammonium chloride (Et<sub>4</sub>N<sup>+</sup>Cl<sup>-</sup>) as substrate, being the results obtained from <sup>1</sup>H NMR titrations.<sup>54-55</sup>

The researchers were able to report the binding activities for most of the receptors studied, although low solubility appeared as a major issue, particularly for tris-urea derivatives. In chloroform these limitations were more evident than in DMSO. A closer analysis at the affinity values obtained lead them to conclude that the aryl groups play an important role in the binding affinity to chloride anions.<sup>54-55</sup>

Table 1 – Binding and transport data regarding the tris(thio)urea studied by Anthony P. Davis and co-workers.

	Binding to Bu <sub>4</sub> N <sup>+</sup> Cl <sup>-</sup> in	Binding to Et <sub>4</sub> N <sup>+</sup> Cl <sup>-</sup>	Cl <sup>-</sup> /NO <sub>3</sub> <sup>-</sup> exchange	
	DMSO-d <sub>6</sub> /H <sub>2</sub> O	in CHCl <sub>3</sub>	in LUV	
	K <sub>a</sub> [M <sup>-1</sup> ]	K <sub>a</sub> [M <sup>-1</sup> ]	t <sub>1/2</sub> (s)	[I] (s <sup>-1</sup> )
Cholapod	12000	4.3x10 <sup>9</sup>	6	<5
51OD	57	n.d.	n.d.	n.d.
51SD	99	2.4x10 <sup>6</sup>	160	14
51SF	68	n.d.	440	<5
51SN	79	n.d.	340	<5
51OP	27	n.d.	n.d.	n.d.
52OD	390	n.d.	25	140
52SD	670	3.0x10 <sup>7</sup>	13	460
52SF	400	n.d.	36	89
52SN	480	2.9x10 <sup>5</sup>	66	<5
52OP	180	n.d.	n.d.	n.d.
52SP	340	n.d.	190	<5
53OD	390	n.d.	110	50
53SD	450	6.8x10 <sup>8</sup>	19	350
53SF	300	1.5x10 <sup>7</sup>	81	56
53SN	380	n.d.	310	5
53SP	130	1.9x10 <sup>4</sup>	510	<5

By observing the results depicted in Table 1, for both Bu<sub>4</sub>N<sup>+</sup>Cl<sup>-</sup> and Et<sub>4</sub>N<sup>+</sup>Cl<sup>-</sup>, one can detect an increase in K<sub>a</sub> values from the P to D thiourea substituents, more specifically in the order P < F < N < D.<sup>54-55</sup> This means that the presence of more electron-withdrawing aryl groups contribute for a greater affinity to chloride anions in the three series of receptors.

Comparing the receptors directly, the researchers concluded that receptors of series **52** presented the best affinities, followed by series **53** and lastly by **51**. The high affinity of receptors of type **52** was attributed to the presence of methyl groups that constrained the

receptors structure forcing an axial arrangement and enhancing the hydrogen-bonds by constricting the binding site. This structural strictness is absent in receptors **51** and **53**, however the latter is more structurally restrained than the former and hence, receptors **53** demonstrated higher affinities for chloride anion than receptors **51**.

For the anion transport studies, the researchers used the lucigenin assay.<sup>54-55</sup> The receptor was encapsulated in large unilamellar vesicles (LUVs, 200nm) of POPC and cholesterol (with a ratio of 7:3).<sup>54-55</sup> The transporter:lipid ratio was set to 1:2500 and was suspended in aqueous solution of sodium nitrate (225mM on both sides).<sup>54-55</sup> To study the chloride influx an external pulse of sodium chloride (25mM) was applied and the consequent decay of lucigenin was recorded.<sup>54-55</sup>

These results showed the same trend as before, in other words, receptors **52** presented the best transport activity, followed by receptors **53** and then came receptors **51**.<sup>54-55</sup> Nonetheless, this was only true for the tris-thiourea containing receptors, since the tris-urea receptors had either low solubility or had no transport activity. The pattern observed lead the researchers to conclude that the receptors **52** continue to benefit from the restrains imposed by the methyl groups.<sup>54-55</sup> The best transporter, **52SD**, showed similar activity to the cholapod derivative studied whilst the second best transporter, **53SD**, showed approximately 70% of the **52SD** activity.<sup>54-55</sup> Consequently, the receptors **52SD** and **53SD**, studied by Anthony P. Davis and further analysed in this thesis, belong to the select group of the most active anionophores available.<sup>54-55</sup>

### *1.6. Objectives*

With this information in mind, one can establish the objectives of this thesis. The greatest motivation of this thesis lays in the rationalization of the results presented, since the scientific community still does not fully understand all the issues regarding the complex process of transmembrane transport of ions. Accordingly, the work to be developed here is of the utmost importance for the future comprehension on the topic of designing selective and efficient anion transporters. To fulfil this goal, one will have to understand the similarities between receptors and, thus, establish the reason for the differences observed in the transport activity essays. This thorough analysis will involve all the tris-thiourea transporters mentioned above since these have presented the most promising results for chloride affinity. Therefore, the project will include the twelve tris-thiourea putative transporters in a first stage and then turn its focus on the transporters that previously presented good transport activity, *i.e.*, **52SD** and **53SD**, as well as **51SD**, for more in-depth computational studies.



Accomplishing such results requires the use of the Molecular Modelling Group's vast know-how and computational resources. In the end, this thesis hopes to take part in the right path to the development of new possibilities regarding the design and study of effective anion transporters. In a nutshell, extremely important molecules that can serve as a powerful tool in the cure of serious health issues, helping to improve life conditions of the ones in need, as well as representing a great milestone for modern medicine.

Regarding the structure of this thesis, after this first chapter one will take an in depth look regarding the methodology (chapter 2). This chapter shall describe all the steps performed to follow through with the experimental part of the present thesis. In turn, chapter 3 will provide all the results obtained as well as their analysis. Moreover, chapter 3 will be divided in two parts: the first part consists of structure optimization and DFT calculations (which will include all twelve transporters), the second part comprises MD simulations for the transporters with the best transport properties previously reported – **51SD**, **52SD** and **53SD** – and the plot of the free energy profile for the best transporter reported – **52SD**. Lastly, a conclusion, with the final thoughts regarding the thesis subject, will be present accompanied by perspective possibilities for future developments on the topic.

## 2. Computational Methods

The MM calculations and the MD simulations were performed using the AMBER 16 software package,<sup>56</sup> with force field parameters from GAFF<sup>43-44</sup> and atomic Restrained Electrostatic Potential (RESP)<sup>57</sup> charges for all the receptors. For the POPC phospholipids, force field parameters from Lipid14 were used.<sup>45</sup>

### 2.1. Calculation of atomic RESP Charges for the Transporters

#### 2.1.1. Structure Assembly for the Free and Complexed Transporters

The structure of 53SD was obtained directly from the x-ray crystal structure of its chloride complex present deposited in the CSD database<sup>58</sup> (with the *ref code* RUSBIS)<sup>55</sup>. From this structure, all the remaining eleven tris-thiourea transporters were created using the programs *Avogadro*<sup>59</sup>

#### 2.1.2. Optimization of the Free Transporters

The optimizations of the free transporters, that is the energy minimization of the molecules, were performed with Gaussian 09<sup>60</sup> at the Hartree-Fock (HF) functional with 6-31G\* basis set. The optimization was followed by a single point calculation of the electrostatic potential, at the same level of theory, and using Merz-Singh-Kollman scheme with 4 concentric layers per atom and 6 density points for each layer (Gaussian IOp (6/33 = 2, 6/41 = 4, 6/42 = 6) consistent with the development of GAFF. The initial charges of each molecule were then calculated by single RESP fitting, along with the attribution of atom types, using *antechamber*,<sup>61</sup> a tool present in the AMBER software package.<sup>56</sup> The process continued with creation the of the frcmod file, a force field modification file, which included parameters missing from GAFF, and were calculated with *parmchk*<sup>43-44, 61</sup> which is part of the AMBER software package.<sup>56</sup> From the mol2 file and the frcmod file, it was then possible to create the topology and coordinate files, using LEaP.

It is known that most of the RESP charge are depend on molecular conformation,<sup>62</sup> thus, to obtain less conformationally dependent charges, all transporters were subjected to a conformational analysis, as follows. This gas phase conformational analysis consisted in an initial MM energy minimization of the receptors, with the initial charges, followed by a heating stage where they were heated to 500 K for 50 ps, before the collection run of 1 ns, using a time step of 1 fs. The use of this high temperature allows the stochastic search of the conformational space since the energetic barriers are easily overcome.<sup>63</sup> This lead to a trajectory file composed of 10000 structures for each molecule, since frames were saved every 0.1 ps. Afterwards, all of these structures were further minimized by MM using a steepest descendent gradient followed by the conjugate gradient algorithm, until the

convergence criterion of  $0.0001 \text{ kcal mol}^{-1} \text{ \AA}^{-1}$  was met. The minimized structures were then clustered with UCSF Chimera software<sup>64</sup> and, for each transporter three structures with tripod shape, composed of three binding groups adopting a *syn* conformation and pointing to the centre of the transporter, and with substantially different RMS values, were selected. Afterwards, the selected structures were submitted to geometry optimization (HF/6-31G\* level) and electrostatic potential (ESP) calculations, just as described above. The esp data of each conformation were concatenated to provide the input files needed for two-stage RESP fitting with, performed by the resp program. The final multi-esp charges were used to replace the initial ones derived from a single conformation on each receptor's mol2 file. These files were later employed as inputs in LEaP to create proper AMBER topology and coordinate files for all MM calculations and MD simulations reported ahead in this chapter. This procedure was followed for the twelve transporters since the initial idea was to proceed with MD studies for all of them, however, due to time constraints, only the three molecules with the best transport characteristics (51SD, 52SD and 53SD) moved to MD simulations, see below. The multi RESP charges obtained for those three molecules are given in the Supporting Information (see, section S1).

## 2.2. Optimization of the chloride complexes

The twelve complexes were optimized with Gaussian 09<sup>60</sup> with the Minnesota '06 family (M06-2X) functional, used in systems with non-covalent interactions, and the 6-31+G\*\* basis set (where the "+" sign designates the introduction of a diffusion function to provide more accurate description of the anion), both in gas phase and with Polarizable Continuum Model (PCM) for DMSO solvent model ( $\epsilon = 46.826$ ), which was added as implicit solvent. The optimized structures are discussed in section 3, along with the dimensions, strength and covalency of the hydrogen bonds established in each receptor.

The optimized structures for the complexes of 51SD, 52SD and 53SD were used for the MD simulations in the POPC membrane model, as discussed above.

### 2.2.1. Natural Bond Orbital Analysis

Natural bond orbital (NBO) analysis was carried out for the twelve complexed transporters after their optimization, both in the gas phase and in DMSO. The theory level used was the same as the one used for complex optimization and this process was carried out with NBO Version 3.1<sup>65</sup> as implemented in Gaussian 09 software package.<sup>60</sup> From this process one was able to obtain both the second order perturbation energies ( $E^2$ ) and the Wiberg Bond Indexes (WBI).

### 2.2.2. Obtaining the Molecular Electrostatic Potential Surfaces

The single point electrostatic potential energy calculations, run at the same level of theory of the optimizations, were performed with the twelve free ligands' geometries extracted from the complexes' optimized structures, both in gas phase and in DMSO. From here it was possible to obtain the  $V_S$  mapped onto the electron density surface of each transporter with a contour of 0.001 electron per Bohr<sup>3</sup>.  $V_{S,max}$  of  $V_S$  were computed using the *multiwfn* program, a multifunctional wavefunction analyser.<sup>66</sup>

### 2.3. Simulations in POPC Bilayer Model

At this stage the goal was to evaluate the ability of the transporters to permeate the phospholipid membrane by passive diffusion. To do so, the 51SD, 52SD and 53SD transporters were put through extensive MD simulations, at atomistic level, carried out in two different setups: the complexes were either placed in the water slab (setup A) or were inserted in the core of the POPC bilayer (setup B).

#### 2.3.1. The Free POPC Bilayer

The phospholipid bilayer used is composed of 128 POPC phospholipids, 6500 water molecules, 18 chloride anions and 18 sodium cations (corresponding to a 0.15M NaCl solution), described with suitable parameters,<sup>67</sup> and was built with a water per lipid ratio of 50.8. This free membrane had already been pre-equilibrated according to the simulation protocol developed by the Molecular Modelling Group, and was also used in previous studies.

The process of equilibration of the free membrane involved a 150 ns simulation, under periodic boundary conditions at 303 K (above POPC membrane phase transition) with force field parameters taken from Lipid14<sup>45</sup> and the ions described with van der Waals parameters developed to be used along with the transferable intermolecular potential 3 point (TIP3P) water model<sup>68</sup>. Structural parameters, such as area per lipid, bilayer thickness, order parameters and electron density profiles for the last 70 ns of simulation were obtained and compared to parameters originally reported for the POPC bilayer system, showing a great level of similarity<sup>69</sup>

### 2.3.2. Simulation of the Chloride Complexes in the POPC Membrane Model

As stated before, two different setups were simulated, one where the complexes started in the water slab (setup A) and another where the complexes were placed in the core of the POPC bilayer (setup B). The protocol for both setups was the same and is presented below. For the placement of the complexes on either setups it was used *Packmol*<sup>70</sup>. For setup A the transporters were placed roughly over 10 Å of the water/lipid interface, see Fig. 19.

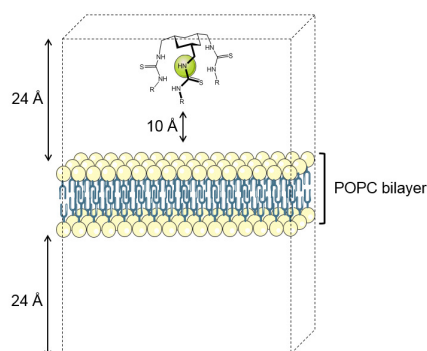


Fig. 19 – Sketch representation of the membrane system for setup A used to carry out the MD simulations.

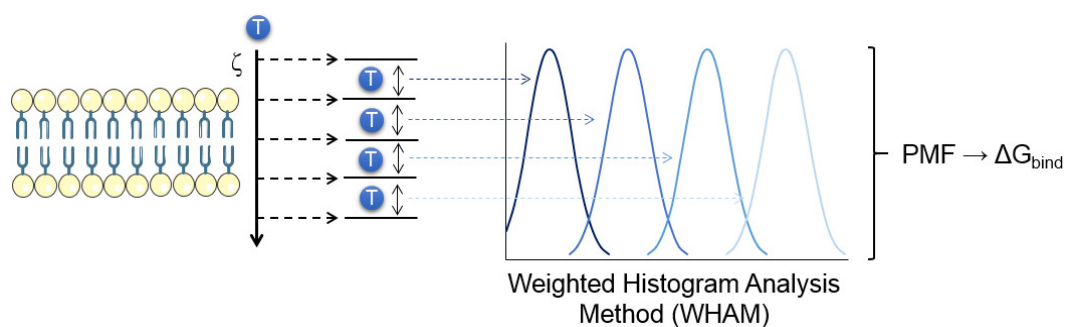
Next followed the MD simulation that consisted in a series of steps starting with 20000 steps (10000 in steepest descent and 10000 in conjugated gradient) of MM energy minimization of the solvent, with a  $500 \text{ kcal mol}^{-1} \text{ \AA}^{-2}$  positional restraint both on the complex and the membrane. Subsequently, the entire system was put through another minimization, equally for 20000 steps. Then, the system was heated to 303 K during 100 ps, using the Langevin thermostat<sup>71</sup> in a canonical ensemble (NVT), with a  $10 \text{ kcal mol}^{-1} \text{ \AA}^{-2}$  restraint on the chloride complex and lipid molecules. Afterwards, the system was adjusted, for 5 ns, in a isothermal-isobaric ensemble (NPT) at 1 atm, controlled by the Berendsen barostat,<sup>72</sup> with isotropic pressure scaling, using a relaxation time of 1 ps, with a  $5 \text{ kcal mol}^{-1} \text{ \AA}^{-2}$  restraint on the complex. Lastly, the positional restraint was removed and the simulation continued for 250ns. The SHAKE algorithm<sup>73</sup> was used to constrain all bonds involving hydrogen atoms, allowing the use of a 2 fs time step. In both setups a 10 Å cutoff was used for the nonbonded interactions. Moreover, these simulations were performed with the pmemd.cuda executable in AMBER16, which allowed to accelerate the explicit solvent Particle Mesh Ewald (PME) calculations,<sup>74</sup> through the use of Graphics Processing Units (GPUs).

This process was applied for the 3 replicates made for the 3 transporters, on both setups.

### 2.4. Computation of Potential of Mean Force

This last part of the experimental procedure regarded the potential of mean force (PMF), which consists of an energy profile along a certain reaction coordinate extracted from a series of umbrella sampling simulations.<sup>75</sup>

In general terms, the process of umbrella sampling consists of a simulation following a determined reaction coordinate,  $\zeta$ , which originates a series of configurations along that same coordinate, this process is designated as Steered Molecular Dynamics (SMD).<sup>75</sup> Then, these coordinates are used for an independent simulation conducted within each sampling window, with the centre of mass (COM) of the transporter restrained in that window by an umbrella biasing potential.<sup>75</sup> The result of these simulations can be traced as histogram with neighbouring windows overlapping such that a continuous energy function can later be derived from these simulations (see Scheme 6).



Scheme 6 – Summary of all the steps involved in obtaining the energy profiles for the transporters being studied.

Therefore, to obtain the PMF profile needed for the 52SD transporter one had to start by performing a SMD, which went as follows.

The first step that was made in this part of the experimental process was to relax the initial structure of the transporter. The structure corresponded to the one used for the MD simulations. The relaxation process consisted of three steps being the first one a 10000 step minimization of the whole system, followed by heating process to 303 K during 100 ps, using the Langevin thermostat<sup>71</sup> in a NVT ensemble, with a 10 kcal mol<sup>-1</sup> Å<sup>-2</sup> restraint on both the chloride complex and the lipids on the membrane. Lastly, and still with this ensemble and temperature, the system was subject of a relaxation step for 100 ps and with a 10 kcal mol<sup>-1</sup> Å<sup>-2</sup> restraint solely on the complex. Afterwards, the complex was pulled along the Z axis using the umbrella method with a harmonic restraint of 5 kcal mol<sup>-1</sup> Å<sup>-2</sup> and a pulling rate of 2.5 Å ns<sup>-1</sup> during a 36 ns simulation. It is also important to note that the positions along the Z axis were sampled in the direction of the normal of the POPC bilayer

and also that the transporter was allowed to move freely in the X-Y plane. The temperature and pressure were set at 303 K and 1 atm, respectively.

Once the SMD process was completed, the windows selection process for the Umbrella Sampling (US) simulations ensued, in which 71 windows were chosen. These 71 independent starting geometries, with the chloride complex evenly spaced by *ca.* 1 Å were simulated for 40 ns in the same conditions as previously described. The receptor was subjected to a force constant of 5 kcal mol<sup>-1</sup> Å<sup>-2</sup> along the Z axis, while the chloride anion was subjected to six N···Cl<sup>-</sup> distance restrains of 5 kcal mol<sup>-1</sup> Å<sup>-2</sup> to preserve the complex. The remaining simulation parameters were the same as for the ones reported for passive diffusion of the transporters across the phospholipid bilayer.

Next, the histograms were plotted and, thus, the PMF curve for the transporter was obtained. The energy profile provided in section 3.3.4 corresponds to the last 20 ns of simulation for 52SD, with the initial half of the US simulations discarded as equilibration periods. Again, the MD simulations were performed with pmemd.cuda executable AMBER16.

### 3. Results and Discussion

#### 3.1. Database Search Analysis

A cornerstone for a molecular modelling study is a good starting structure. Crystallographic databases are crucial regarding the search for chemical structures, if not the pretended, at least similar structures that might work as a starting point. The search intended to gather structures that resembled or matched the transporters being studied in the present thesis, meaning that the starting structures should be cyclohexane- or benzene-based, branched in alternated carbon atoms, have thiourea groups in its composition and aryl substituents.

The framework used as a query in the CSD Database search is depicted in Fig. 20. In the fragment the centre motif in dashed lines can represent either a cyclohexane or a benzene ring, while the X can symbolise both a sulfur atom and an oxygen atom, from a urea or a thiourea group, respectively. This fragment allowed a broad search that yielded a total of 103 hits.

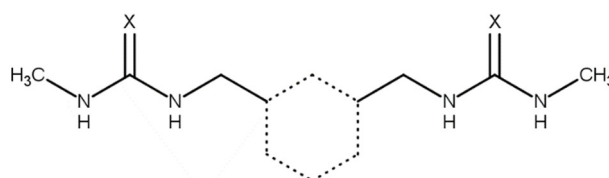


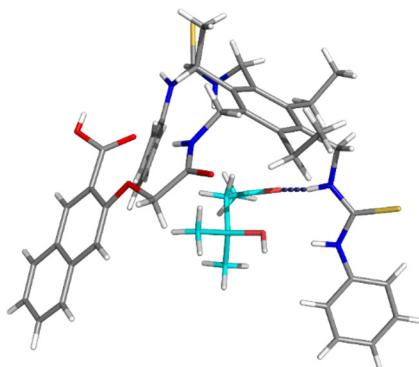
Fig. 20 – Framework used as query for the CSD Database search, where X = S, O.

Out of these 103 structures, only two of them had a tripodal framework, which were deposited in the CSD Database with the *ref codes* RONJUB<sup>76</sup> and RUSBIS<sup>55</sup>. The former contains two thiourea binding units coupled with an amide binding unit and serves as a chemical sensor for glyphosate herbicide.<sup>76</sup> The crystal structure presented in Fig. 21(a) shows the receptor in a tripodal shape that is able to encapsulate a disordered glyphosate by hydrogen bond interactions. The latter crystal structure, RUSBIS, is an anion complex containing two ligands and two chloride anions assembled by water bridges  $[\text{Cl}\mu(\text{OH}_2)_2\text{Cl}]$ . The ligands are actually two 52SD tripodal receptors, which recognise the anions *via* multiple  $\text{NH}\cdots\text{Cl}$  bonds, as shown in Fig. 21(b) (drawn in pink and purple dashed lines).

Indeed, the assemble of two ligands provides enough room to accommodate this  $[\text{Cl}\mu(\text{OH}_2)_2\text{Cl}]$  structural unit, leading to a 2:2 stoichiometry.



(a)



(b)

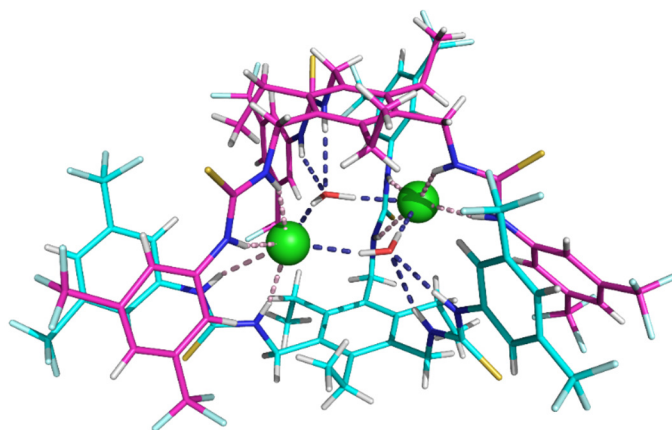


Fig. 21 – 3D representation of (a) molecule with the ref code RONJUB, where the purple dashed lines represent the hydrogen bonds between the ligand and the glyosate molecule, and (b) the anion complex with the ref code RUSBIS, where both the pink and purple dashed lines represent the multiple hydrogen interactions established within the structure's central core.

One of these ligands, together with a chloride anion, was taken from the crystal structure and subsequently used to build the structures of all remaining complexes, by adequate atomic manipulations for them to be used in further molecular investigations. The 1:1 stoichiometry used is in agreement with previous binding and transport studies.

In the Supporting Information section, one can find a table that summarises the most relevant structural parameters of the crystal structure of RUSBIS, as the torsion angle C–C–N–C, starting in the carbon atom of the benzene ring and ending at the carbon atom of thiourea group, as well as the dimensions of the hydrogen bonding interactions (see, section S2). In this table one can see solely measurements for one of the ligands and for just one of the water molecules due to the symmetry of the aggregate ( $C_{2/c}$ ). This means there is a second degree axis, which goes through both chloride anions, allowing the distances and

angles established between a water molecule and a ligand to be the same as the ones established by the other molecule and the remaining ligand.

### 3.2. DFT Geometry Optimizations

The transport ability of an anion carrier is determined by several structural parameters including its lipophilicity, the binding affinity of the transporter for the anion in water phase as well as its ability to release the chloride anion after crossing the phospholipid bilayer. Thus, concerning the binding affinity, all twelve chloride complexes (which chemical structure is represented in Fig. 22) were optimized by DFT using the M06-2X functional and the 6-31+G\*\* basis set, in gas phase and in DMSO. The resulting structures for gas phase are presented in Fig. 23. The optimized structures were further used for the MD simulations.

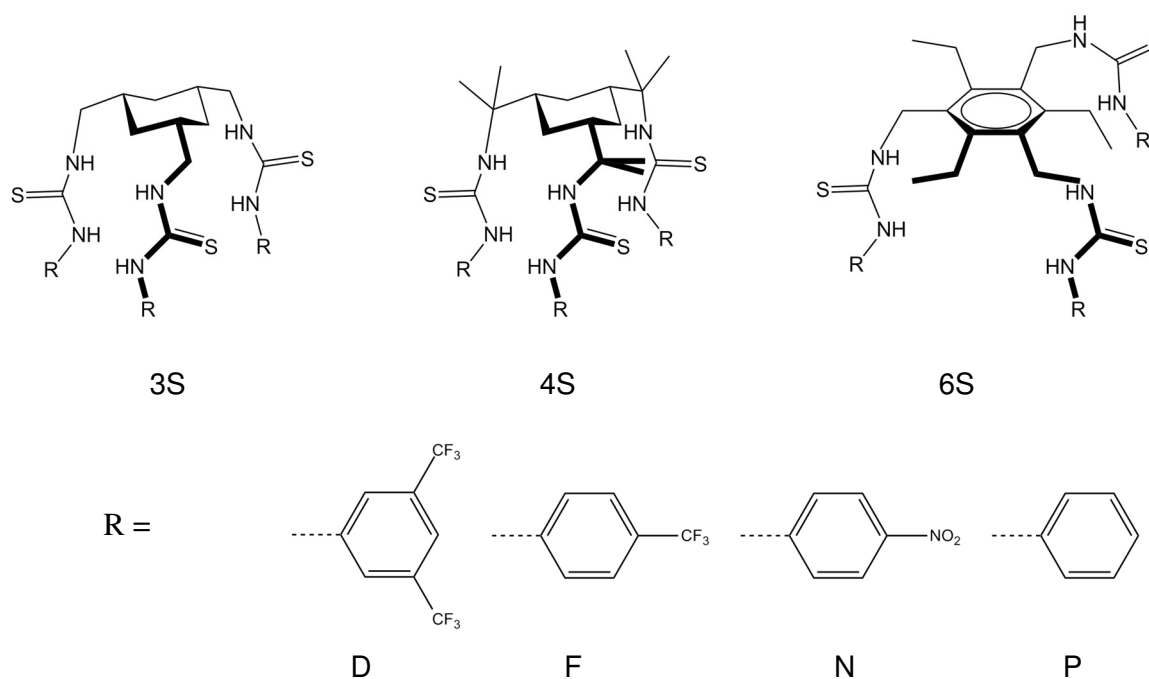


Fig. 22 – Chemical structures of the twelve transporters being studied in the present thesis, where the numbers 3, 4 and 6 represent the scaffold, the “S” identifies the presence of thiourea groups and the letters “D”, “F”, “N” and “P” symbolize the aromatic substituents.

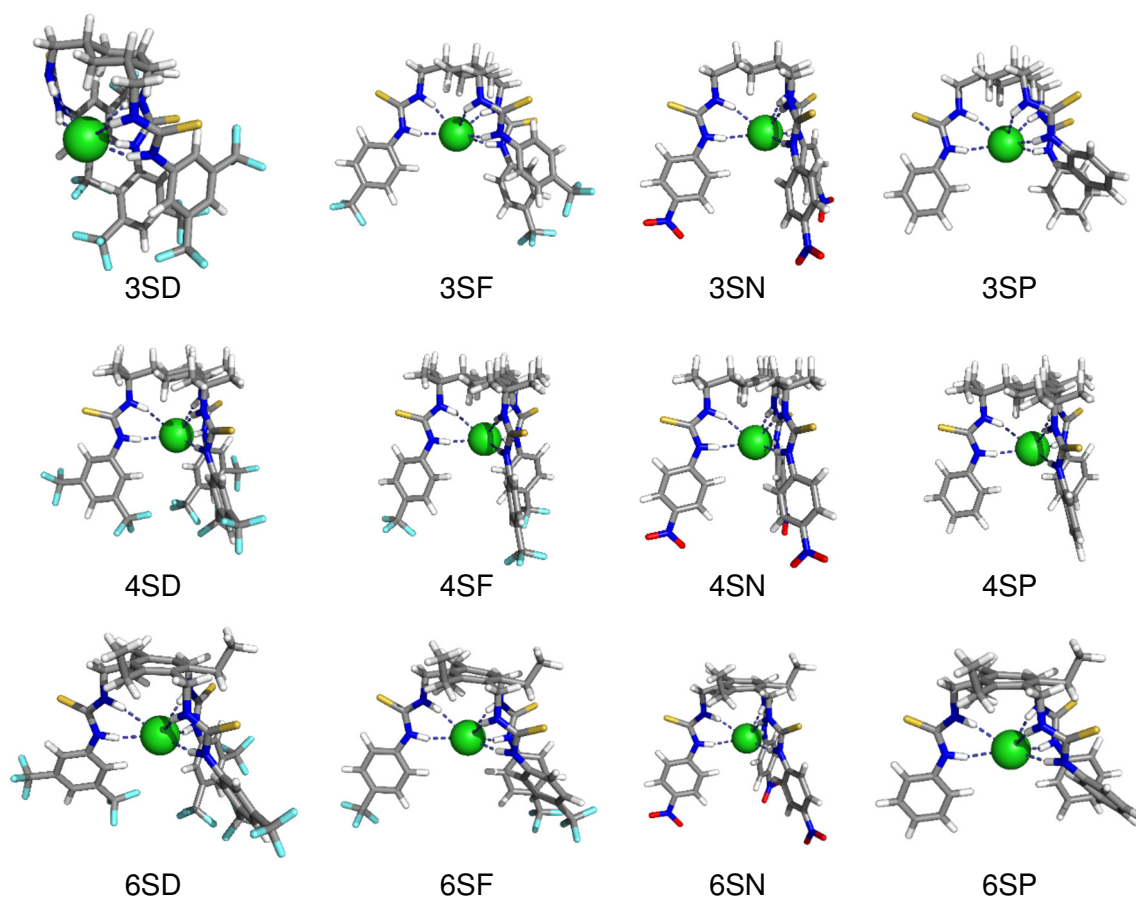


Fig. 23 – Optimized structure of the twelve transporters with a theory level of M062X/6-31+G\*\*, in gas phase.

Overall each complex preserves six putative hydrogen bonds. The hydrogen bonds are almost linear, as shown by the values of the N-H $\cdots$ Cl $\cdots$  angles listed in Table 2, together with the corresponding N $\cdots$ Cl $\cdots$  distances, both in gas phase and in DMSO. Moreover, the individual N $\cdots$ Cl $\cdots$  distances for each binding unit are systematically inequivalent, differing by *ca.* 0.12 Å.

The transporters preserve the tripodal conformational shape, with individual appendages assuming a *trans* configuration characterized by C–C–N–C torsion angles roughly around  $\pm 180^\circ$ . Still, the 3SD complex, which still displays a tripodal shape, has two C–C–N–C torsion angles of  $92.7^\circ$  and  $-90.2^\circ$ , much closer to an ideal *gauche* conformation ( $\pm 60^\circ$ ), while the remaining one of  $-168.2^\circ$  is constant with *trans* configuration. In summary, along these series the most common configuration is *ttt*, with exception of 3SD which is *ggt*.

Table 2 – Summary of the DFT optimization results for all transporters in gas phase and in DMSO (values in italic).

Receptor	N...Cl- Distance (Å)			N-H...Cl- Angle (°)			C-C-N-C Torsion (°)								
	Binding Unit			Binding Unit			Chain								
	3	2	1	3	2	1	3	2	1						
3SD	3.312	3.597	3.186	3.493	3.266	3.445	169.1	155.8	146.8	149.2	153.8	151.4	-168.2	-90.2	92.7
	<i>3.306</i>	<i>3.611</i>	<i>3.195</i>	<i>3.556</i>	<i>3.249</i>	<i>3.493</i>	<i>170.8</i>	<i>154.8</i>	<i>146.4</i>	<i>146.0</i>	<i>153.2</i>	<i>149.0</i>	<i>-171.0</i>	<i>-90.1</i>	<i>93.2</i>
3SF	3.309	3.681	3.392	3.436	3.415	3.365	154.8	141.5	166.1	159.4	164.6	164.9	94.5	-158.2	178.5
	<i>3.338</i>	<i>3.704</i>	<i>3.357</i>	<i>3.517</i>	<i>3.41</i>	<i>3.306</i>	<i>152.0</i>	<i>139.3</i>	<i>167.4</i>	<i>146.4</i>	<i>161.2</i>	<i>161.4</i>	<i>99.6</i>	<i>-139.9</i>	<i>-168.2</i>
3SN	3.461	3.43	3.444	3.426	3.456	3.432	165.8	164.8	166.4	164.2	165.8	163.5	-177.3	-171.8	-169.2
	<i>3.354</i>	<i>3.369</i>	<i>3.361</i>	<i>3.563</i>	<i>3.328</i>	<i>3.977</i>	<i>164.2</i>	<i>160.5</i>	<i>146.9</i>	<i>144.2</i>	<i>155.4</i>	<i>106.7</i>	<i>-160.1</i>	<i>113.2</i>	<i>-99.7</i>
3SP	3.354	3.717	3.434	3.411	3.452	3.378	163.3	137.3	161.2	163.7	164.3	165.7	102.7	-176.0	179.7
	<i>3.34</i>	<i>3.872</i>	<i>3.421</i>	<i>3.433</i>	<i>3.439</i>	<i>3.388</i>	<i>158.6</i>	<i>122.0</i>	<i>160.4</i>	<i>162.8</i>	<i>160.2</i>	<i>162.7</i>	<i>99.9</i>	<i>-170.2</i>	<i>166.0</i>
4SD	3.335	3.458	3.309	3.463	3.312	3.463	168.9	162.7	170.4	161.9	170.9	162.1	178.9	176.1	-179.0
	<i>3.304</i>	<i>3.466</i>	<i>3.285</i>	<i>3.477</i>	<i>3.283</i>	<i>3.475</i>	<i>168.6</i>	<i>161.3</i>	<i>169.4</i>	<i>160.2</i>	<i>171.6</i>	<i>160.5</i>	<i>178.9</i>	<i>173.5</i>	<i>-177.0</i>
4SF	3.348	3.465	3.353	3.473	3.353	3.47	168.8	162.8	169.3	163.1	168.5	163.0	177.6	177.7	178.4
	<i>3.34</i>	<i>3.481</i>	<i>3.345</i>	<i>3.48</i>	<i>3.34</i>	<i>3.487</i>	<i>167.1</i>	<i>161.3</i>	<i>165.3</i>	<i>162.0</i>	<i>167.5</i>	<i>161.3</i>	<i>177.4</i>	<i>176.1</i>	<i>177.5</i>
4SN	3.358	3.477	3.359	3.471	3.35	3.473	170.2	163.2	169.0	163.3	169.5	163.2	-178.3	-178.1	-179.8
	<i>3.31</i>	<i>3.483</i>	<i>3.328</i>	<i>3.473</i>	<i>3.312</i>	<i>3.481</i>	<i>166.4</i>	<i>161.0</i>	<i>163.9</i>	<i>161.5</i>	<i>168.1</i>	<i>161.3</i>	<i>-172.9</i>	<i>-175.0</i>	<i>178.7</i>
4SP	3.354	3.464	3.348	3.459	3.365	3.457	169.4	163.5	169.9	163.4	168.9	163.8	178.7	-179.2	179.0
	<i>3.364</i>	<i>3.484</i>	<i>3.37</i>	<i>3.487</i>	<i>3.377</i>	<i>3.481</i>	<i>165.1</i>	<i>162.3</i>	<i>165.1</i>	<i>162.4</i>	<i>164.0</i>	<i>162.8</i>	<i>176.9</i>	<i>178.3</i>	<i>178.3</i>
6SD	3.404	3.489	3.422	3.451	3.453	3.36	167.5	158.8	164.0	157.1	163.9	165.4	-151.2	140.2	179.1
	<i>3.37</i>	<i>3.516</i>	<i>3.358</i>	<i>3.479</i>	<i>3.444</i>	<i>3.368</i>	<i>167.2</i>	<i>151.7</i>	<i>165.5</i>	<i>149.8</i>	<i>162.6</i>	<i>162.1</i>	<i>-142.9</i>	<i>132.8</i>	<i>164.5</i>
6SF	3.454	3.385	3.431	3.524	3.413	3.388	164.3	164.1	166.0	158.3	157.5	163.0	-166.8	126.8	-150.6
	<i>3.478</i>	<i>3.408</i>	<i>3.381</i>	<i>3.524</i>	<i>3.571</i>	<i>3.381</i>	<i>160.7</i>	<i>159.2</i>	<i>165.3</i>	<i>149.8</i>	<i>147.1</i>	<i>167.4</i>	<i>-155.4</i>	<i>125.7</i>	<i>-143.3</i>
6SN	3.454	3.433	3.524	3.388	3.443	3.431	166.3	163.0	162.8	166.1	166.1	161.7	-164.2	166.9	158.8
	<i>3.451</i>	<i>3.422</i>	<i>3.426</i>	<i>3.464</i>	<i>3.467</i>	<i>3.403</i>	<i>162.7</i>	<i>158.4</i>	<i>164.6</i>	<i>152.9</i>	<i>162.6</i>	<i>159.2</i>	<i>-155.1</i>	<i>136.8</i>	<i>160.9</i>
6SP	3.467	3.403	3.432	3.515	3.47	3.353	163.9	163.4	165.4	157.2	157.7	166.3	-160.3	128.0	-153.0
	<i>3.556</i>	<i>3.408</i>	<i>3.384</i>	<i>3.557</i>	<i>3.585</i>	<i>3.369</i>	<i>158.0</i>	<i>163.0</i>	<i>166.3</i>	<i>150.8</i>	<i>152.8</i>	<i>169.7</i>	<i>-161.9</i>	<i>124.8</i>	<i>-155.8</i>

The strength of the hydrogen bond interactions was ascertained using the following quantum descriptors:  $E^2$ , WBI and  $V_{S,max}$  of molecular electrostatic potential (MEP) surface. The  $E^2$  value as well as the WBI were obtained from the NBO analysis. This analysis takes into account the interactions established between occupied (that is, bonding or lone pair) Lewis-type NBOs and antibonding non-Lewis NBOs, being the former designated donor and the latter acceptor. The energy of said interactions is estimated by second order perturbation theory analysis of the Fock matrix<sup>77</sup>, according to the following equation:

$$E^2 = \Delta E_{ij} = q_i \frac{F(i,j)^2}{\varepsilon_j - \varepsilon_i} \quad (6)$$

Where  $i$  and  $j$  represent the donor and acceptor orbitals, respectively,  $q_i$  symbolizes the donor orbital occupancy,  $F(i,j)$  is the Fock matrix elements between the NBO  $i$  and  $j$ , and lastly,  $\varepsilon_i$  and  $\varepsilon_j$  are the orbital energies.<sup>77</sup>

The WBI and  $E^2$  values for hydrogen bonds, calculated in gas phase and in DMSO, are summarized in Table 3, along with  $V_{S,max}$  values, binding affinity constants ( $K_a$ ) measured in DMSO (provided by previous studies)<sup>54-55</sup> and the fluorescence decay half-lives ( $t_{1/2}$ ) for the chloride-nitrate exchange reported for transport ability purposes (also provided by previous studies).<sup>54-55</sup> Along the three series of chloride complexes, the WBI, in both environments, mirror the pattern of the  $N \cdots Cl^-$  distances found for each binding unit.

The MEP surfaces for all the twelve transporters were calculated, both in gas phase and also using PCM for DMSO solvent model, through a single point calculation on the complex's previously optimized structure at the same theory level, removing the chloride anion (the remaining computational details are given in the experimental section, see chapter 2.2.2). The mapped distribution on the transporter's molecular surfaces are illustrated for 3SD, 3SP, 4SD, 4SP, 6SD and 6SP, which are molecules with markedly distinct electron properties, in Fig. 24, together with the position of three highest values of electrostatic potential identified as black dots.

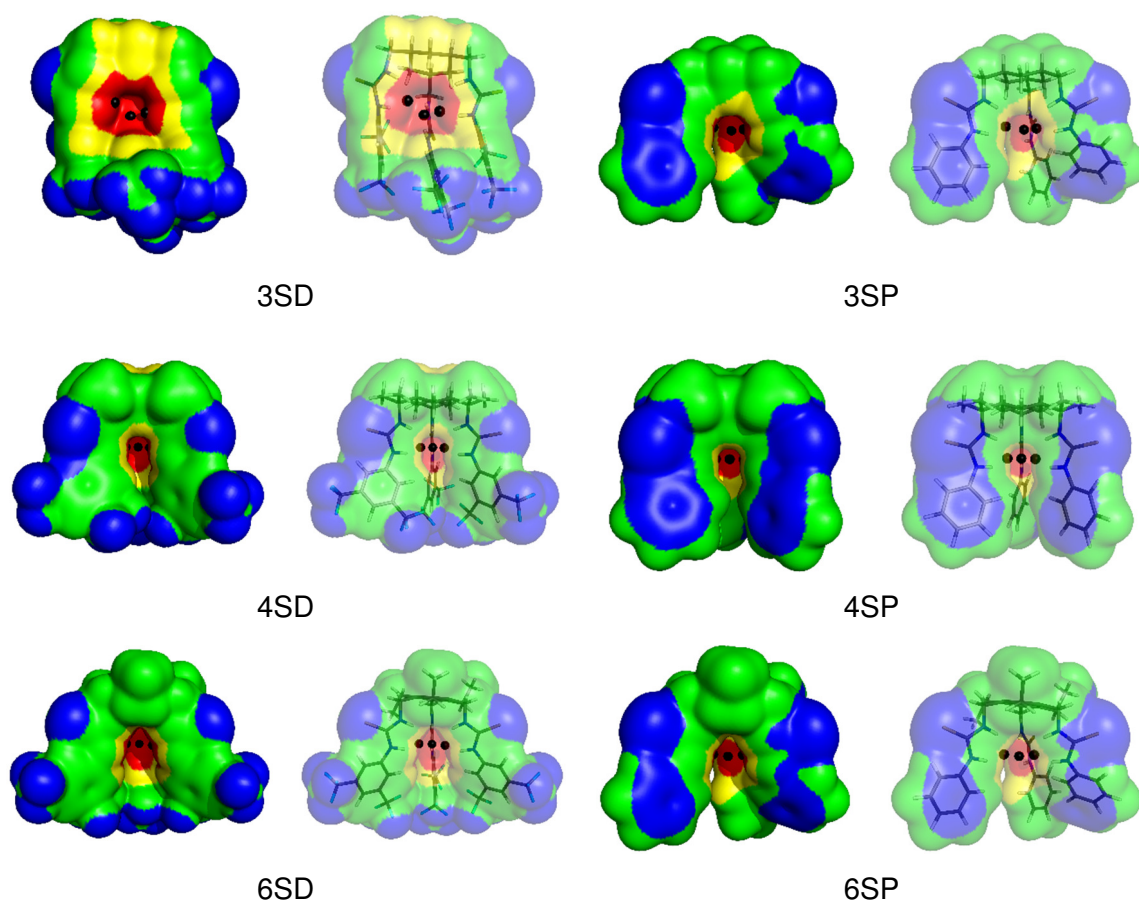


Fig. 24 – Electrostatic potential mapped on the molecular electron density surface (0.001 electron per Bohr<sup>3</sup>) of 3SD, 3SP, 4SD, 4SP, 6SD and 6SP. The three highest values for each transporter are represented as black dots on the molecular surfaces. The colour scales range from blue to red from -16 kcal mol<sup>-1</sup> to 77 kcal mol<sup>-1</sup> in all representations.

Throughout the series of transporters, all molecules exhibit the most positive region (red) inside of the tripodal binding pocket and three local maxima of  $V_S$ , placed in the middle of each binding unit, and one of them corresponds to the molecule's  $V_{S,max}$ . In contrast, the negative regions enclose the thiourea's sulfur atoms as well as the electron withdrawing substituents (-CF<sub>3</sub> and -NO<sub>2</sub>).

All twelve transporters display higher  $V_{S,max}$  values in DMSO than in gas phase due to the presence of the solvent.

Distinct electron withdrawing groups present in the molecules lead to a difference in the acidic character of the NH binding group, that is, they give a different binding ability for hydrogen bonding, which might play a role in the modulation of the chloride transport.

In Fig. 25 the log of dissociation constant (logK) are plotted against the  $V_{S,max}$ , estimated in gas phase and DMSO, for the three series of transporters. The  $V_{S,max}$  increase with association constants (logK) in both media reflecting the electronic withdrawing effects of the substituents. This trend follows the order P < F < D < N, so transporters that have in

their constitution *p*-nitrophenyl substituents, have the highest  $V_{S,max}$  followed by the transporters that are composed of two 3,5-phenyl(trifluoromethyl) groups, then by the one that have a *p*-trifluoromethyl substituent and lastly the transporters with phenyl substituents. In other words, in compounds with *p*-nitrophenyl substituents (the strongest withdrawing group) the NH protons are more acidic while the unsubstituted molecules the NH protons have less propensity to bind the chloride anion.

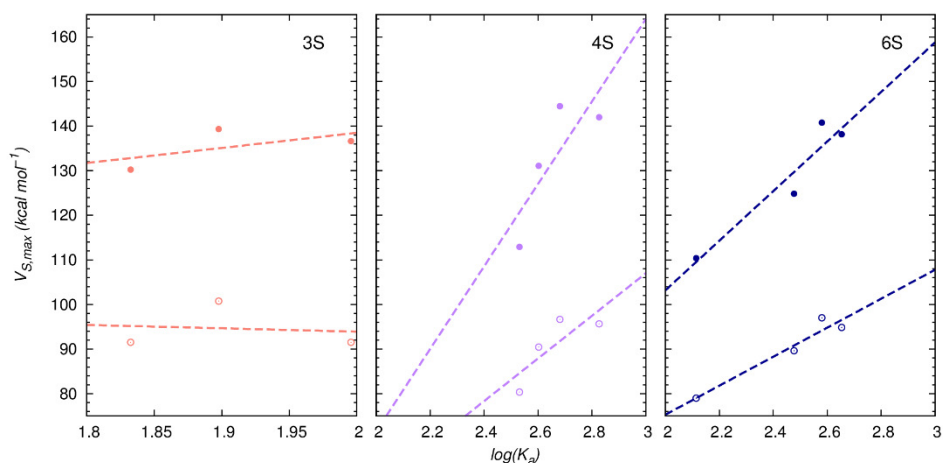


Fig. 25 – Plot of the  $V_{S,max}$  values against  $\log(K_a)$  for the three series of transporters in gas phase (unfilled dots) and in DMSO (solid dots). For the 3S series  $R^2=0.013$  and  $R^2=0.351$ , for gas phase and DMSO, respectively. For the 4S series  $R^2=0.657$  and  $R^2=0.662$ , for gas phase and DMSO, respectively. For the 6S series  $R^2=0.936$  and  $R^2=0.906$ , for gas phase and DMSO, respectively.

By plotting  $\log(E^2)$  against the values for  $V_{S,max}$ , or even  $E^2$  against  $\log(K_a)$ , one can say that it is not possible to establish a straightforward relationship between none of these descriptors, apart of the 4S series, see Fig. 26.

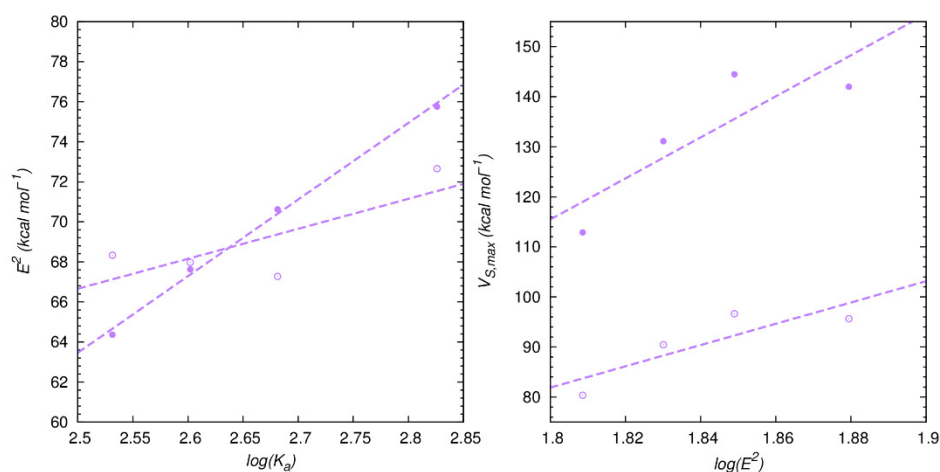


Fig. 26 – Plot of the  $E^2$  values against  $\log(K_a)$  (provided in Anthony Davis' paper regarding these transporters)<sup>54-55</sup> and for  $V_{S,max}$  against  $\log(E^2)$  for the 4S series in gas phase (unfilled dots) and in DMSO (solid dots). The correlation coefficients for the  $E^2$  vs  $\log(K_a)$  plot in gas phase and in DMSO are  $R^2 = 0.600$  and  $R^2 = 0.996$ , respectively. As for the  $V_{S,max}$  vs  $\log(E^2)$  plot they are  $R^2 = 0.735$  and  $R^2 = 0.733$  in the gas phase and DMSO, respectively.

Table 3 – Summary of quantum descriptors for all transporters in gas phase and in DMSO (values in italic).  
The values for  $K_a$  and  $t_{1/2}^f$  were taken from previous studies.<sup>54-55</sup>

	<b>H...Cl<sup>-</sup> E<sup>2</sup></b> <b>(kcal mol<sup>-1</sup>)</b>	<b>WBI</b> <b>(sum)</b>	<b>V<sub>S,max</sub></b> <b>(kcal mol<sup>-1</sup>)</b>	<b>logP</b>	<b>K<sub>a</sub> in</b> <b>DMSO (M<sup>-1</sup>)</b>	<b>t<sub>1/2</sub><sup>f</sup> (s)</b>
3SD	67.38	0.2191	91.524	12.62	99	160
	<i>65.24</i>	<i>0.2130</i>	<i>136.615</i>			
3SF	63.08	0.2060	91.525	6.70	68	440
	<i>57.59</i>	<i>0.1893</i>	<i>130.227</i>			
3SN	63.18	0.2090	100.733	5.04	79	340
	<i>54.37</i>	<i>0.1796</i>	<i>139.359</i>			
3SP	60.71	0.1995	81.935	3.67	-	-
	<i>58.07</i>	<i>0.1919</i>	<i>114.350</i>			
4SD	72.66	0.2332	95.657	14.71	670	13
	<i>75.76</i>	<i>0.2407</i>	<i>141.990</i>			
4SF	67.97	0.2221	90.463	8.79	400	36
	<i>67.62</i>	<i>0.2219</i>	<i>131.095</i>			
4SN	67.27	0.2203	96.644	7.13	480	66
	<i>70.63</i>	<i>0.2290</i>	<i>144.471</i>			
4SP	68.33	0.2227	80.362	5.76	340	190
	<i>64.36</i>	<i>0.2129</i>	<i>112.890</i>			
6SD	65.58	0.2179	94.850	15.48	450	19
	<i>65.01</i>	<i>0.2141</i>	<i>138.162</i>			
6SF	64.47	0.2147	89.628	9.57	300	81
	<i>58.87</i>	<i>0.1990</i>	<i>124.823</i>			
6SN	63.97	0.2145	96.997	7.91	380	310
	<i>61.61</i>	<i>0.2062</i>	<i>140.789</i>			
6SP	64.07	0.2136	78.988	6.53	130	510
	<i>59.41</i>	<i>0.1998</i>	<i>110.377</i>			



For this series, the  $E^2$  values estimated in gas phase plotted against  $\log K$  do not follow a linear trend, leading to a  $R^2$  value of 0.600. In contrast, when this plot is made with the values obtained in DMSO a linear relationship emerges with a  $R^2 = 0.996$ . This linear relation between the  $E^2$  and  $\log K$  in DMSO indicates that polar nature of the solvent may have an important role on the strength of the hydrogen bonding interactions, *i.e.* on the transporters' binding affinity for chloride. The  $E^2$  values increase linearly with  $V_{S,max}$  only for the P, F and N transporters ( $R^2 = 0.87$ ), excluding the 3,5-trifluoromethyl derivative. Given that the  $V_{S,max}$  is a measure of the acidic character of the NH binding units, (*i.e.* a compound with a high  $V_{S,max}$  value has a higher propensity to take part in hydrogen bond interactions, as a proton donor) these facts suggests that the  $NH\cdots Cl^-$  interactions have a certain degree of covalence. Indeed, the sum of the WBI listed in Table 3, for the six binding units increases with the  $E^2$  values, as shown in Fig. 27.

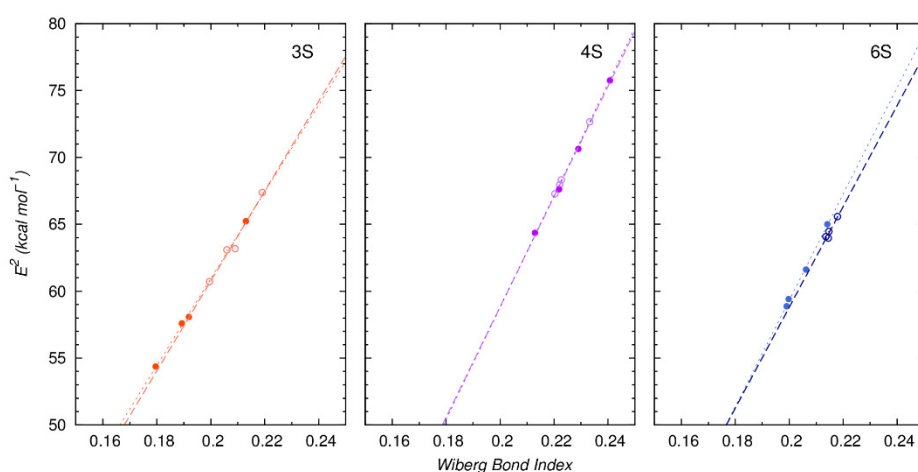


Fig. 27 – Plot of the  $E^2$  values against the WBI for the three series of transporters in gas phase (unfilled dots) and in DMSO (solid dots). The correlation coefficients for the 3S series are  $R^2 = 0.978$  and  $R^2 = 0.999$  in gas phase and DMSO, respectively; for the 4S series are  $R^2 = 0.999$  and  $R^2 = 0.0998$  in gas phase and DMSO, respectively; as for the 6S series are  $R^2 = 0.923$  and  $R^2 = 0.997$  in gas phase and DMSO, respectively.

By looking at Table 3, one can clearly see a trend. Among the three series, the best transporters (3,5-trifluoromethyl derivatives) are the ones with the highest values for  $E^2$ ,  $K_a$  and  $\log P$ . The best transporters are the most lipophilic ones with higher affinity towards chloride anion. In other words, the high values of the quantum descriptors allow these transporters to uptake a chloride from water phase and then transport it across the phospholipid bilayer and subsequently release the chloride anion to the opposite water phase, as illustrated further by MD simulations.

Moreover, when comparing the three D transporters, where the only structural difference is the scaffold, the best transporter is 4SD, with higher  $E^2$  and  $K_a$ , and a slightly lower  $\log P$  than 6SD ( $\log P_{4SD}=14.71$  and  $\log P_{6SD}=15.48$ ). This comparison suggests that the transport ability is a delicate balance between the binding affinity and lipophilicity.

### 3.3. Receptor's MD Simulations Analysis

The MD simulations in POPC model were performed using two different initial configurations, as depicted in Fig. 28. In setup A the chloride complexes 3SD, 4SD and 6SD, obtained *via* DFT optimizations (*vide supra*), were initially placed in the water slab, free of restrains, so that they could move freely. On the other hand, in setup B the anion complexes were located inside the bilayer membrane, between the membrane's phospholipids.

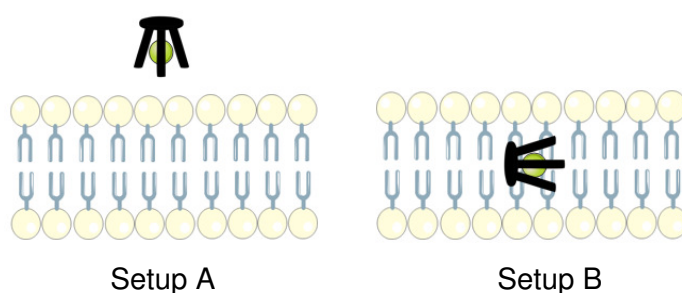


Fig. 28 – Schematic representation of both MD setups used. The tripodal structures are represented as a black stool-like shape.

These two initial configurations allowed to evaluate the diffusion ability of the transporters and their complexes through the membrane, as well as, the eventual uptake and/or release of chloride anion and, finally, the interaction between the transporters and the phospholipid head groups at the water/lipid interface.

In this analysis, solely three transporters (3SD, 4SD and 6SD, see Fig. 22) were investigated by MD simulations due to time constraints. Among the three series, these transporters were selected given their recognized transport abilities. Three independent replicates, of 250 ns, were carried out at 303K for each transporter in both setups.

To ease the interpretation of the results an ID system is applied derived from the combination of the initial setup, replicate and receptor, for instance, A<sub>1</sub>3SD stands for the first replicate of 3SD transporter in setup A.

### 3.3.1. Structural Impact of the Transporters in the POPC Membrane Model

The structural impact of the transporters in the bilayer model was evaluated by ascertaining several structural parameters, namely area per lipid, membrane thickness, electron density profiles and order parameters. The average values obtained for area per lipid and the membrane thickness, for the three transporters, in both setups, are compared in Table 4 to the values obtained for the free membrane.<sup>69</sup> A more detailed version of this table is given in the Supporting Information, along with the plots of the electron density profiles and the order parameters (see, sections S3 and S4).

Overall, all the average values for area per lipid and membrane thickness are similar to those reported for the free simulated POPC membrane model, as well as the profiles for electron density and order parameters. In other words, the transporters have a marginal impact on the membrane's structure, turning these molecules potential candidates to assist anion transmembrane transport in replacement therapies.

Table 4 – Summary of the results obtained for area per lipid and membrane thickness, for the three transporters in study, in both setups, in comparison with the values for the POPC model.

	Area per Lipid ( $\text{\AA}^2$ )			Membrane Thickness ( $\text{\AA}$ )			
	Avg $\pm$ SD	Min	Max	Avg $\pm$ SD	Min	Max	N
POPC Model	65.58 $\pm$ 1.19	61.98	68.98	37.75 $\pm$ 0.57	36.05	39.60	7000
A3SD	65.70 $\pm$ 1.18	61.61	70.34	37.87 $\pm$ 0.55	35.79	39.76	30000
A4SD	65.96 $\pm$ 1.37	62.08	71.02	37.84 $\pm$ 0.65	35.47	39.74	30000
A6SD	65.85 $\pm$ 1.12	62.27	69.82	37.90 $\pm$ 0.53	36.16	40.06	30000
B3SD	65.99 $\pm$ 1.17	62.02	70.06	37.87 $\pm$ 0.55	36.16	40.16	30000
B4SD	65.62 $\pm$ 1.17	62.32	69.16	38.03 $\pm$ 0.56	35.97	39.81	30000
B6SD	65.28 $\pm$ 1.17	61.66	69.13	38.14 $\pm$ 0.55	36.26	39.87	30000

### 3.3.2. Transporters' Diffusion in the Phospholipid Bilayer

The analysis of the passive diffusion was started with simulations carried out in setup A, for all three transporters, followed by the simulations performed in setup B.

The relative position of each transporter relatively to the membrane's interface was evaluated by the  $P_{\text{int}} \cdots \text{Core}_{\text{COM}}$ , throughout the simulation time, in which  $P_{\text{int}}$  represents the

COM determined by the phosphorus atoms of the phospholipid head groups, from the closest leaflet of the membrane lipid interface, while  $Core_{COM}$  denotes the COM of the transporters' centre motif (see Fig. 29, in red). Moreover, the  $P_{int} \cdots CF_{3COM}$  distance was also tracked, where  $CF_{3COM}$  is the COM defined by the carbon atoms from terminal  $CF_3$  substituent groups, (see Fig. 29, in blue). The simultaneous use of these two distances also gives the transporter's orientation in the bilayer membrane.

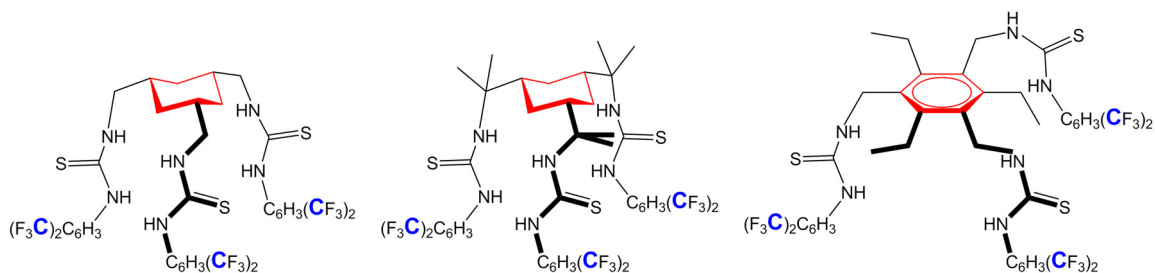


Fig. 29 – Chemical structure of the three transporters put through MD simulations (3SD, 4SD and 6SD, from left to right) were the atoms that define  $Core_{COM}$  are highlighted in red and the atoms that define  $CF_{3COM}$  are highlighted in blue.

The evolution of the  $P_{int} \cdots Core_{COM}$  (red line) and  $P_{int} \cdots CF_{3COM}$  (blue line) distances for a 250 ns simulation time are presented in Fig. 30, Fig. 31 and Fig. 32 for the three replicates of 3SD, 4SD and 6SD, respectively.

These figures also include the counting of the  $NH \cdots Cl^-$  hydrogen bonds (green line) established between the thiourea binding sites and any of the 18 chloride anions present in the bilayer system as well as the counting of  $NH \cdots PO_4$  hydrogen bonds (orange line) established between the thiourea binding site and the phosphate head groups of the phospholipid bilayer. The counting of the  $NH \cdots Cl^-$  interactions allowed to ascertain the eventual chloride uptake events when the transporters were in the water phase or within the phospholipid bilayer. Furthermore, the  $NH \cdots Cl^-$  and  $NH \cdots PO_4$  interactions were counted using  $N \cdots Cl^-/PO_4$  distance and  $NH \cdots Cl^-/PO_4$  angle cut-off of 3.5 Å and 120°, respectively, in agreement with  $NH \cdots Cl^-/PO_4$  dimensions found in CSD database for single crystal x-ray structures of similar tripodal chloride complexes.<sup>33, 78</sup>

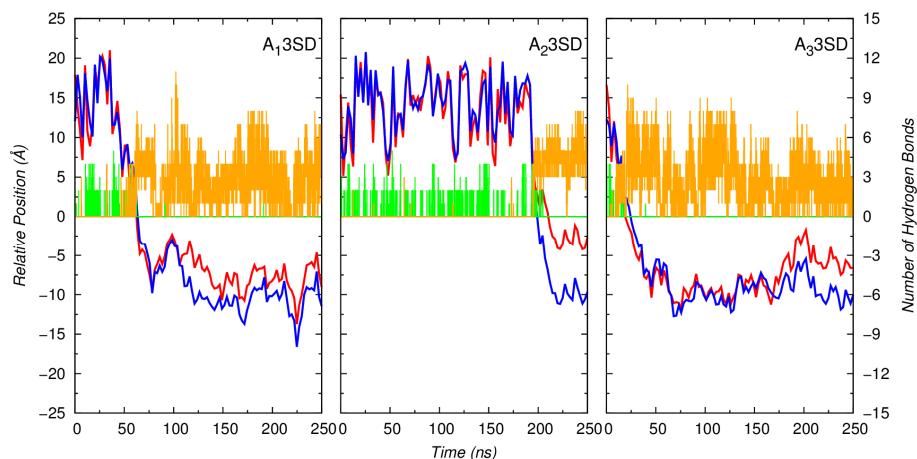


Fig. 30 – Evolution of the  $P_{int} \cdots Core_{COM}$  (in red) and the  $P_{int} \cdots CF_{3COM}$  (in blue) distances for the 3SD transporter. The water/lipid interface is at a relative position of 0 Å. The counting of hydrogen bonds to chloride anions and phospholipid head groups is represented in green and orange, respectively. The data for  $P_{int} \cdots Core_{COM}$  and  $P_{int} \cdots CF_{3COM}$  was smoothed with Béziers curves.

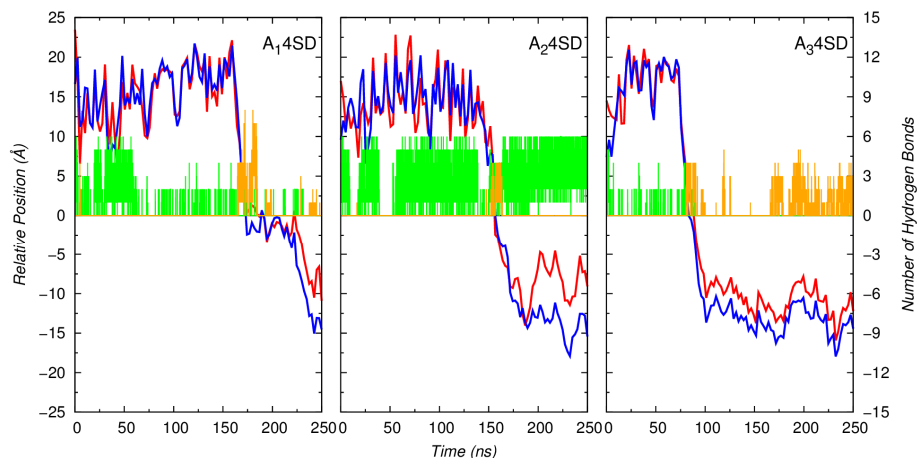


Fig. 31 – Evolution of the  $P_{int} \cdots Core_{COM}$  (in red) and the  $P_{int} \cdots CF_{3COM}$  (in blue) distances for the 4SD transporter. The water/lipid interface is represented at a relative position of 0 Å. Remaining details as given in Fig.30.

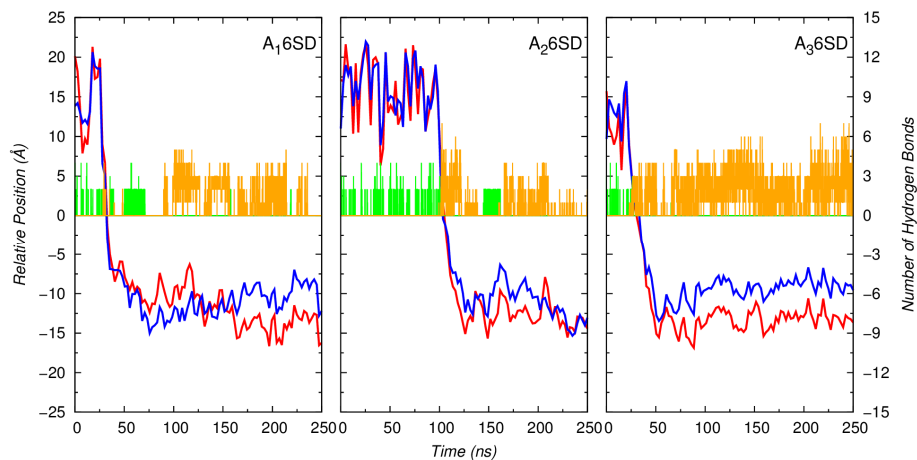
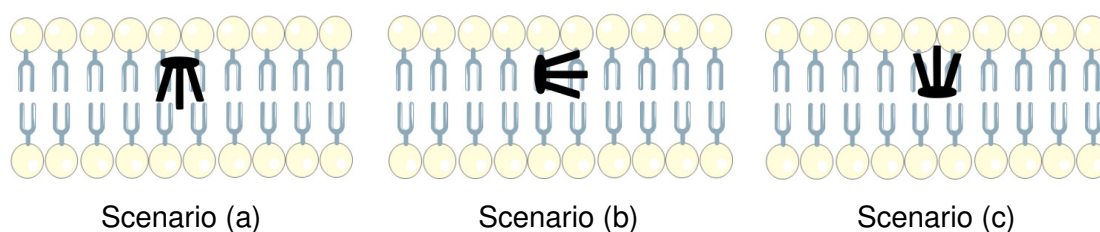


Fig. 32 – Evolution of the  $P_{int} \cdots Core_{COM}$  (in red) and the  $P_{int} \cdots CF_{3COM}$  (in blue) distances for the 6SD transporter. The water/lipid interface is represented line at a relative position of 0 Å. Remaining details as given in Fig.30.

Overall, all the transporters passively migrate from the water slab towards the water/lipid interface and subsequently permeate the phospholipid bilayer. In the water phase, as expected, all transporters exhibit a random orientation. On the other hand, when inside the phospholipid bilayer, they assume three preferential orientations with the transporter almost preserving the tripodal shape, as depicted in Scheme 7. In scenario (a) the  $-CF_3$  alkyl chains are pointing towards the centre of phospholipid bilayer, almost parallel to the membrane's normal, while  $Core_{COM}$  is closer to the membrane interface; in scenario (b)  $Core_{COM}$  and  $CF_{3COM}$  are equidistant to the membrane's interface and the transporter is nearly orthogonal to the membrane's normal; lastly, in scenario (c) the transporter adopts a spatial disposition antiparallel to scenario (a).



Scheme 7 – Schematic representation of the main spatial dispositions adopted by the transporters throughout the MD simulations. The tripodal structures are represented as a black stool-like shape.

Indeed, while in the scenarios (b) and (c), the thiourea binding units are closer to the membrane interface enabling the transporters to establish potential hydrogen bonding interaction with water molecules from the water slab, phospholipid head groups or chloride anions.

For 3SD, after membrane permeation, the transporter evidently adopts the spatial disposition (a) in  $A_23SD$ . This disposition is also observed in the last 150 ns of  $A_13SD$  and between 175<sup>th</sup> and the 250<sup>th</sup> ns in  $A_33SD$ . For these two replicates, during the remaining simulation time, within the phospholipid bilayer, the transporter adopts the disposition of scenario (b).

Regarding 4SD, when it diffuses through the bilayer membrane, in all three replicates, it is clear that the transporter adopts the disposition in scenario (a).

Considering the 6SD transporter, when permeating the membrane bilayer, in the first replicate,  $A_16SD$ , the transporter oscillates between scenarios (a) and (c), passing by a transition to scenario (b). On the other hand, in the second replicate the transporter adopts both scenario (c) and (b), in this order, while in the third one it prefers the spatial disposition (c).

Noteworthy, the three transporters, in water phase, are able to recognize several chloride anions via intermittent hydrogen bonding interactions, and subsequently they permeate the membrane as a chloride complexes, nesting below the lipid interface. Overall, apart of A<sub>2</sub>4SD, the transporters release the chloride anion to the water phase as they permeate the membrane. Concomitantly, these N-H···Cl<sup>-</sup> bonds are replaced by new ones with phospholipid head groups, as shown in Fig. 30, Fig. 31 and Fig. 32, for the three transporters.. An inset on hydrogen bonding interactions to the phospholipid head groups are shown in Fig. 33.

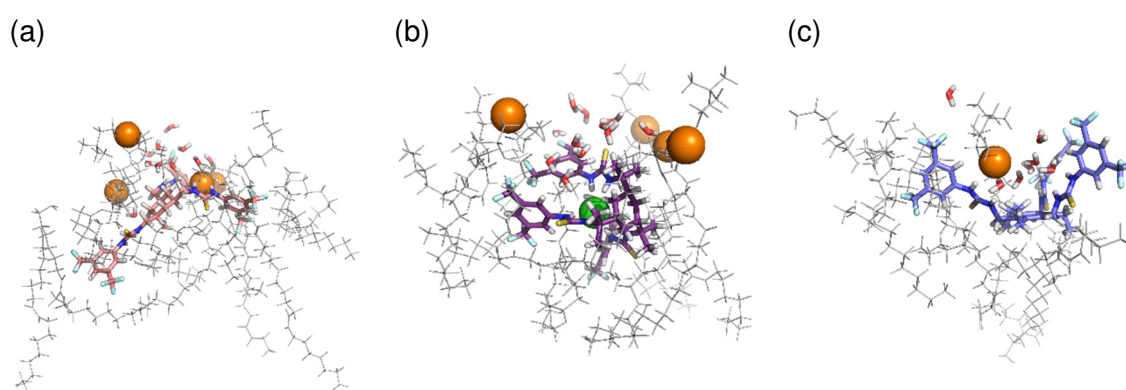


Fig. 33 – Snapshots of the interactions between the transporters (a) 3SD, (b) 4SD and (c) 6SD with the phosphate head groups of the bilayer membrane and water molecules at a distance of 3 Å. The carbon atoms of the transporters are represented in salmon, purple and dark blue for (a), (b) and (c), respectively, while the hydrogen atoms are represented in white, the nitrogen atoms in blue and the sulfur atoms in yellow. The chloride and phosphorus atoms are represented as green and orange spheres, respectively, as for the carbon atoms of the POPC lipids are represented as grey lines. The snapshot in (a) was taken from A<sub>1</sub>3SD, from A<sub>2</sub>4SD for (b) and A<sub>1</sub>6SD for (c).

Overall, the increase of these hydrogen bonding interactions leads to a decrease in hydrogen bonds between the thiourea binding sites and water molecules for all transporters, (see Fig. 34, Fig. 35 and Fig. 36). On other hand, in the second replicate of the 4SD transporter, A<sub>2</sub>4SD, the chloride complex is maintained until the end of the simulation time with all CF<sub>3</sub> alkyl substituents pointing to the centre of the membrane bilayer. Furthermore, the transporter adopts the spatial disposition described in scenario (b), sheltering the anion from the water phase until the end of the simulation time, as shown in Fig. 31. In other words, the third step of the anion carrier mechanism, *i.e.* the release of the chloride anion to the opposite water slab, was not observed. To observe this event, it was decided to extend the simulation time, which is currently in progress.

Fig. 32 shows that in the first and second replicates of 6SD, this transporter is able to sporadically uptake chloride anions for significant simulation periods of time (*ca.* 25 ns)

while it is within the membrane bilayer. This event, in the first replicate, is observed while the transporter adopting a spatial disposition (b), whereas in the second replicate it exhibits disposition (c), showing that both spatial dispositions allow chloride recognition.

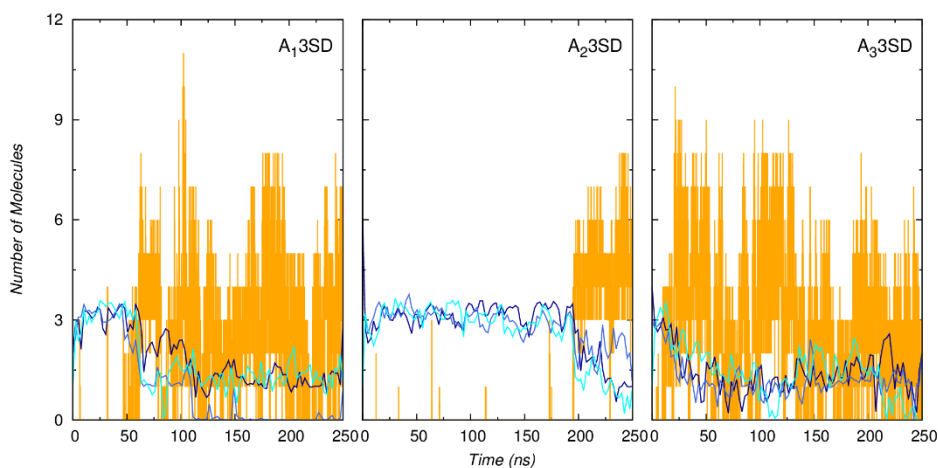


Fig. 34 – Evolution of the number of water molecules at a distance of 3.4 Å of the three binding sites of 3SD (in three different shades of blue) and evolution of the number of hydrogen bonds with the phosphate head groups (in orange). The hydration data was smoothed with Bézier curves.

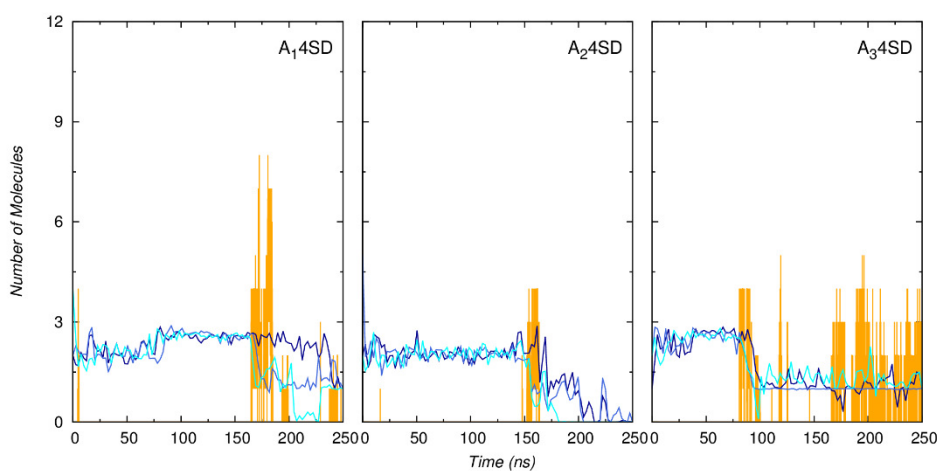


Fig. 35 – Evolution of the number of water molecules at a distance of 3.4 Å for the three binding sites of 4SD (in three different shades of blue) and evolution of the number of hydrogen bonds with the phosphate head groups (in orange). The hydration data was smoothed with Bézier curves.



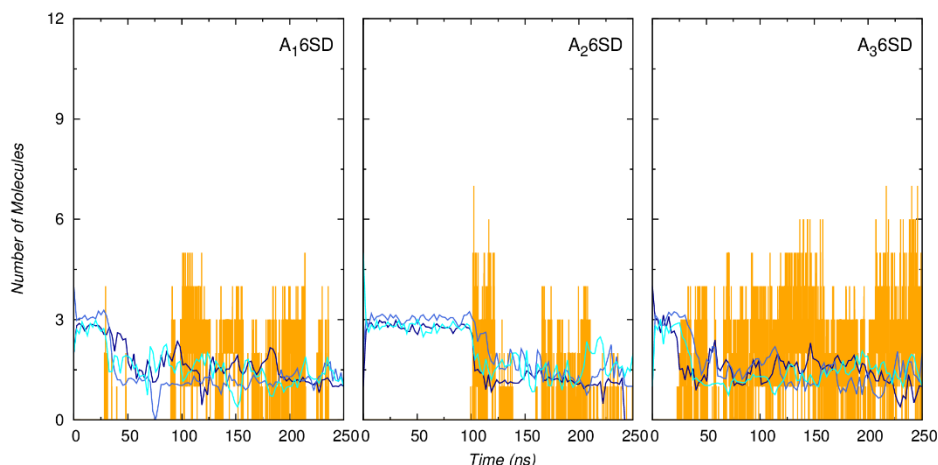


Fig. 36 – Evolution of the number of water molecules at a distance of 3.4 Å for the three binding sites of 6SD (in three different shades of blue) and evolution of the number of hydrogen bonds with the phosphate head groups (in orange). The hydration data was smoothed with Bézier curves.

The passive diffusion events reported above for the three transporters are depicted in detail in Fig. 37, Fig. 38 and Fig. 39, with selected snapshots, taken from a single replicate for 3SD, 4SD and 6SD, respectively. In Fig. 37, the first replicate for 3SD shows that the transporter permeates the membrane, with the 3,5-trifluoromethyl substituent first, losing the tripod-like conformational shape, which is further restored during the last nanoseconds of simulation, with the transporter nested in the spatial disposition (a). Fig. 38 shows that the 4SD transporter permeates the membrane associated to a chloride anion, adopting, unequivocally inside of the membrane, a spatial disposition (a) which prevented the release of the chloride anion during the simulation time. Lastly, Fig. 39 shows that the passive diffusion of 6SD occurs likewise 3SD through the phospholipid bilayer via a tumbling movement with the transporter being able to recognise intermittently a chloride anion in a (b) spatial disposition.

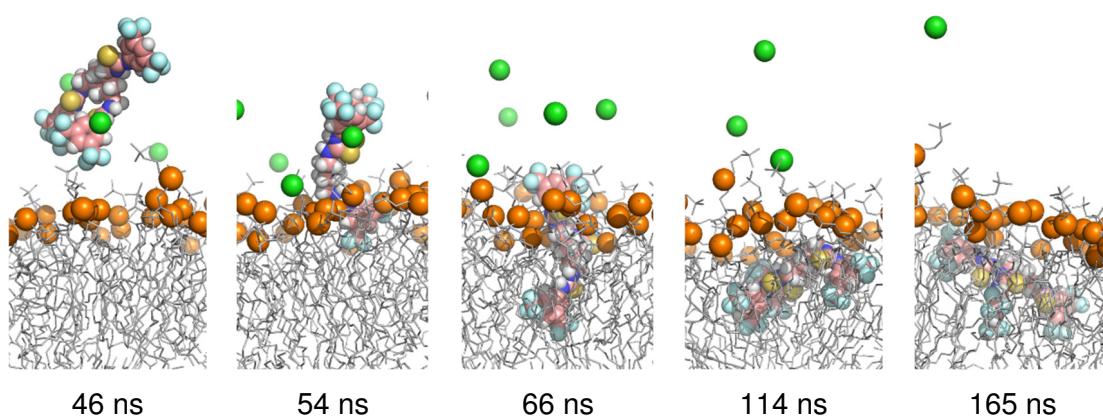


Fig. 37 – Five frames of A<sub>1</sub>3SD demonstrating 3SD entering the membrane bilayer. 3SD is represented in a space filling model with carbon atoms in salmon, hydrogen atoms in white, nitrogen atoms in blue and sulfur atoms in yellow. The chloride and phosphorus atoms are represented as green and orange spheres,

respectively, and the POPC lipids are drawn in grey lines (the hydrogen atoms in the C-H bonds of POPC lipids and the sodium atoms were omitted for clarity).

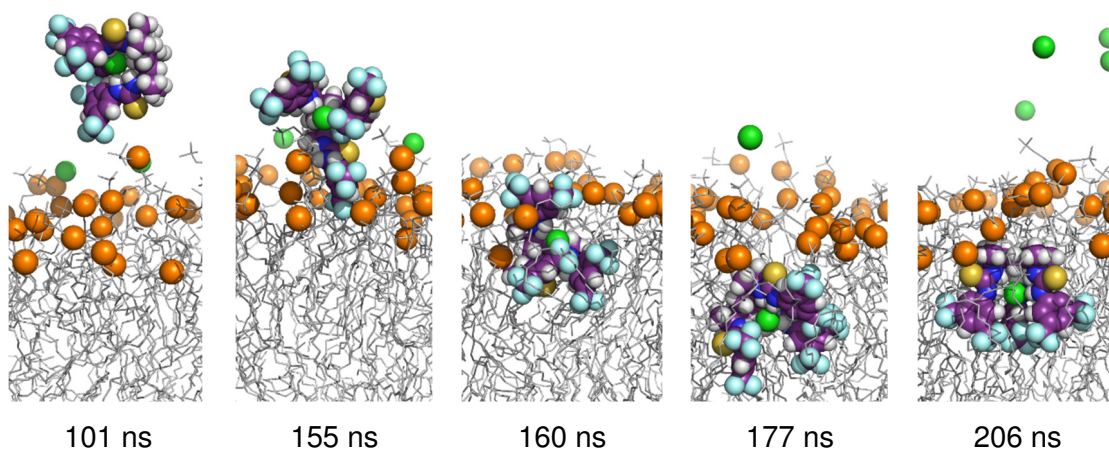


Fig. 38 – Five frames of A<sub>2</sub>4SD demonstrating the transporter entering the membrane bilayer. 4SD is represented in a space filling model with carbon atoms in purple. Remaining details as given in Fig. 37.

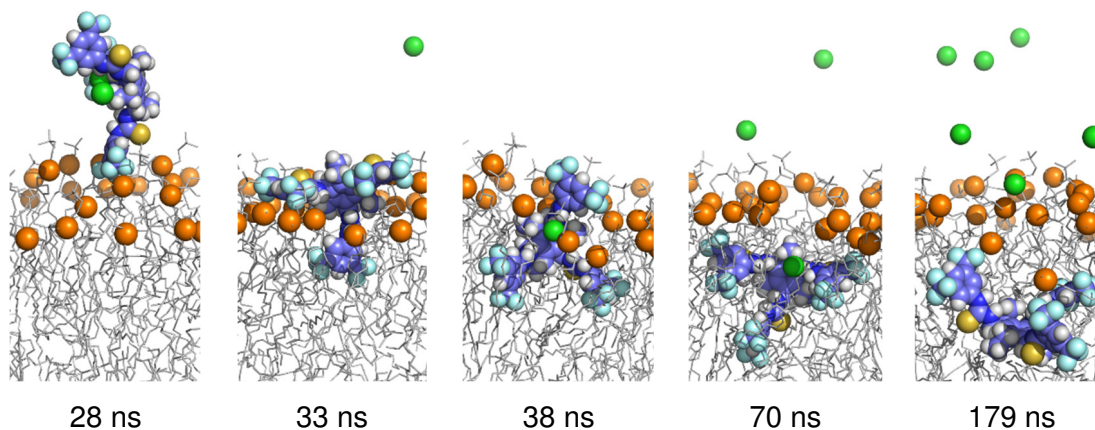


Fig. 39 – Five frames of A<sub>1</sub>6SD demonstrating the transporter entering the membrane bilayer. 6SD is represented in a space filling model with carbon atoms in blue. Remaining details as given in Fig. 37.

Then the transporters were placed in the middle of the membrane bilayer, setup B, with trinary  $Core_{COM}$  and  $CF_{3COM}$  (*vide supra*) axis almost orthogonal to the membrane's normal, as scenario (b), see Scheme 7. As plotted in Fig. 40, Fig. 41 and Fig. 42 the three molecules exhibit different diffusion patterns. The less lipophilic transporter, 3SD, in the three replicates, promptly diffuses towards the membrane's interface, reorienting itself between the phospholipids assuming scenario (a), which prevents the chloride release, as well as the interaction with phospholipid head groups, with exception of the third replicate, B<sub>3</sub>3SD. In this MD run, during *ca.* 10 ns, the hydrogen bonding some interactions with chloride are replaced by hydrogen bonds with phosphate head groups, see Fig. 40 and Fig. 43. Likewise 3SD, the 4SD transporter also diffuses to the water/lipid interface, but in lesser extension, oscillating between the spatial dispositions (b) and (a), efficiently sheltering the

chloride anion from the phosphate head groups as well as from water molecules, see Fig. 41 and Fig. 44, respectively.

In contrast with the other transporters, the diffusion of 6SD to the interface, along the three replicates, occurs with a flip movement leading to scenario (c), with the  $\text{CF}_3$  substituents pointing to the interface. Consequently, the chloride anions are released to the water phase and the NH binding sites interact either with phosphate groups or water molecules, see Fig. 42, Fig. 45 and Fig. 46.

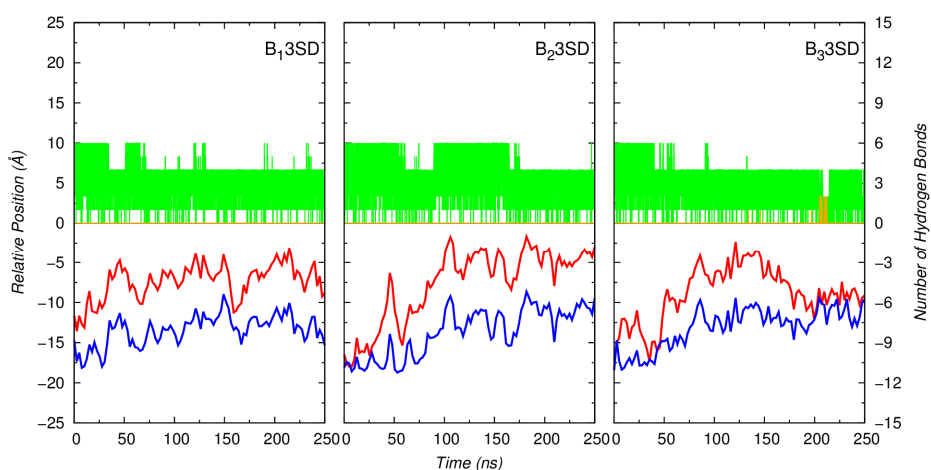


Fig. 40 – Evolution of the  $P_{\text{int}} \cdots \text{Core}_{\text{COM}}$  (in red) and the  $P_{\text{int}} \cdots \text{CF}_3_{\text{COM}}$  (in blue) distances for the 3SD transporter. The water/lipid interface is represented at a relative position of 0 Å. Remaining details as given in Fig.30.

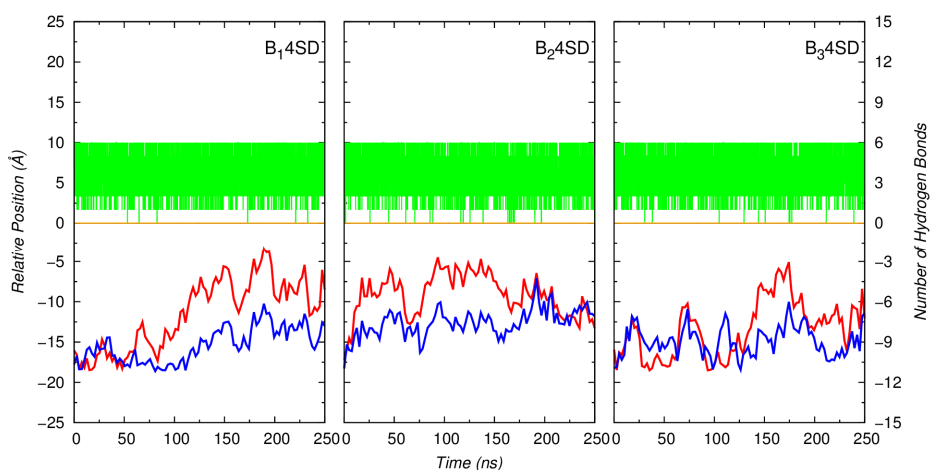


Fig. 41 – Evolution of the  $P_{\text{int}} \cdots \text{Core}_{\text{COM}}$  (in red) and the  $P_{\text{int}} \cdots \text{CF}_3_{\text{COM}}$  (in blue) distances for the 4SD transporter. The water/lipid interface is represented at a relative position of 0 Å. Remaining details as given in Fig.30.

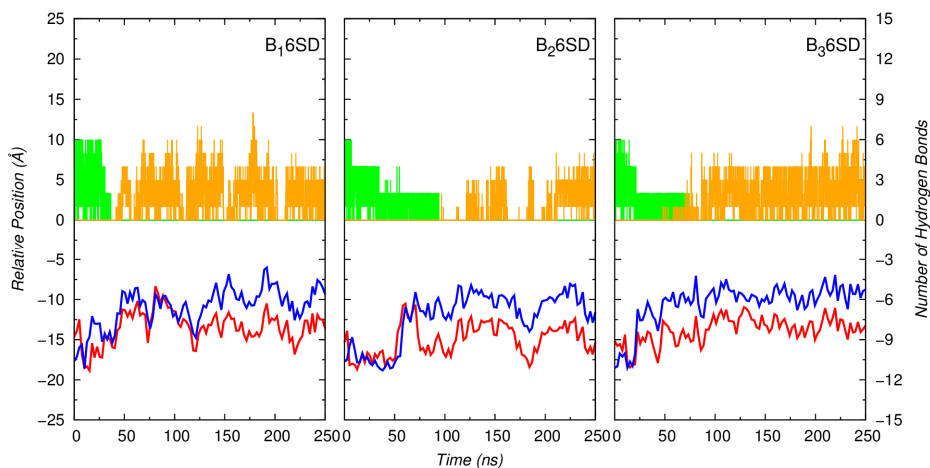


Fig. 42 – Evolution of the  $P_{\text{int}} \cdots \text{Core}_{\text{COM}}$  (in red) and the  $P_{\text{int}} \cdots \text{CF}_3\text{COM}$  (in blue) distances for the 6SD transporter. The water/lipid interface is represented at a relative position of 0 Å. Remaining details as given in Fig.30.

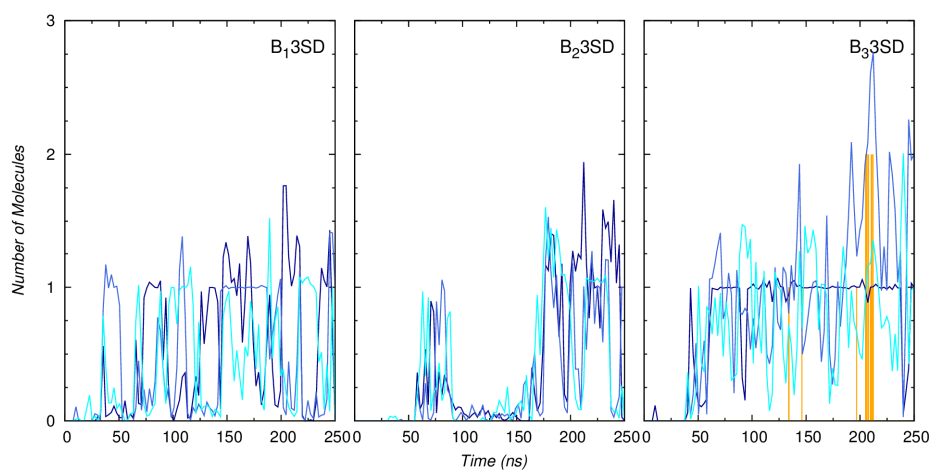


Fig. 43 – Evolution of the number of water molecules at a distance of 3.4 Å of the three binding sites of 3SD (in three different shades of blue) and evolution of the number of hydrogen bonds with the phosphate head groups (in orange). The hydration data was smoothed with Bézier curves.

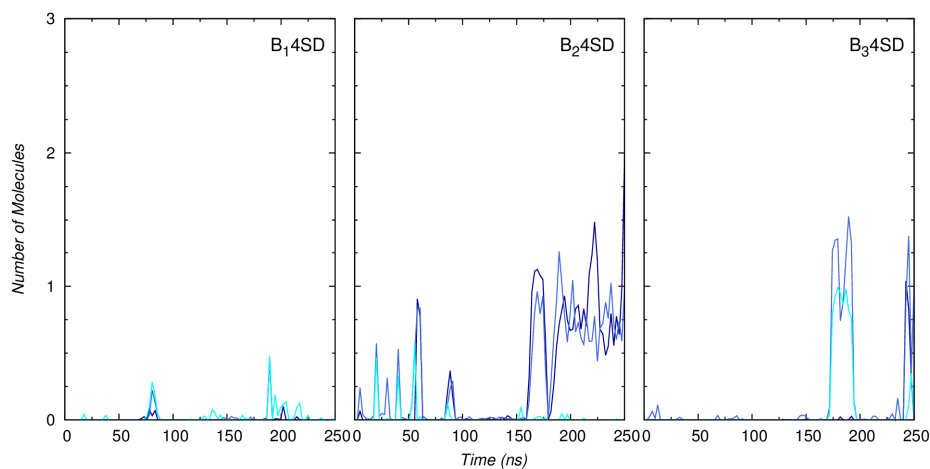


Fig. 44 – Evolution of the number of water molecules at a distance of 3.4 Å of the three binding sites of 4SD (in three different shades of blue) and evolution of the number of hydrogen bonds with the phosphate head groups (in orange). The hydration data was smoothed with Bézier curves.

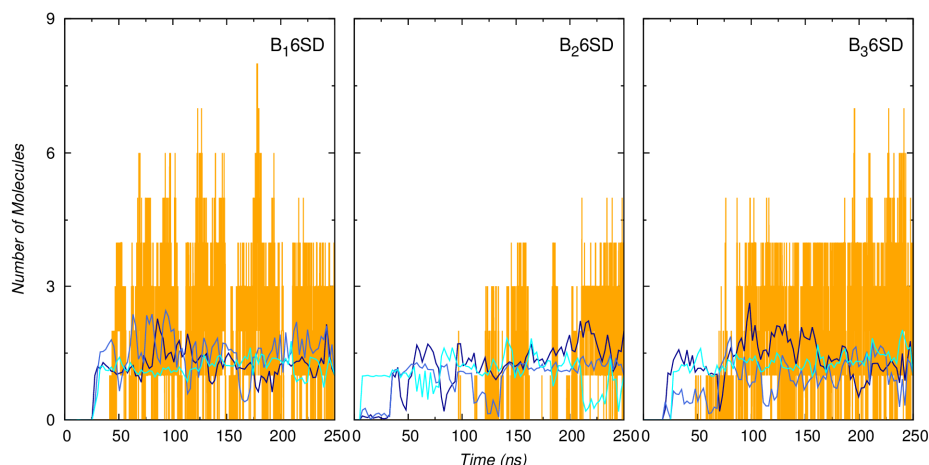


Fig. 45 – Evolution of the number of water molecules at a distance of 3.4 Å of the three binding sites of 6SD (in three different shades of blue) and evolution of the number of hydrogen bonds with the phosphate head groups (in orange). The hydration data was smoothed with Bézier curves.

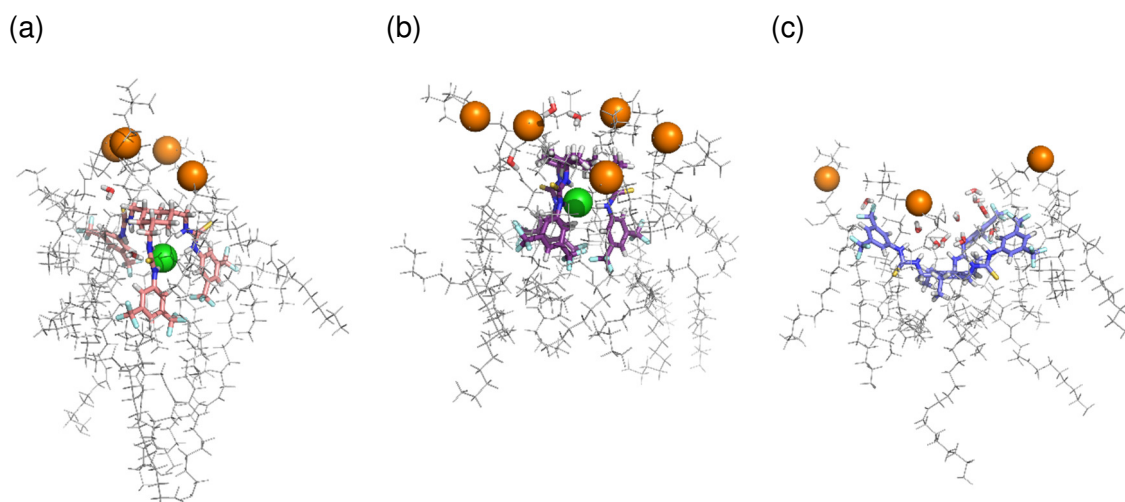


Fig. 46 – Snapshots of the interactions between the transporters (a) 3SD, (b) 4SD and (c) 6SD with the phosphate head groups of the bilayer membrane and water molecules at a distance of 3 Å. The snapshot in (a) was taken from B1\_3SD, from B1\_4SD for (b) and B1\_6SD for (c). Remaining detail as given in Fig.33.

The passive diffusion of all transporters across phospholipid bilayer, along the MD simulations, in both setups, are presented in Fig. 47, Fig. 48 and Fig. 49, plotting their  $Core_{COM}$  distances relatively to the interface throughout the simulation time. It is clear that for each transporter, throughout the *ca.* 50 last nanoseconds of the MD simulations, the transporters sit below the interface at nearly the same relative position, independently of the starting scenario. Furthermore, the average  $Core_{COM}$  distances estimated for the individual replicates in both setups, for the last 50 ns of the MD simulations, follow the order  $3SD < 4SD < 6SD$ , indicating that the molecules permeate the phospholipid bilayer in agreement with their lipophilic character, see Table 5.

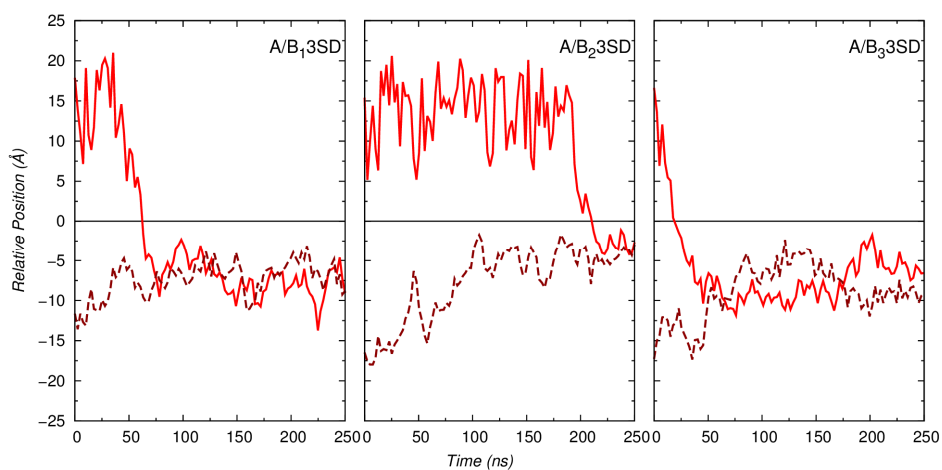


Fig. 47 – Evolution of the  $P_{int} \dots Core_{COM}$  for the 3SD transporter in setup A (red continuous line) and in setup B (dark red dashed line). The water/lipid interface is represented at a relative position of 0 Å. Data was smoothed with Bézier curves.

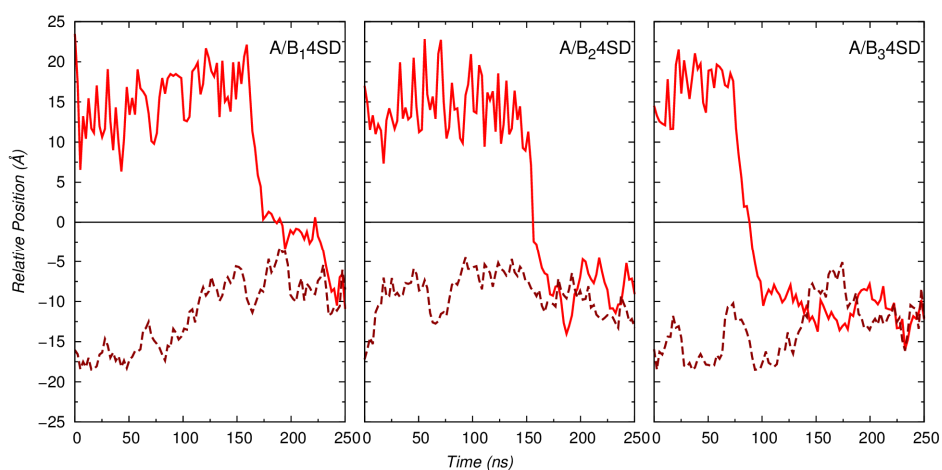


Fig. 48 – Evolution of the  $P_{int} \dots Core_{COM}$  for the 4SD transporter in setup A (red continuous line) and in setup B (dark red dashed line). The water/lipid interface is represented at a relative position of 0 Å. Data was smoothed with Bézier curves.

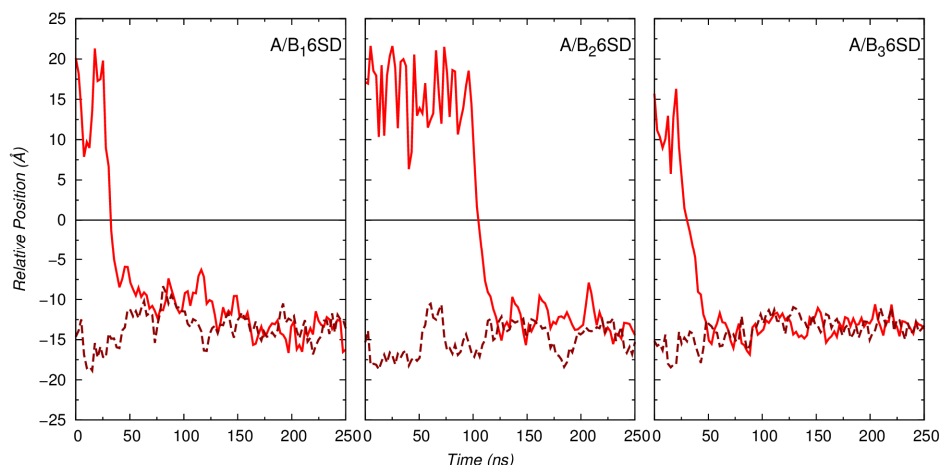


Fig. 49 – Evolution of the  $P_{\text{int}} \cdots \text{Core}_{\text{COM}}$  for the 6SD transporter in setup A (red continuous line) and in setup B (dark red dashed line). The water/lipid interface is represented at a relative position of 0 Å. Data was smoothed with Bézier curves.

Table 5 – Average  $P_{\text{int}} \cdots \text{Core}_{\text{COM}}$  distances for the last 50 ns of MD simulations for the three transporters in both setups.

Receptor	Core <sub>COM</sub> distance to	Receptor	Core <sub>COM</sub> distance to
In setup A	water/lipid interface (Å)	In setup B	water/lipid interface (Å)
A3SD	5.1±3.1	B3SD	6.6±2.4
A4SD	7.7±3.8	B4SD	10.8±1.7
A6SD	13.2±0.5	B6SD	13.6±0.5

### 3.3.4. Free Energy Calculations

Further insights into the anion transmembrane transport were obtained from US MD simulations followed by PMF calculations. The starting configurations for each US window were previously generated by a SMD simulation, as follows: the chloride complex of 4SD was initially positioned in the water phase and subsequently was dragged across the phospholipid bilayer, along the Z coordinate, to the opposite water phase, at constant velocity and using a force constant of  $5 \text{ kcal mol}^{-1} \text{ \AA}^{-2}$ . Seventy one simulation windows of 40 ns were performed leading to a total simulation time of 2.8  $\mu\text{s}$ . An equivalent protocol was applied for the free chloride anion. The remaining details are given in the experimental section.

The huge simulation time precluded us to undertake to investigate remaining two transporters along this one year MSc project, which is a very short period of time for this kind of theoretical investigation. The SMD and US simulations are currently in progress for 3SD and 6SD chloride complexes, as well as for the three free transporters.

The free energy profiles for the 4SD complex and for the chloride anion were restored from US simulations through the PMF. To assure the correct overlap between sampling windows, an histogram was built with the positions occupied by the chloride complex along the seventy one windows, see Fig. 50. Indeed, one can see the overlapping of vicinal windows, meaning that a continuous energy function can in fact be derived from the seventy one independent simulations. The same approach was followed for the chloride anion.

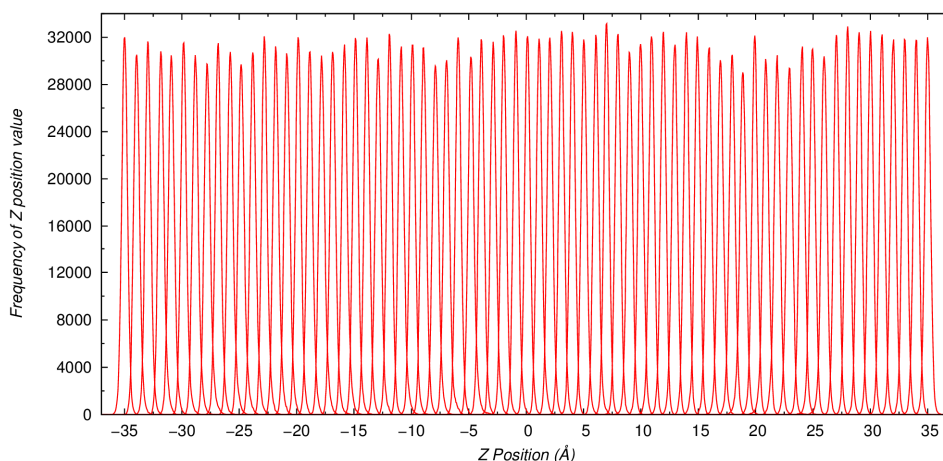


Fig. 50 – Histogram obtained for the 4SD complex showing the correct overlapping of neighboring windows.

The energy profiles plotted in Fig. 51 indicate that the chloride anion transmembrane transport is energetically favoured when the anion is carried by 4SD. Indeed, the profile of the free chloride indicates that the translocation of the anion through the phospholipids is disfavoured, with a sharp maximum of *ca.* 16.5 kcal mol<sup>-1</sup> (green line) close to the membrane's centre, at a Z coordinate of -3 Å. On the other hand, the most favourable energetic position for the chloride complex is below the membrane's interface, *ca.* 6 Å. This energetic result is entirely consistent with structural findings observed in the unrestrained MD simulations. The permeation of the chloride complex across the membrane's interface is favoured by 6 kcal mol<sup>-1</sup>. Subsequently, in remarkable contrast, the transport of the complexed chloride across the highly-packed phospholipid bilayer is accompanied by a slightly increase of the free energy, with a broad maximum, at *ca.* Z = -6 Å of only -1 kcal mol<sup>-1</sup>. In addition, when nearly located on the middle of the membrane the chloride complex is favoured by *ca.* 17.5 kcal mol<sup>-1</sup> relatively to the free chloride. Finally, the chloride complex's exit is disfavoured by 4 kcal mol<sup>-1</sup>.



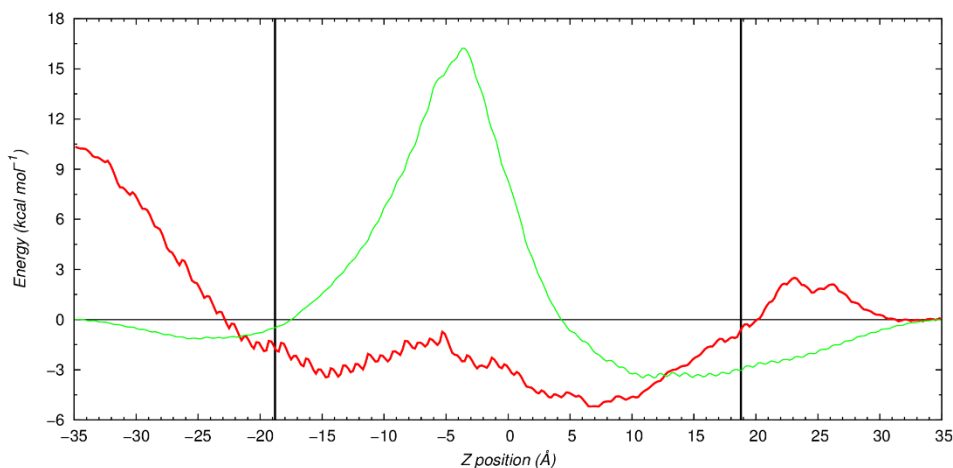


Fig. 51 – Free energy profiles for the 4SD chloride complex (in red) and the free chloride anion (in green).

The energy profile of the chloride complex is clearly asymmetric due to the spatial dispositions of the complex monitored along the US windows, which are depicted in Fig. 52(a). The complex enters and exits with the aromatic substituents pointing to the phospholipid head groups, leading to different interactions with the two water/lipid interfaces, namely with the phospholipid head groups. In contrast, in the hypothetical diffusion of the chloride complex sketched in Fig. 52(b), the complex enters with the same spatial orientation but reorients itself within the phospholipid bilayer and leaves with the phenyl substituents facing the centre of the bilayer core, in other words, the complex permeates and leaves the membrane the phenyl substituents by interacting with the lipids in a similar fashion, which should lead to a symmetric energy profile.

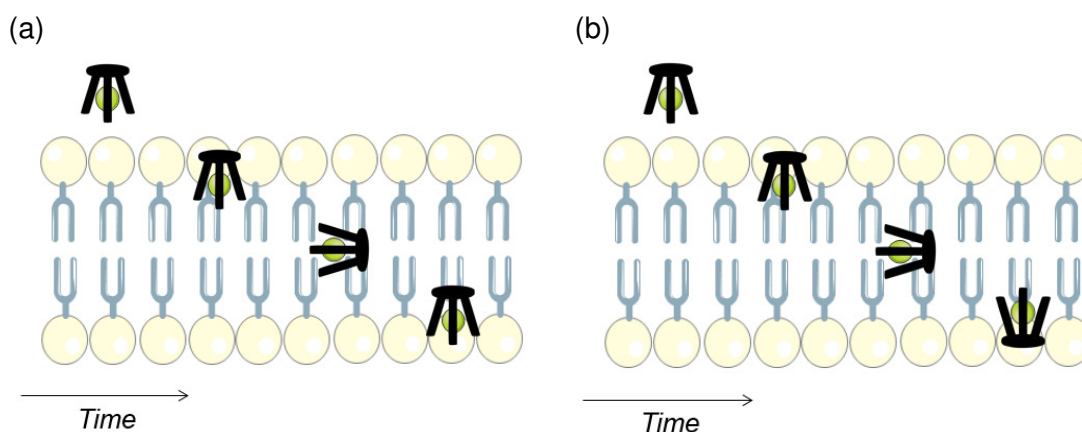


Fig. 52 – Sketch of the spatial dispositions adopted by the chloride complex that would (a) reflect the free energy profile plotted in Fig. 51 and (b) a symmetric free energy profile.

At this stage of the current research, from this energetic comparison 4SD is able to promote the chloride transport as an anion carrier, however a key question concerning the anion

transporter mechanism persists: does the transporter uptake and release the chloride anion in water solution or, alternatively, these processes occur at the water/lipid interface with the transporter positioned inside the membrane.

#### 4. Conclusion

In summary, when DFT optimized, the twelve putative chloride transporters exhibited a tripodal shape characterized by an electrostatic potential energy surface with a positive region enclosing the six binding units and a negative region over the sulfur atoms and the aryl substituents. Thus, these molecules provide a binding pocket to encapsulate a chloride anion through six convergent  $\text{NH}\cdots\text{Cl}^-$  hydrogen bonds. Furthermore, the outcome of the  $E^2$  values obtained from the second order perturbation theory and the WBI showed that the binding affinity can be modulated increasing with the introduction of p-nitro, p-trifluoromethyl, 3,5-trifluoromethyl electron withdrawing groups. On the other hand, the fluorination increases the lipophilicity of the molecules, making 3SD, 4SD and 6SD, with the 3,5-trisfluoromethyl appendages, the most lipophilic molecules while also exhibit higher chloride affinities and better transport properties. However, along this series the molecule with hexamethyl cyclohexane motif (4SD) has an intermediate logP value and has been experimentally demonstrated to be a superior chloride transporter. This outcome suggests the existence of a fine balance between transport ability and lipophilicity.

Further atomistic level insights on the transport ability of the three 3,5-trisfluoromethyl transporters were obtained by MD simulations. A preliminary analysis shows that the complexes had a marginal impact on the POPC membrane model, apart of the negligible structural changes required to accommodate the transporters within the membrane.

When the chloride complexes were initially positioned in the water slab, all tripodal receptors were able to release and, subsequently, recognise chloride anions before permeating the membrane bilayer. In addition, the hexamethyl scaffold based transporter permeated the membrane with a chloride anion, as monitored in a single MD run, A<sub>2</sub>4SD. Moreover, the molecule with benzene scaffold was able to bind and release a chloride anion when it was nested below the membrane's interface.

When the chloride complexes were placed inside the membrane, the desmethyl transporter and the hexamethyl derivatives maintained the chloride anion sheltered from the water molecules with the aryl substituents pointing to the bilayer core. In contrast, during the diffusion towards the bilayer membrane's interface, the benzene-based transporter reoriented itself within the high packet phospholipid bilayer leading to the chloride release, as requested by the anion carrier mechanism. These apparent contractor outcomes may

suggest a lack of sampling or different interactions established with phospholipids. This matter continuous under investigation in our lab. Furthermore, comparing the simulations in both setups, the distances of the transporters relatively to water/lipid interface, along the bilayer normal, were found to be directly related to the transporters' lipophilicity and independent of the starting setup.

The PMF energy profile for the chloride complex of 3,5-trifluoromethyl hexamethyl cyclohexane transporter, when compared to the energy profile of the free chloride anion, indicates that the transport of the anion was heavily favoured by the presence of the transporter (ca. 17.5 kcal mol<sup>-1</sup>). Moreover, the entry of the complex in the membrane is favoured by 6 kcal mol<sup>-1</sup>, while the chloride complex has to overcome an energy barrier of 4 kcal mol<sup>-1</sup> to exit the phospholipid bilayer. However, the pronounced increase of the energy from -25 to -35 Å indicates that this results should be considered as preliminary as discussed above in this thesis. New PMF profiles will be estimated from US simulations carried out with different starting points for these putative transporters.

Given the time available for this master's project, the results reported are in line with the main goals initially drawn for this thesis.

## 5. Bibliography

1. Marques, I.; Colaco, A. R.; Costa, P. J.; Busschaert, N.; Gale, P. A.; Felix, V., Tris-thiourea tripodal-based molecules as chloride transmembrane transporters: insights from molecular dynamics simulations. *Soft Matter* **2014**, *10* (20), 3608-21.
2. Langton, M. J.; Robinson, S. W.; Marques, I.; Felix, V.; Beer, P. D., Halogen bonding in water results in enhanced anion recognition in acyclic and rotaxane hosts. *Nat Chem* **2014**, *6* (12), 1039-43.
3. Nelson, D. L.; Cox, M. M., *Lehninger Principles of Biochemistry*. 5 ed.; Macmillan Publishers: New York, 2008.
4. Patrick, G. L., *An Introduction to Medicinal Chemistry*. 4 ed.; Oxford University Press: New York, 2009.
5. Strehler, E. E.; Zacharias, D. A., Role of alternative splicing in generating isoform diversity among plasma membrane calcium pumps. *Physiol. Rev.* **2001**, *81* (1), 21-50.
6. Yuan, Z.; Cai, T.; Tian, J.; Ivanov, A. V.; Giovannucci, D. R.; Xie, Z., Na/K-ATPase tethers phospholipase C and IP3 receptor into a calcium-regulatory complex. *Mol Biol Cell* **2005**, *16* (9), 4034-45.

7. Yu, S. P.; Choi, D. W., Na(+)-Ca<sup>2+</sup> exchange currents in cortical neurons: concomitant forward and reverse operation and effect of glutamate. *Eur. J. Neurosci.* **1997**, *9* (6), 1273-81.
8. Wright, E. M.; Turk, E., The sodium/glucose cotransport family SLC5. *Pflugers Arch* **2004**, *447* (5), 510-8.
9. Alberts, B.; Johnson, A.; Lewis, J.; Raff, M.; Roberts, K.; Walter, P., *Molecular Biology of the Cell*. Garland Science, Taylor & Francis Group: New York, 2007.
10. Fyles, T. M., Synthetic ion channels in bilayer membranes. *Chem. Soc. Rev.* **2007**, *36* (2), 335-47.
11. Gale, P. A., From anion receptors to transporters. *Acc. Chem. Res.* **2011**, *44* (3), 216-26.
12. Sessler, J. L.; Eller, L. R.; Cho, W. S.; Nicolaou, S.; Aguilar, A.; Lee, J. T.; Lynch, V. M.; Magda, D. J., Synthesis, anion-binding properties, and in vitro anticancer activity of prodigiosin analogues. *Angew. Chem. Int. Ed. Engl.* **2005**, *44* (37), 5989-92.
13. Santacroce, P. V.; Davis, J. T.; Light, M. E.; Gale, P. A.; Iglesias-Sanchez, J. C.; Prados, P.; Quesada, R., Conformational control of transmembrane Cl<sup>-</sup> transport. *J. Am. Chem. Soc.* **2007**, *129* (7), 1886-7.
14. Matile, S.; Vargas Jentsch, A.; Montenegro, J.; Fin, A., Recent synthetic transport systems. *Chem. Soc. Rev.* **2011**, *40* (5), 2453-74.
15. Sisson, A. L.; Shah, M. R.; Bhosale, S.; Matile, S., Synthetic ion channels and pores (2004-2005). *Chem. Soc. Rev.* **2006**, *35* (12), 1269-86.
16. Gale, P. A.; Busschaert, N.; Haynes, C. J.; Karagiannidis, L. E.; Kirby, I. L., Anion receptor chemistry: highlights from 2011 and 2012. *Chem. Soc. Rev.* **2014**, *43* (1), 205-41.
17. Clark, T.; Hennemann, M.; Murray, J. S.; Politzer, P., Halogen bonding: the sigma-hole. Proceedings of "Modeling interactions in biomolecules II", Prague, September 5th-9th, 2005. *J. Mol. Model.* **2007**, *13* (2), 291-6.
18. Jentsch, A. V.; Emery, D.; Mareda, J.; Nayak, S. K.; Metrangolo, P.; Resnati, G.; Sakai, N.; Matile, S., Transmembrane anion transport mediated by halogen-bond donors. *Nat Commun* **2012**, *3*, 905.
19. Giese, M.; Albrecht, M.; Bannwarth, C.; Raabe, G.; Valkonen, A.; Rissanen, K., From attraction to repulsion: anion-pi interactions between bromide and fluorinated phenyl groups. *Chem. Commun.* **2011**, *47* (30), 8542-4.
20. Benz, S.; Macchione, M.; Verolet, Q.; Mareda, J.; Sakai, N.; Matile, S., Anion Transport with Chalcogen Bonds. *J. Am. Chem. Soc.* **2016**, *138* (29), 9093-6.

21. Beno, B. R.; Yeung, K. S.; Bartberger, M. D.; Pennington, L. D.; Meanwell, N. A., A Survey of the Role of Noncovalent Sulfur Interactions in Drug Design. *J. Med. Chem.* **2015**, *58* (11), 4383-438.
22. McDonald, K. P.; Hua, Y.; Lee, S.; Flood, A. H., Shape persistence delivers lock-and-key chloride binding in triazolophanes. *Chem. Commun.* **2012**, *48* (42), 5065-75.
23. Maeda, H.; Bando, Y.; Shimomura, K.; Yamada, I.; Naito, M.; Nobusawa, K.; Tsumatori, H.; Kawai, T., Chemical-stimuli-controllable circularly polarized luminescence from anion-responsive pi-conjugated molecules. *J. Am. Chem. Soc.* **2011**, *133* (24), 9266-9.
24. Iglesias Hernandez, P.; Moreno, D.; Javier, A. A.; Torroba, T.; Perez-Tomas, R.; Quesada, R., Tambjamine alkaloids and related synthetic analogs: efficient transmembrane anion transporters. *Chem. Commun.* **2012**, *48* (10), 1556-8.
25. Busschaert, N.; Kirby, I. L.; Young, S.; Coles, S. J.; Horton, P. N.; Light, M. E.; Gale, P. A., Squaramides as potent transmembrane anion transporters. *Angew. Chem. Int. Ed. Engl.* **2012**, *51* (18), 4426-30.
26. Lipinski, C. A.; Lombardo, F.; Dominy, B. W.; Feeney, P. J., Experimental and computational approaches to estimate solubility and permeability in drug discovery and development settings. *Adv Drug Deliv Rev* **2001**, *46* (1-3), 3-26.
27. Lipinski, C. A., Lead- and drug-like compounds: the rule-of-five revolution. *Drug Discov Today Technol* **2004**, *1* (4), 337-41.
28. Ghose, A. K.; Viswanadhan, V. N.; Wendoloski, J. J., A knowledge-based approach in designing combinatorial or medicinal chemistry libraries for drug discovery. 1. A qualitative and quantitative characterization of known drug databases. *J. Comb. Chem.* **1999**, *1* (1), 55-68.
29. Veber, D. F.; Johnson, S. R.; Cheng, H. Y.; Smith, B. R.; Ward, K. W.; Kopple, K. D., Molecular properties that influence the oral bioavailability of drug candidates. *J. Med. Chem.* **2002**, *45* (12), 2615-2623.
30. Congreve, M.; Carr, R.; Murray, C.; Jhoti, H., A 'Rule of Three' for fragment-based lead discovery? *Drug Discovery Today* **2003**, *8* (19), 876-877.
31. Gale, P. A.; Perez-Tomas, R.; Quesada, R., Anion transporters and biological systems. *Acc. Chem. Res.* **2013**, *46* (12), 2801-13.
32. Haynes, C. J. E.; Moore, S. J.; Hiscock, J. R.; Marques, I.; Costa, P. J.; Felix, V.; Gale, P. A., Tunable transmembrane chloride transport by bis-indolylureas. *Chemical Science* **2012**, *3* (5), 1436-1444.

33. Busschaert, N.; Wenzel, M.; Light, M. E.; Iglesias-Hernandez, P.; Perez-Tomas, R.; Gale, P. A., Structure-activity relationships in tripodal transmembrane anion transporters: the effect of fluorination. *J. Am. Chem. Soc.* **2011**, *133* (35), 14136-48.
34. Busschaert, N.; Bradberry, S. J.; Wenzel, M.; Haynes, C. J. E.; Hiscock, J. R.; Kirby, I. L.; Karagiannidis, L. E.; Moore, S. J.; Wells, N. J.; Herniman, J.; Langley, G. J.; Horton, P. N.; Light, M. E.; Marques, I.; Costa, P. J.; Felix, V.; Frey, J. G.; Gale, P. A., Towards predictable transmembrane transport: QSAR analysis of anion binding and transport. *Chemical Science* **2013**, *4* (8), 3036-3045.
35. Olivari, M.; Montis, R.; Berry, S. N.; Karagiannidis, L. E.; Coles, S. J.; Horton, P. N.; Mapp, L. K.; Gale, P. A.; Caltagirone, C., Tris-ureas as transmembrane anion transporters. *Dalton Trans* **2016**, *45* (29), 11892-7.
36. Karagiannidis, L. E.; Haynes, C. J.; Holder, K. J.; Kirby, I. L.; Moore, S. J.; Wells, N. J.; Gale, P. A., Highly effective yet simple transmembrane anion transporters based upon ortho-phenylenediamine bis-ureas. *Chem. Commun.* **2014**, *50* (81), 12050-3.
37. Leach, A. R., *Molecular Modelling. Principles and Applications*. 2 ed.; Pearson Education Limited: Essex, 2001.
38. Vanommeslaeghe, K.; Mackerell, A. D., Jr., CHARMM additive and polarizable force fields for biophysics and computer-aided drug design. *Biochim. Biophys. Acta* **2015**, *1850* (5), 861-71.
39. Brooks, B. R.; Brooks, C. L., 3rd; Mackerell, A. D., Jr.; Nilsson, L.; Petrella, R. J.; Roux, B.; Won, Y.; Archontis, G.; Bartels, C.; Boresch, S.; Caflisch, A.; Caves, L.; Cui, Q.; Dinner, A. R.; Feig, M.; Fischer, S.; Gao, J.; Hodoscek, M.; Im, W.; Kuczera, K.; Lazaridis, T.; Ma, J.; Ovchinnikov, V.; Paci, E.; Pastor, R. W.; Post, C. B.; Pu, J. Z.; Schaefer, M.; Tidor, B.; Venable, R. M.; Woodcock, H. L.; Wu, X.; Yang, W.; York, D. M.; Karplus, M., CHARMM: the biomolecular simulation program. *J. Comput. Chem.* **2009**, *30* (10), 1545-614.
40. Jorgensen, W. L.; Maxwell, D. S.; TiradoRives, J., Development and testing of the OPLS all-atom force field on conformational energetics and properties of organic liquids. *J. Am. Chem. Soc.* **1996**, *118* (45), 11225-11236.
41. Addicoat, M. A.; Vankova, N.; Akter, I. F.; Heine, T., Extension of the Universal Force Field to Metal-Organic Frameworks. *J Chem Theory Comput* **2014**, *10* (2), 880-91.
42. Vanommeslaeghe, K.; Hatcher, E.; Acharya, C.; Kundu, S.; Zhong, S.; Shim, J.; Darian, E.; Guvench, O.; Lopes, P.; Vorobyov, I.; Mackerell, A. D., Jr., CHARMM general force field: A force field for drug-like molecules compatible with the CHARMM all-atom additive biological force fields. *J. Comput. Chem.* **2010**, *31* (4), 671-90.

43. Wang, J.; Wolf, R. M.; Caldwell, J. W.; Kollman, P. A.; Case, D. A., Development and testing of a general amber force field. *J. Comput. Chem.* **2004**, *25* (9), 1157-74.
44. Wang, J.; Wolf, R. M.; Caldwell, J. W.; Kollman, P. A.; Case, D. A., Junmei Wang, Romain M. Wolf, James W. Caldwell, Peter A. Kollman, and David A. Case, "Development and testing of a general amber force field" *Journal of Computational Chemistry*(2004) *25*(9) 1157-1174. *J. Comput. Chem.* **2005**, *26* (1), 114-114.
45. Dickson, C. J.; Madej, B. D.; Skjevik, A. A.; Betz, R. M.; Teigen, K.; Gould, I. R.; Walker, R. C., Lipid14: The Amber Lipid Force Field. *J Chem Theory Comput* **2014**, *10* (2), 865-879.
46. Skjevik, A. A.; Madej, B. D.; Walker, R. C.; Teigen, K., LIPID11: a modular framework for lipid simulations using amber. *J. Phys. Chem. B* **2012**, *116* (36), 11124-36.
47. Dickson, C. J.; Rosso, L.; Betz, R. M.; Walker, R. C.; Gould, I. R., GAFFlipid: a General Amber Force Field for the accurate molecular dynamics simulation of phospholipid. *Soft Matter* **2012**, *8* (37), 9617-9627.
48. Jambeck, J. P.; Lyubartsev, A. P., Derivation and systematic validation of a refined all-atom force field for phosphatidylcholine lipids. *J. Phys. Chem. B* **2012**, *116* (10), 3164-79.
49. Chiu, S. W.; Pandit, S. A.; Scott, H. L.; Jakobsson, E., An improved united atom force field for simulation of mixed lipid bilayers. *J. Phys. Chem. B* **2009**, *113* (9), 2748-63.
50. Marrink, S. J.; de Vries, A. H.; Mark, A. E., Coarse grained model for semiquantitative lipid simulations. *J. Phys. Chem. B* **2004**, *108* (2), 750-760.
51. Jojart, B.; Martinek, T. A., Performance of the general amber force field in modeling aqueous POPC membrane bilayers. *J. Comput. Chem.* **2007**, *28* (12), 2051-8.
52. Saggiomo, V.; Otto, S.; Marques, I.; Felix, V.; Torroba, T.; Quesada, R., The role of lipophilicity in transmembrane anion transport. *Chem. Commun.* **2012**, *48* (43), 5274-6.
53. Santos, M. M.; Marques, I.; Carvalho, S.; Moiteiro, C.; Felix, V., Recognition of bio-relevant dicarboxylate anions by an azacalix[2]arene[2]triazine derivative decorated with urea moieties. *Org Biomol Chem* **2015**, *13* (10), 3070-85.
54. Cooper, J. A.; Street, S. T.; Davis, A. P., A flexible solution to anion transport: powerful anionophores based on a cyclohexane scaffold. *Angew. Chem. Int. Ed. Engl.* **2014**, *53* (22), 5609-13.
55. Valkenier, H.; Dias, C. M.; Porter Goff, K. L.; Jurcek, O.; Puttreddy, R.; Rissanen, K.; Davis, A. P., Sterically geared tris-thioureas; transmembrane chloride transporters with unusual activity and accessibility. *Chem. Commun.* **2015**, *51* (75), 14235-8.

56. Case, D. A.; Betz, R. M.; Botello-Smith, W.; Cerutti, D. S.; Cheatham, I., T.E. ; Darden, T. A.; Duke, R. E.; Giese, T. J.; Gohlke, H.; Goetz, A. W.; Homeyer, N.; Izadi, S.; Janowski, P.; Kaus, J.; Kovalenko, A.; Lee, T. S.; LeGrand, S.; Li, P.; Lin, C.; Luchko, T.; Luo, R.; Madej, B.; Mermelstein, D.; Merz, K. M.; Monard, G.; Nguyen, H.; Nguyen, H. T.; Omelyan, I.; Onufriev, A.; Roe, D. R.; Roitberg, A.; Sagui, C.; Simmerling, C. L.; Swails, J.; Walker, R. C.; Wang, J.; Wolf, R. M.; Wu, X.; Xiao, L.; York, D. M.; Kollman, P. A. *AMBER16*, San Francisco, 2016.
57. Bayly, C. I.; Cieplak, P.; Cornell, W. D.; Kollman, P. A., A Well-Behaved Electrostatic Potential Based Method Using Charge Restraints for Deriving Atomic Charges - the Resp Model. *J. Phys. Chem.* **1993**, *97* (40), 10269-10280.
58. Groom, C. R.; Bruno, I. J.; Lightfoot, M. P.; Ward, S. C., The Cambridge Structural Database. *Acta Crystallogr B Struct Sci Cryst Eng Mater* **2016**, *72* (Pt 2), 171-9.
59. Hanwell, M. D.; Curtis, D. E.; Lonie, D. C.; Vandermeersch, T.; Zurek, E.; Hutchison, G. R., Avogadro: an advanced semantic chemical editor, visualization, and analysis platform. *J Cheminform* **2012**, *4* (1), 17.
60. Frisch, M. J.; Trucks, G. W.; Schlegel, H. B.; Scuseria, G. E.; Robb, M. A.; Cheeseman, J. R.; Scalmani, G.; Barone, V.; Mennucci, B.; Petersson, G. A.; Nakatsuji, H.; Caricato, M.; Li, X.; Hratchian, H. P.; Izmaylov, A. F.; Bloino, J.; Zheng, G.; Sonnenberg, J. L.; Hada, M.; Ehara, M.; Toyota, K.; Fukuda, R.; Hasegawa, J.; Ishida, M.; Nakajima, T.; Honda, Y.; Kitao, O.; Nakai, H.; Vreven, T.; Montgomery, J., J. A. ; Peralta, J. E.; Ogliaro, F.; Bearpark, M.; Heyd, J. J.; Brothers, E.; Kudin, K. N.; Staroverov, V. N.; Kobayashi, R.; Normand, J.; Raghavachari, K.; Rendell, A.; Burant, J. C.; Iyengar, S. S.; Tomasi, J.; Cossi, M.; Rega, N.; Millam, J. M.; Klene, M.; Knox, J. E.; Cross, J. B.; Bakken, V.; Adamo, C.; Jaramillo, J.; Gomperts, R.; Stratmann, R. E.; Yazyev, O.; Austin, A. J.; Cammi, R.; Pomelli, C.; Ochterski, J. W.; Martin, R. L.; Morokuma, K.; Zakrzewski, V. G.; Voth, G. A.; Salvador, P.; Dannenberg, J. J.; Dapprich, S.; Daniels, A. D.; Farkas, O.; Foresman, J. B.; Ortiz, J. V.; Cioslowski, J.; Fox, D. J. *Gaussian 09, Revision A.02*, Pittsburg, 2009.
61. Wang, J.; Wang, W.; Kollman, P. A.; Case, D. A., Automatic atom type and bond type perception in molecular mechanical calculations. *J Mol Graph Model* **2006**, *25* (2), 247-60.
62. Bachrach, S. M., *Reviews in Computational Chemistry*. John Wiley & Sons, Inc.: New York, 2007; Vol. 5.
63. Rappe, A. K.; Casewit, C. J. R., *Molecular Mechanics across Chemistry*. 1 ed.; University Science Books: Virginia, 1997.



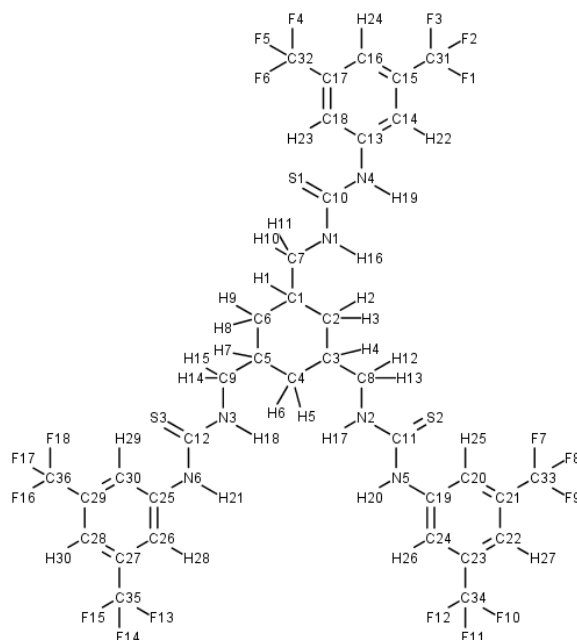
64. Pettersen, E. F.; Goddard, T. D.; Huang, C. C.; Couch, G. S.; Greenblatt, D. M.; Meng, E. C.; Ferrin, T. E., UCSF Chimera--a visualization system for exploratory research and analysis. *J. Comput. Chem.* **2004**, *25* (13), 1605-12.
65. Glendening, J., E. D. ; Badenhop, K.; Reed, A. E.; Carpenter, J. E.; Bohmann, J. A.; Morales, C. M.; Landis, C. R.; Weinhold, F. *NBO 3.1*, Madison, 2013.
66. Lu, T.; Chen, F., Multiwfn: a multifunctional wavefunction analyzer. *J. Comput. Chem.* **2012**, *33* (5), 580-92.
67. Joung, I. S.; Cheatham, T. E., 3rd, Determination of alkali and halide monovalent ion parameters for use in explicitly solvated biomolecular simulations. *J. Phys. Chem. B* **2008**, *112* (30), 9020-41.
68. Jorgensen, W. L.; Chandrasekhar, J.; Madura, J. D.; Impey, R. W.; Klein, M. L., Comparison of Simple Potential Functions for Simulating Liquid Water. *J. Chem. Phys.* **1983**, *79* (2), 926-935.
69. Edwards, S. J.; Marques, I.; Dias, C. M.; Tromans, R. A.; Lees, N. R.; Felix, V.; Valkenier, H.; Davis, A. P., Tilting and Tumbling in Transmembrane Anion Carriers: Activity Tuning through n-Alkyl Substitution. *Chemistry* **2016**, *22* (6), 2004-2011.
70. Martinez, L.; Andrade, R.; Birgin, E. G.; Martinez, J. M., PACKMOL: a package for building initial configurations for molecular dynamics simulations. *J. Comput. Chem.* **2009**, *30* (13), 2157-64.
71. Loncharich, R. J.; Brooks, B. R.; Pastor, R. W., Langevin dynamics of peptides: the frictional dependence of isomerization rates of N-acetylalanyl-N'-methylamide. *Biopolymers* **1992**, *32* (5), 523-35.
72. Berendsen, H. J. C.; Postma, J. P. M.; Vangunsteren, W. F.; Dinola, A.; Haak, J. R., Molecular-Dynamics with Coupling to an External Bath. *J. Chem. Phys.* **1984**, *81* (8), 3684-3690.
73. Ryckaert, J.-P.; Ciccotti, G.; Berendsen, H. J. C., Numerical integration of the cartesian equations of motion of a system with constraints: molecular dynamics of n-alkanes. *Journal of Computational Physics* **1977**, *23* (3), 327-341.
74. Darden, T.; York, D.; Pedersen, L., Particle mesh Ewald: An N-log(N) method for Ewald sums in large systems. *J. Chem. Phys.* **1993**, *98* (12), 10089-10092.
75. Lemkul, J. A. GROMACS Tutorial: Umbrella Sampling.  
<http://www.bevanlab.biochem.vt.edu/Pages/Personal/justin/gmx-tutorials/umbrella/index.html>.

76. Minami, T.; Liu, Y.; Akdeniz, A.; Koutnik, P.; Esipenko, N. A.; Nishiyabu, R.; Kubo, Y.; Anzenbacher, P., Jr., Intramolecular indicator displacement assay for anions: supramolecular sensor for glyphosate. *J. Am. Chem. Soc.* **2014**, *136* (32), 11396-401.
77. Weinhold, F.; Glendening, E. D., *NBO 6.0 Program Manual*. Madison, 2013.
78. Gogoi, A.; Das, G., Electronic substitution effects on anion coordination of a tripodal thiourea receptor: evidences of deprotonation of oxy- anions in solid and solution. *Supramol. Chem.* **2013**, *25* (12), 819-830.

## Supporting Information

### S1: Multi RESP charges for 51SD, 52SD and 53SD

#### 51SD

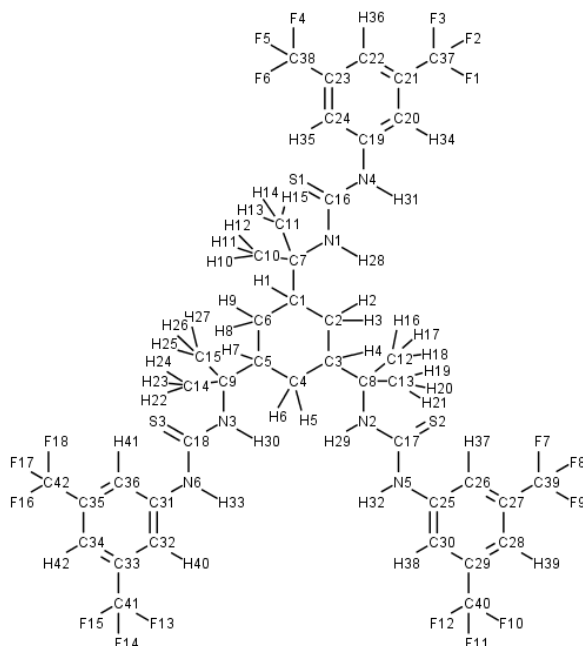


S1. 1 – Chemical structure for the 51SD transporter with all the atoms labeled.

Table 6 – Atom type and correspondent charge for all atoms of 51SD obtained after the multi RESP analysis.

Atom Name	Atom Type	Charge	Atom Name	Atom Type	Charge
<b>C1, C3, C5</b>	c3	0.166832	<b>N1, N2, N3</b>	n	-0.317750
<b>C2, C4, C6</b>	c3	-0.146012	<b>N4, N5, N6</b>	n	-0.368576
<b>C7, C8, C9</b>	c3	-0.006465	<b>S1, S2, S3</b>	s	-0.400800
<b>C10, C11, C12</b>	c	0.250633	<b>H1, H4, H7</b>	hc	-0.005756
<b>C13, C19, C25</b>	ca	0.197251	<b>H2, H3, H5, H6, H8, H9</b>	hc	0.025503
<b>C14, C20, C26</b>	ca	-0.220397	<b>H10, H11, H12, H13, H14, H15</b>	h1	0.050000
<b>C15, C21, C27</b>	ca	-0.033399	<b>H16, H17, H18</b>	hn	0.266445
<b>C16, C22, C28</b>	ca	-0.168532	<b>H19, H20, H21</b>	hn	0.316587
<b>C17, C23, C29</b>	ca	-0.033399	<b>H22, H23, H25, H26, H28, H29</b>	ha	0.180042
<b>C18, C24, C30</b>	ca	-0.220397	<b>H24, H27, H30</b>	ha	0.172576
<b>C31 to C36</b>	c3	0.676290	<b>F1 to F18</b>	f	-0.218752

## 52SD

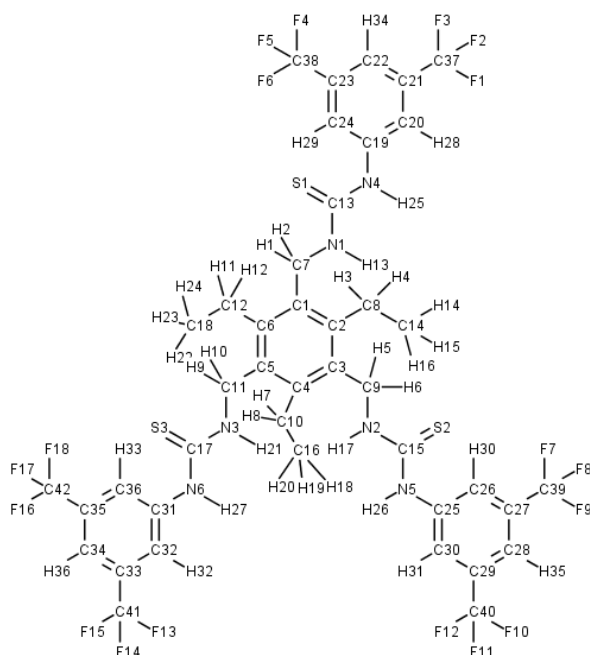


S1. 2 – Chemical structure for the 52SD transporter with all the atoms labeled.

Table 7 – Atom type and correspondent charge for all atoms of 52SD obtained after the multi RESP analysis.

Atom Name	Atom Type	Charge	Atom Name	Atom Type	Charge
<b>C1, C3, C5</b>	c3	-0.120107	<b>N4, N5, N6</b>	n	-0.339462
<b>C2, C4, C6</b>	c3	-0.026560	<b>S1, S2, S3</b>	s	-0.404750
<b>C7, C8, C9</b>	c3	0.520634	<b>H1, H4, H7</b>	hc	0.035859
<b>C10 to C15</b>	c3	-0.359859	<b>H2, H3, H5, H6, H8, H9</b>	hc	0.019144
<b>C16, C17, C18</b>	c	0.268168	<b>H10 to H27</b>	hc	0.090486
<b>C19, C25, C31</b>	ca	0.138521	<b>H28, H29, H30</b>	hn	0.252299
<b>C20, C24, C26, C30, C32, C36</b>	ca	-0.190016	<b>H31, H32, H33</b>	hn	0.324146
<b>C21, C23, C27, C29, C33, C35</b>	ca	-0.040621	<b>H34, H35, H37, H38, H40, H41</b>	ha	0.174682
<b>C22, C28, C34</b>	ca	-0.157441	<b>H36, H39, H42</b>	ha	0.164729
<b>C37 to C42</b>	c3	0.649722	<b>F1 to F18</b>	f	-0.211834
<b>N1, N2, N3</b>	n	-0.434053			

## 53SD



S1. 3 – Chemical structure for the 53SD transporter with all the atoms labeled.

Table 8 – Atom type and correspondent charge for all atoms of 53SD obtained after the multi RESP analysis.

Atom Name	Atom Type	Charge	Atom Name	Atom Type	Charge
<b>C1, C3, C5</b>	ca	0.083125	<b>N1, N2, N3</b>	n	-0.403062
<b>C2, C4, C6</b>	ca	-0.217917	<b>N4, N5, N6</b>	n	-0.317919
<b>C7, C9, C11</b>	c3	0.051454	<b>S1, S2, S3</b>	s	-0.404890
<b>C8, C10, C12</b>	c3	0.150703	<b>H1, H2, H5, H6,</b> <b>H9, H10</b>	h1	0.072200
<b>C13, C15, C17</b>	c	0.301505	<b>H3, H4, H7, H8,</b> <b>H11, H12</b>	hc	0.009851
<b>C14, C16, C18</b>	c3	-0.196876	<b>H13, H17, H21</b> <b>H14 - H16, H18</b>	hn	0.272638
<b>C19, C25, C31</b>	ca	0.135880	<b>- H20, H22 -</b> <b>H24</b>	hc	0.053395
<b>C20, C24, C26,</b> <b>C30, C32, C36</b>	ca	-0.186387	<b>H25, H26, H27</b>	hn	0.298973
<b>C21, C23, C27,</b> <b>C29, C33, C35</b>	ca	-0.049417	<b>H28, H30, H31,</b> <b>H33, H34, H36</b>	ha	0.169136
<b>C22, C28, C34</b>	ca	-0.147988	<b>H29, H32, H35</b>	ha	0.164615
<b>C37 to C42</b>	c3	0.668182	<b>F1 to F18</b>	f	-0.216259

S2: Structural parameters of the crystal structure of RUSBIS

Table 9 – Results for the dimensions of the interactions established in the crystal structure of RUSBIS:

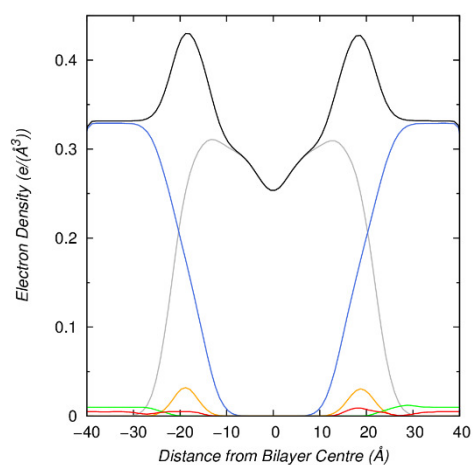
Torsion Angle (°)		Distances (Å)				Angle (°)			
Chain 1	Chain2	Chain3	N...O	O...Cl	N...Cl1	N...Cl2	NH...O	NH...Cl1	NH...Cl2
172.4	173.8	169.9	2.969	3.197	3.325	3.418	157.6	159.0	149.0
			2.955	3.108	3.284	3.496	156.1	164.4	166.5

*S3: Complete results for the structural parameters of area per lipid and membrane thickness*

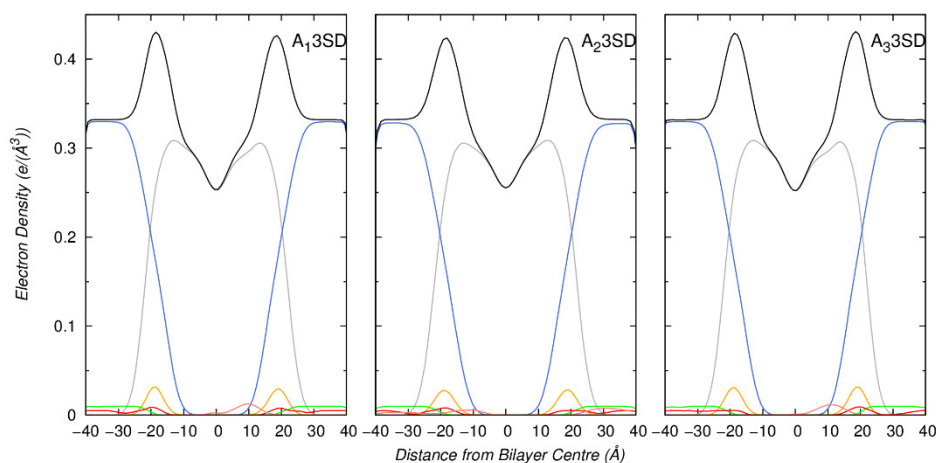
Table 10 – Results obtained for area per lipid and membrane thickness for the last 100 ns of MD simulation of the three transporters being studied, in both setups, in comparison with the values for the POPC model.

	Area per Lipid (Å <sup>2</sup> )			Membrane Thickness (Å <sup>2</sup> )			
	Avg±SD	Min	Max	Avg±SD	Min	Max	N
POPC model	65.58±1.19			37.75±0.57			7000
A <sub>1</sub> 3SD	65.78±1.10	62.85	69.07	37.89±0.52	36.26	39.50	10000
A <sub>2</sub> 3SD	65.77±1.48	61.61	70.34	37.74±0.67	35.79	39.76	10000
A <sub>3</sub> 3SD	65.54±0.84	62.82	68.15	37.98±0.42	36.58	39.31	10000
A <sub>1</sub> 4SD	66.40±1.59	62.08	71.02	37.58±0.73	35.47	39.73	10000
A <sub>2</sub> 4SD	66.01±1.33	62.70	69.80	37.85±0.63	35.82	39.74	10000
A <sub>3</sub> 4SD	65.48±0.96	63.23	68.50	38.10±0.46	36.53	39.48	10000
A <sub>1</sub> 6SD	66.27±1.04	62.66	69.71	37.70±0.51	36.16	39.81	10000
A <sub>2</sub> 6SD	65.88±1.11	62.27	69.31	37.90±0.53	36.27	40.06	10000
A <sub>3</sub> 6SD	65.41±1.05	63.02	69.82	38.10±0.48	36.19	39.37	10000
B <sub>1</sub> 3SD	65.93±1.26	62.02	70.06	37.90±0.57	36.21	40.16	10000
B <sub>2</sub> 3SD	65.95±1.00	63.04	69.26	37.89±0.48	36.23	39.23	10000
B <sub>3</sub> 3SD	66.09±1.23	62.30	69.33	37.83±0.59	36.16	39.66	10000
B <sub>1</sub> 4SD	65.66±0.99	62.62	68.96	38.03±0.50	36.50	39.72	10000
B <sub>2</sub> 4SD	65.81±1.25	62.32	69.16	37.94±0.59	35.97	39.79	10000
B <sub>3</sub> 4SD	65.40±1.23	62.48	68.98	38.12±0.58	36.51	39.81	10000
B <sub>1</sub> 6SD	65.52±0.87	62.78	68.71	37.99±0.41	36.45	39.42	10000
B <sub>2</sub> 6SD	65.58±1.19	62.06	68.86	38.08±0.60	36.43	39.87	10000
B <sub>3</sub> 6SD	64.75±1.23	61.66	69.13	38.35±0.57	36.26	39.85	10000

S4: Results for the structural parameters of electron density profiles and order parameters

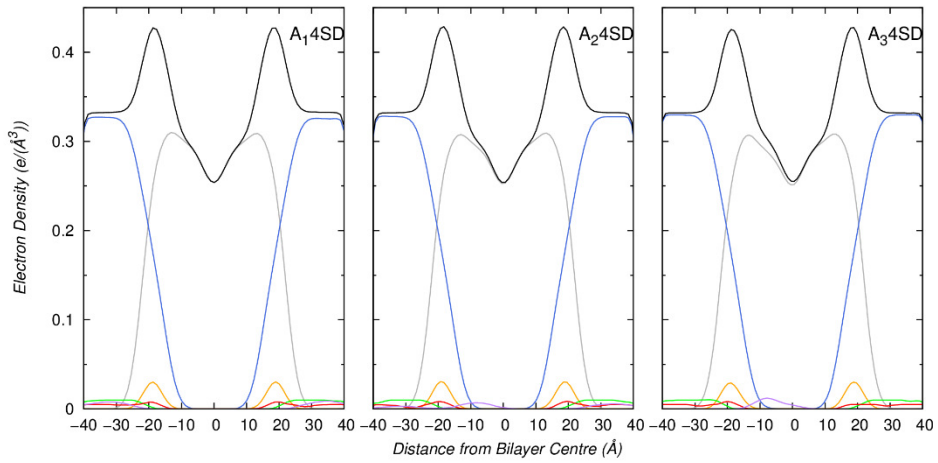


S4. 1 – Electron density profile for the POPC membrane model. The profile of the whole system is represented in a black line, of water is represented in a blue line, of the phospholipid membrane in a grey line, of the phosphorus atoms in an orange line, of the sodium cations in a red line and of the chloride anion in a green line. The data for the sodium cations and the chloride anions was scaled five times.

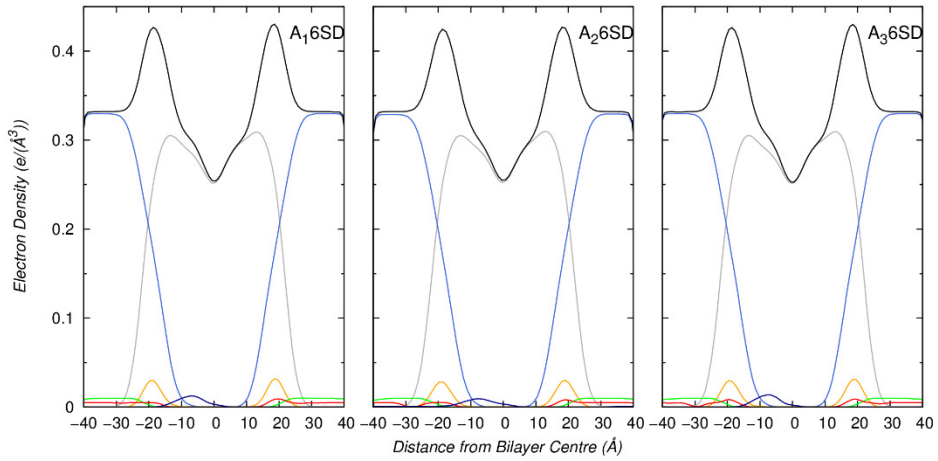


S4. 2 – Electron density profile for 3SD in setup A represented in a salmon solid line. Remaining details as given in S4.1.

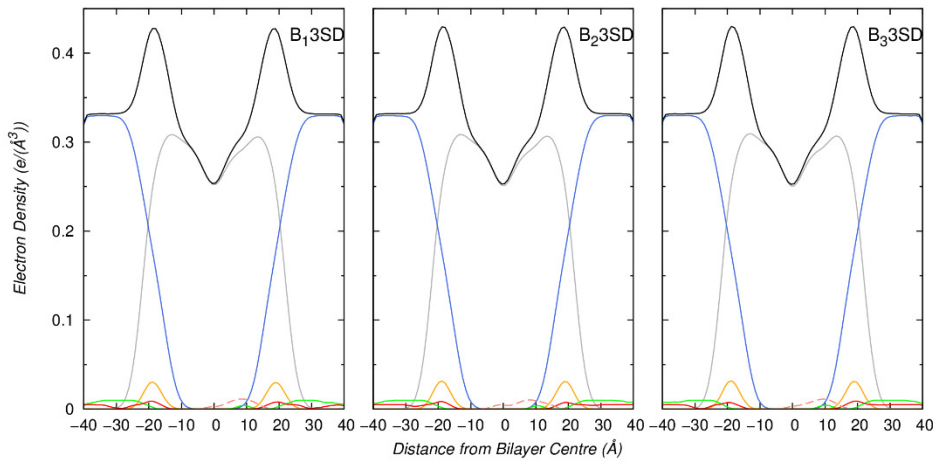




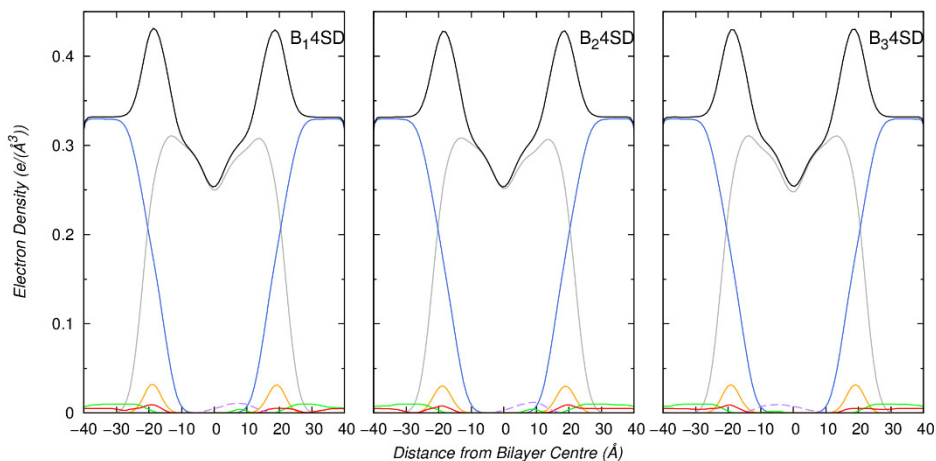
S4. 3 – Electron density profile for 4SD in setup A represented in a purple solid line. Remaining details as given in S4.1.



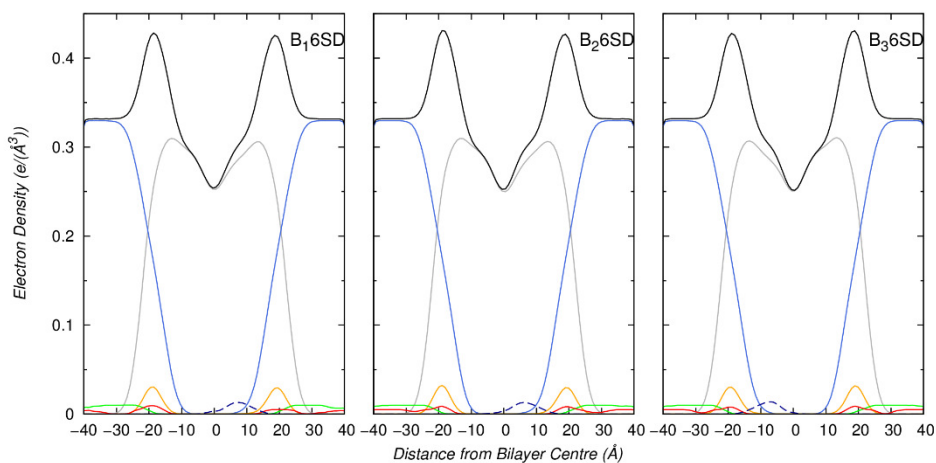
S4. 4 – Electron density profile for 6SD in setup A represented in a blue solid line. Remaining details as given in S4.1.



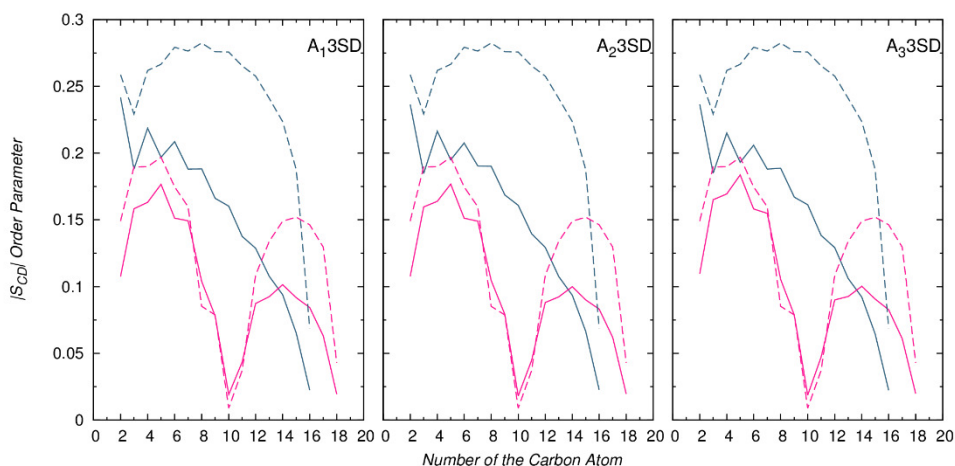
S4. 5 – Electron density profile for 3SD in setup B represented in a salmon dashed line. Remaining details as given in S4.1.



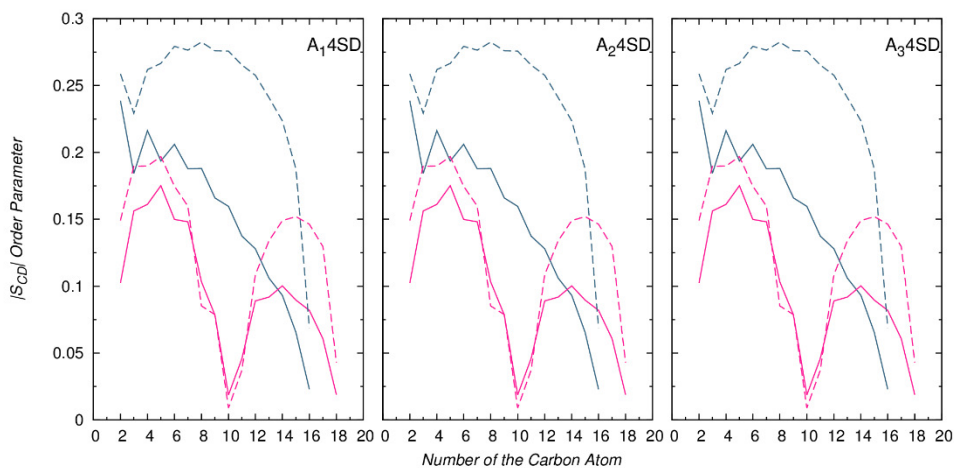
S4. 6 – Electron density profile for 4SD in setup B represented in a purple dashed line. Remaining details as given in S4.1.



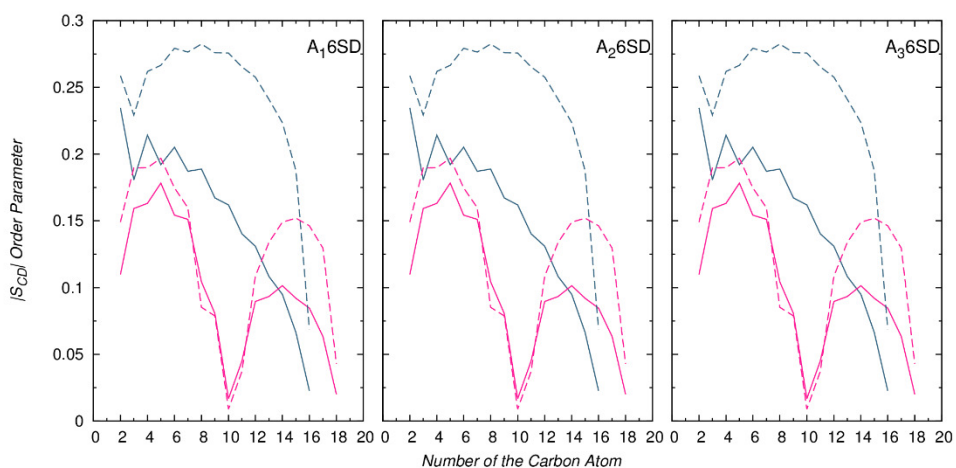
S4. 7 – Electron density profile for 6SD in setup B represented in a blue dashed line. Remaining details as given in S4.1.



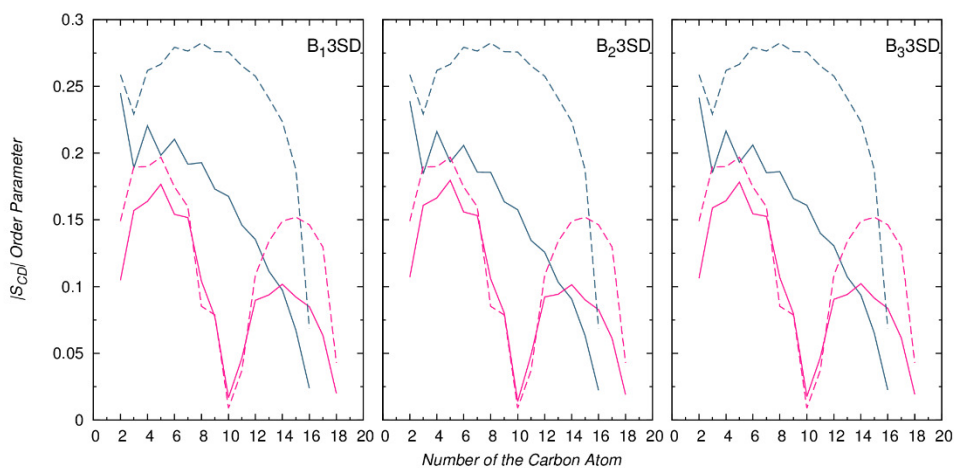
S4. 8 – Order parameters for  $sn-1$  and  $sn-2$  of 3SD in setup A are represented in light blue and pink solid lines, respectively. The order parameters for  $sn-1$  and  $sn-2$  for the POPC membrane model are represented in light blue and pink dashed lines.



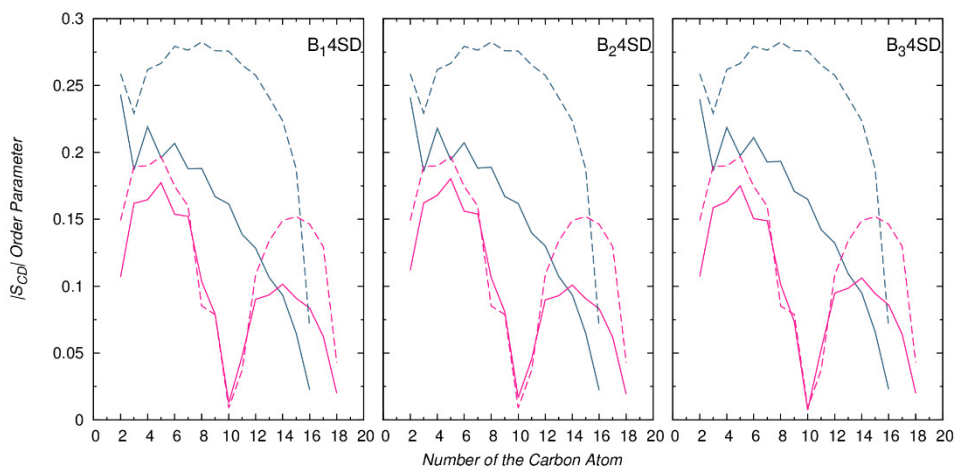
S4. 9 – Order parameters for  $sn-1$  and  $sn-2$  of 4SD in setup A are represented in light blue and pink solid lines, respectively. Remaining details as given in S4.8.



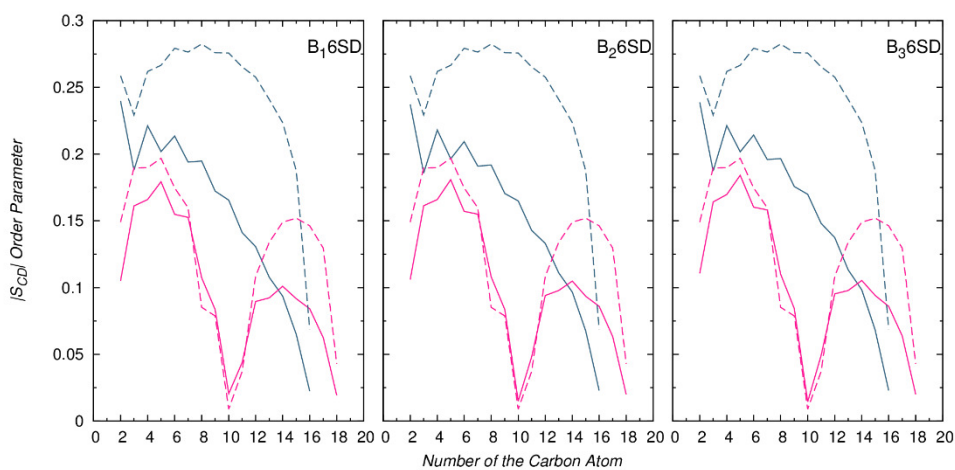
S4. 10 – Order parameters for  $sn-1$  and  $sn-2$  of 6SD in setup A are represented in light blue and pink solid lines, respectively. Remaining details as given in S4.8.



S4. 11 – Order parameters for  $sn-1$  and  $sn-2$  of 3SD in setup B are represented in light blue and pink solid lines, respectively. Remaining details as given in S4.8.



S4. 12 – Order parameters for *sn*-1 and *sn*-2 of 4SD in setup B are represented in light blue and pink solid lines, respectively. Remaining details as given in S4.8.



S4. 13 – Order parameters for *sn*-1 and *sn*-2 of 6SD in setup B are represented in light blue and pink solid lines, respectively. Remaining details as given in S4.8.